Scientific Analysis/Calculation Administrative Change Notice

Complete only applicable items.

1. Document Number:	ANL-NBS-HS-000039	2. Revision:	02	3. ACN:	01
4. Title:	Saturated Zone In-Situ Testing				
5. No. of Pages Attached:	129				

6. Approvals:

Preparer:	Paul Reimus (Paul W. Reimus) Print Name and Sign	8/30/07 Date
Checker:	Robert Roback (RC Roback) Print name and sign	8/30/07 Date
QCS/Lead Lab QA Reviewer:	Sounia Kassabian-Darnell (Sounia K. Darnell) Print name and sign	08/31/2007 Date
Responsible Manager:	Stephanie Kuzio (Stephanie Kuzio) Print name and sign	9/5/2007 Date

7. Affected Pages	8. Description of Change:
vii, viia	Editorial changes to titles of Appendices F and K – Title change to Appendix F was a DOE Comment.
xx	Figure G-32 caption changed from "diffusion-into-blocks" to "diffusion-into-grains"
xxvi	Added "Groundwater" to the beginning of the table titles for Tables 6.5-5 and 6.5-6
xxviii	Added "Groundwater" to the beginning of the table titles for Tables G-8, G-9, and G-10. Also changed "diffusion-into-blocks" to "diffusion-into-grains" in title for Table G-11.
1-1	'BSC 2004 [DIRS 177390]' changed to 'SNL 2007 [DIRS 181650]'.
1-3	'BSC 2004 [DIRS 177390]' changed to 'SNL 2007 [DIRS 181650]' and 'BSC 2004 [DIRS 170042]' changed to 'SNL 2007 [DIRS 181006]'.
6-3	Added note to Figure 6.1-1.
6-17	Centered Figure 6.1-10 and changed DTN and DIRs number for the LA FEP list. Changed "model report" to "analysis report". Added a period after "table" (last word on page).
6-18, 6-19, 6-20	'BSC 2004 [DIRS 177390]' changed to 'SNL 2007 [DIRS 181650]' in Table 6.1-3 (numerous places). Also, one carriage return removed between table title and table on each page.
6-40	Subscripted and superscripted appropriate characters in the 2nd and 3rd columns of the header row of Table 6.3-2.
6-41	Moved the superscripted "d" (footnote) outside the parentheses in the last two rows of Table 6.3-3.
6-46	'BSC 2004 [DIRS 177390]' changed to 'SNL 2007 [DIRS 181650]' in two places.
6-53	Changed "sentenes" to "sentences" – DOE comment
6-61	Changed iodide diffusion coefficient from 2.1×10^{-6} to 2.1×10^{-5} in Table 6.5-3. Also, extra header row was removed from table, and "(kg)" was changed to "(g)" in the third-to-last row of table. The latter two items were DOE Comments.
6-69	Added a comma after "flow porosity" to avoid giving the impression that the flow porosity is equal to the subsequent stream of numbers.
6-71	Changed what appeared to be an incomplete sentence to numbered item 3 – DOE comment. Also, removed a space after "v_S" and added a space after "(=".
6-72	Moved "Groundwater" to beginning of Table 6.5-5 title and added "Seepage" before "Velocities" in both the Table title and the header row of this table (inserted spaces in header row as well). Also, changed footnote "a" to read "…in *SZ Flow and Transport Model Abstraction* (SNL 2007 [DIRS 181650])."

Scientific Analysis/Calculation Administrative Change Notice

Complete only applicable items.

1. Document Number:	ANL-NBS-HS-000039	2. Revision:	02	3. ACN:	01
4. Title:	Saturated Zone In-Situ Testing				

6-73	Added "Groundwater" to beginning of Table 6.5-6 title. Also, changed footnote "a" to read "…in *SZ Flow and Transport Model Abstraction* (SNL 2007 [DIRS 181650])." Broke sentence starting at bottom of page 6-73 (and ending on top of p. 6-74) into 2 sentences and made other editorial changes for clarity – This was a DOE comment. One of the new sentences is the last sentence on p. 6-73. The other new sentence is the first sentence on p. 6-75.
6-74, 6-75	There is no longer a sentence that continues from p. 6-73 onto p. 6-74. Also, the first sentence on p. 6-75 is a new sentence that was part of the sentence that previously appeared at the bottom of p. 6-73 and ended on top of p. 6-74.
6-76	Changed "diffusion into blocks" to "diffusion into grains".
6-80	Changed "layers or blocks" to "layers or grains".
7-3, 7-9, 7-12, 7-13	'BSC 2004 [DIRS 177390]' changed to 'SNL 2007 [DIRS 181650]' (4 places). Changed the name for this report on pp. 7-12 and 7-13. Also, removed extra carriage return at end of p. 7-13.
8-3	Removed citations to DIRS 170042 (old citation for *SZ Flow and Transport Model Abstraction*) and DIRS 170037 (old citation for *SZ Site-Scale Flow Model*).
8-14	Added new citations for *SZ Flow and Transport Model Abstraction* [DIRS 181650] and *Particle Tracking Model and Abstraction of Transport Processes* [DIRS 181006].
8-25	Updated citation for LA FEP list.
B-1	Removed the "*" after "N/A" in the second column – there is no * in the footnote and an asterisk isn't used in the 3rd row or the last row. USW WT#1 changed to USW WT-1. Added the following wells to this table that are now referred to in Appendix O: USW WT-10, UE-25 WT#12, USW G-1, USW G-2, USW G-3 and GU-3, USW G-4, USW H-1, USW H-3, USW H-5, and USW H-6.
C-62	Changed the end of the second note to: "which consists largely of friction head loss, is known."
C-66	'BSC 2004 [DIRS 170037]' changed to 'SNL 2007 [DIRS 177391]'
D-2	Inserted "Figure" before "D-1".
D-19	Changed the c's in the note from upper case to lower case.
D-29	Subscripted and superscripted appropriate characters in the 2nd and 3rd columns of the header row of Table D-1, and inserted spaces between the superscripted footnote designators and text in the other rows of this table.
D-30	Slight reformatting of Table D-2. Also, inserted "Not Estimated" where there were blank table entries.
D-32	Inserted "Not Estimated" where there were blank table entries in Table D-3.
D-40, D-41	Inserted new figures with revised y-axis titles for Figures D-19, D-20, and D-21.
D-48, D-48a	Replaced $\phi D_m^{1/2}/b$ with $\frac{\phi}{b}\sqrt{D_m}$, which caused two lines to move to the next page (which is a new page).
D-54	Changed y-axis titles on both plots of Figure D-26.
D-63, D-64	Reformatted $\frac{\phi}{b}\sqrt{D_m}$ on p. D-63, and replaced $\phi D_m^{1/2}/b$ with $\frac{\phi}{b}\sqrt{D_m}$ on p. D-64.
D-72	Moved text from between Figures D-31 and D-32 to bottom of this page.
D-73	Change bar indicates move of text to bottom of p. D-72
D-74	Changed y-axis title of Figure D-32 (inserted new figure).
D-79	Reformatted $\frac{\phi}{b}\sqrt{D_m}$.
D-82	'BSC 2004 [DIRS 170042]' changed to 'SNL 2007 [DIRS 181650]'
E-12, E-14, E-15	Inserted new figures for Figures E-6, E-8, and E-9 so that axes titles would be consistent with other figures in this section. Also, added legend box to Figure E-9.
E-29	Appropriate characters superscripted in Diffusion Coefficient table header row.
E-32	In header row of Table E-7, abbreviated "Lithium Concentration" to "Lithium Conc." to avoid the splitting of Concentration into "Concentrat" and "ion".

1. Document Number:	ANL-NBS-HS-000039	2. Revision:	02	3. ACN:	01
4. Title:	Saturated Zone In-Situ Testing				

E-43	Subscripted the "h" on Bh and italicized this term – to be consistent with subsequent tables containing hydraulic aperture.
E-47, E-47a	Replaced $\phi D_m^{1/2}/b$ with $\frac{\phi}{b}\sqrt{D_m}$. This change caused the last two lines on the page to move to the next page, which is a new page (E-47a).
E-58, E-62	Changed "Li^+ Retardation factor" to "Li^+ Matrix retardation factor" and also changed "Li^+ Partition coefficient" to "Li^+ Matrix partition coefficient" in Tables E-16 and E-17.
E-67	Removed the superscripted "*" after "D_m" for Diffusion Cells. There is no corresponding footnote or explanation for this symbol. Also, inserted a space between the "10" and the "b" in the superscripted portion of the last column of the Lower Prow Pass (3) row (to be consistent with elsewhere).
Appendix F title page	Title changed from "Details of Hydraulic Testing and Test Interpretations at the Alluvial Testing Complex (ATC) and Nye County Site 22" to "Details of Hydraulic Testing and Hydraulic Test Interpretations in Saturated Alluvium South of Yucca Mountain".
F-1	Several changes to the first two paragraphs to include discussion of testing and test interpretations for Nye County Site 22 – DOE comment
F-6, F-8, F-10, F-12	Subscripted the "w" of "Lw" in the notes of Figures F-4, F-6, F-8, and F-10.
F-37	Inserted a dash (-) between "north" and "northwest" – DOE comment
F-39, F-39a	Added a footnoted definition of "bgs" to the bottom of Table F-1.
F-40	Removed the period after "20.5".
F-43	Made several changes to Table F-3 - Changed "Linear Regression Parameters" to "Linear Regression Equations" - In Row 3, removed all the asterisks (which were intended to be multiplication symbols but were not necessary). - In 5th column of 3rd row, changed p_3 to p_2 (this was a typo). - In first column, added "(a)" after "Slope" and "(c)" after "Intercept". - Made "pressure" and "zone" plural in the NOTE.
F-49	Removed "(for illustration purposes only)" from the figure caption – it is redundant with the NOTE.
F-53	Replaced "1" with "I" in χ_{i+I} – DOE Comment
F-59	Added spaces on either side of the equal sign. Also, made the "i" after Equation F-39 italic.
F-60	The first few sentences of Section F6.7.1 have been rewritten for better clarity, and a reference to "Figure 30" has been removed from this block of text – This was a DOE comment.
F-61, F-67, F-68	Added spaces on either side of equal signs. Also, change "S" to "s" on p. F-68
F-80	Inserted a "0" before ".2".
F-83	Removed the extra "s" in front of "storativity" in the last line of the table note. Also, changed "m^2/d" to "m^2/day" in first line of table note.
F-88	Added spaces on either side of equal signs. Also, in last two sentences of Section F6.9, changed "based on all four zone pumping" to "based on pumping all four zones in 22S". Also, changed "test" to "tests" at the end of the 2nd sentence.
F-90	Revised the figure so that there are no spaces between rectangles representing layers.
F-91	Changed "10.3 m/day" to "10.4 m/day" – DOE Comment
F-97, F-98, F-99, F-100	Replaced Figures F-46 to F-49 to improve readability of axes and improve formatting.
G-3	Changed top figure on this page so that all lines are bold/dark – DOE Comment
G-6	Removed a row from this table that contained "Grain diameter in nonadvective layers", which was always listed as N/A – DOE Comment
G-9, G-12, G-13	Inserted "Insets show details of halide and FBA responses near their peak concentrations" in the notes to Figures G-3, G-5, and G-6 – DOE Comment(s)
G-19	Changed "a = 0" to "c = 0" – DOE Comment

1. Document Number:	ANL-NBS-HS-000039	2. Revision:	02	3. ACN:	01
4. Title:	Saturated Zone In-Situ Testing				

G-38	Added ", which" after "Equations G-7 to G-16" – DOE Comment
G-40	'BSC 2004 [DIRS 170042]' changed to 'SNL 2007 [DIRS 181650]'
G-50, G-51, G-52, G-54	Changed "3.1 to 12.4" to "3.0 to 12.2" on pages G-50 and G-54 – DOE Comment(s). Also, removed hyphen from between "Groundwater" and "Velocity" in titles of Sections G4.4 and G4.5 on pp. G-52 and G-54. On p. G-51, added "Groundwater" to beginning of titles of Tables G-8, G-9, and G-10, and also changed footnote "a" for each of these tables to read "…in *SZ Flow and Transport Model Abstraction* (SNL 2007 [DIRS 181650])."
G-57	Changed "22s" to "22S" – DOE Comment. Also, changed "blocks" to "grains" in several places, and replaced '*or "blocks"*' with '*(sometimes also referred to as "blocks")*'.
G-58, G-59, G-60, G-61	Changed "blocks" to "grains" in numerous places – DOE comment noted inconsistent usage.
G-64	Added a space between the "12" and the superscripted "a" in the Longitudinal Dispersivity row of the table.
G-65	Removed an extra space before the first "20", and also changed "m/d" to "m/day." Also, added a comma after "flow porosity" to avoid giving the impression that the flow porosity is equal to the subsequent stream of numbers.
G-66	Changed iodide diffusion coefficient from 2.1×10^{-6} to 2.1×10^{-5} in Table G-13. Also, "(kg)" was changed to "(g)" in the last row on the page. The latter item was a DOE Comment for Table 6.5-3 that also applies here.
G-76	Changed "blocks" to "grains" and made "line" plural ("lines") near bottom of page. The latter item was a DOE Comment.
G-77	Changed "blocks" to "grains".
G-81	Added "(continued)" at the end of the Table G-14 title – DOE Comment
G-91	Added "prior to time zero" at end of figure note.
G-96, G-96a	Revised and clarified block of text to read: : "It can be shown that if advective transport times are long relative to diffusion time scales, a nonsorbing solute will experience an effective physical retardation factor equal to 1.0 plus the ratio of stagnant to flowing porosity in a system (Robinson 1994 [DIRS 101154]). Advective time scales are clearly longer than deduced times scales for diffusion (Table G-20) in the alluvium under ambient flow conditions, so the range of porosity ratios of 0.3 to 1.9 translates to a range of effective physical retardation factors of 1.3 to 2.9 in the alluvium." – DOE Comment. Also, removed "(or "blocks")" and changed "blocks" to "grains" in last paragraph.
G-97	Changed "blocks" to "grains".
G-100	Changed "untracerd water" to "untraced water" – DOE Comment
G-101	In the "Output DTN" footnote, changed "retardation factor" to "partition coefficients (K_d values)".
G-105	Changed "blocks" to "grains".
H-6	Changed "30,000 xg" to "30,000x g (at an acceleration 30,000 times that of gravity)". Also, a colon was added after "from" just before Equation H-1.
H-11	Inserted spaces before superscripted footnote designators in header row of table.
H-18	Reformatted the two equations on this page.
J-2	Inserted spaces before superscripted footnote designators in header row of table.
K-3	'BSC 2004 [DIRS 170037]' changed to 'SNL 2007 [DIRS 177391]'in two places.
N-2	Used carriage returns in header row to move "zone" down to the second line in four of the columns
O-2, O-5	Changed borehole designations of 4 WT wells, as necessary, to be consistent with the following designations that appear in the TDMS: USW WT-10, UE-25 WT#12, UE-25 WT#14, UE-25 WT#17
Q-19	Added a space before "Derivative calculated" in figure note. Also, the "$\pm$" at the end of the second row of the note was moved to the beginning of the third row.

CONTENTS (Continued)

Page

CONTENTS (Continued)

Page

FIGURES (Continued)

Page

TABLES (Continued)

Page

TABLES (Continued)

Page

1. PURPOSE

The purpose of this scientific analysis is to document the results and interpretations of field experiments that test and validate conceptual flow and radionuclide transport models in the saturated zone (SZ) near Yucca Mountain, Nevada. The test interpretations provide estimates of flow and transport parameters used in the development of parameter distributions for total system performance assessment (TSPA) calculations. These parameter distributions are documented in *Site-Scale Saturated Zone Transport* (SNL 2007 [DIRS 177392]), *Saturated Zone Colloid Transport* (BSC 2004 [DIRS 170006]), and *Saturated Zone Flow and Transport Model Abstraction* (SNL 2007 [DIRS 181650]).

Although this TWP was prepared before transition to the Lead Laboratory, it was considered appropriate for developing this report, because it was prepared in compliance with LP-2.29Q-BSC, *Planning for Science Activities* (a BSC procedure (predecessor)), which corresponds to SCI-PRO-002, *Planning for Science Activities* (the Lead Laboratory procedure). Specifically, this scientific analysis contributes the following to the assessment of the capability of the SZ to serve as part of a natural barrier for waste isolation for the Yucca Mountain repository system:

- The bases for selection of conceptual flow and transport models in the saturated volcanics and the saturated alluvium located near Yucca Mountain.

- Results and interpretations of hydraulic and tracer tests conducted in saturated fractured volcanics at the C-wells complex near Yucca Mountain. The test interpretations include estimates of hydraulic conductivities, anisotropy in hydraulic conductivity, storativities, total porosities, effective porosities, longitudinal dispersivities, matrix diffusion mass transfer coefficients, matrix diffusion coefficients, fracture apertures, and colloid transport parameters.

- Results and interpretations of hydraulic and tracer tests conducted in saturated alluvium at the Alluvial Testing Complex (ATC) located at the southwestern corner of the Nevada Test Site (NTS) and at Nye County Site 22, located just east of Fortymile Wash about 4.5 km northeast of the ATC (and about 13 km from the repository). The test interpretations include estimates of hydraulic conductivities, storativities, total porosities, effective porosities, longitudinal dispersivities, matrix diffusion mass transfer coefficients, and colloid transport parameters.

- Comparisons of sorption parameter estimates for a reactive solute tracer (lithium ion) derived from the C-wells field tracer tests and laboratory tests using C-wells core samples.

- Sorption parameter estimates for lithium ion derived from laboratory tests using alluvium samples from ATC well NC-EWDP-19D and from well NC-EWDP-22PC. For the latter well, these estimates allow a comparison of laboratory- and field-derived sorption parameters to be made for saturated alluvium (cross-hole tests were never conducted at the ATC, so a similar comparison is not possible for that location).

believed to be far removed from potential flow pathways from the repository footprint). Also, Eh, pH, and redox couple data relevant to potential radionuclide transport from Yucca Mountain are discussed in considerable detail in *Impacts of Solubility and Other Geochemical Processes on Radionuclide Retardation in the Natural System - Rev 01* (BSC 2006 [DIRS 178672]).

- Comparisons of alluvium hydraulic parameter estimates and specific discharge estimates to estimates obtained from the calibrated SZ site-scale flow model are discussed in *Saturated Zone Site-Scale Flow Model* (SNL 2007 [DIRS 177391]) rather than in this analysis report.

- More software items are listed in Table 3-1 and used in this analysis than are listed in Table 6 of the TWP.

The data and analyses documented in this report are used as scientific supporting information in other Yucca Mountain Project reports including:

- *Saturated Zone Site-Scale Flow Model*
- *Site-Scale Saturated Zone Transport*
- *Saturated Zone Colloid Transport*
- *Saturated Zone Flow and Transport Model Abstraction.*

Figure 1-1 shows the relationship of this report to other analysis and model reports that pertain to flow and transport in the SZ. Figure 1-1 also shows the flow of key information among the SZ reports. It should be noted that Figure 1-1 does not contain a complete representation of the data and parameter inputs and outputs of all SZ reports, nor does it show inputs external to this suite of SZ reports. In addition to the SZ analysis and model reports in Figure 1-1, this analysis report provides input (longitudinal dispersivity estimates from C-wells tracer tests) to *Radionuclide Transport Models Under Ambient Conditions* (SNL 2007 [DIRS 177396]) and *Particle Tracking Model and Abstraction of Transport Processes* (SNL 2007 [DIRS 181006]).

The bases for the conceptual models and the estimates of flow and transport parameters presented in this scientific analysis are derived from tests conducted at only one location in the saturated fractured volcanics (C-wells complex) and two locations in the saturated alluvium (ATC and Nye County Site 22). Consequently, several other sources of information are used to develop broader uncertainty distributions for flow and transport parameters in the TSPA for license application (LA) analyses. The development and bases of these distributions are documented in *SZ Flow and Transport Model Abstraction* (SNL 2007 [DIRS 181650]), where it is shown that the overall parameter distributions used in the TSPA-LA analyses include considerations of literature data, expert elicitation input, and peer review input. The only uncertainty distribution presented in this report is one for the north-south/east-west anisotropy ratio of horizontal hydraulic conductivity in the fractured volcanics (Section 6.2.6).

The SZ FEPs included in the TSPA-LA and supported by the results of this report are listed in Table 6.1-3.

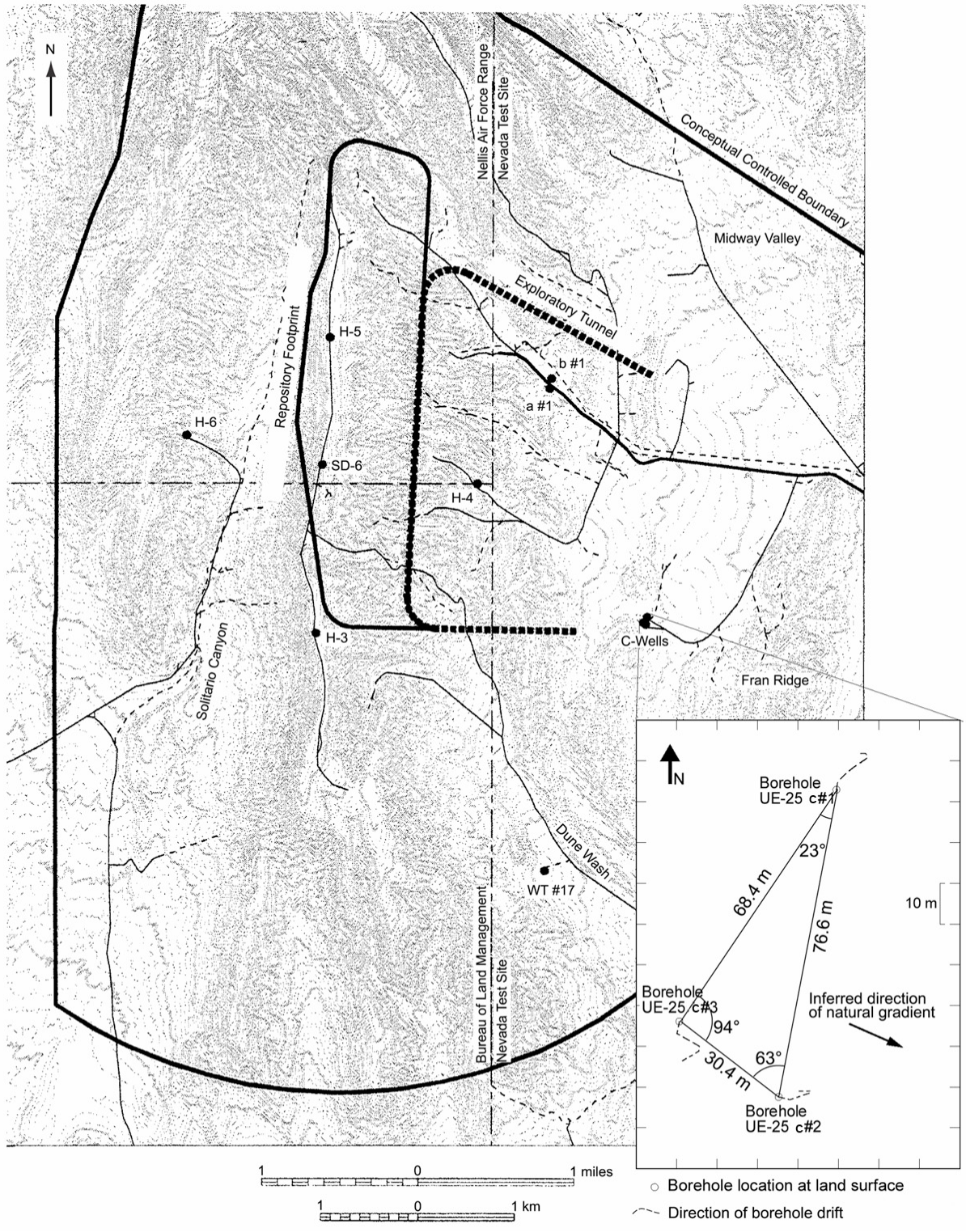

Source: Based on Geldon 1993 [DIRS 101045], p 6, Figure 2.

NOTE: The repository footprint is subject to change and is shown for illustration purposes only.

Figure 6.1-1. Location and Surface Layout of the C-Wells Complex

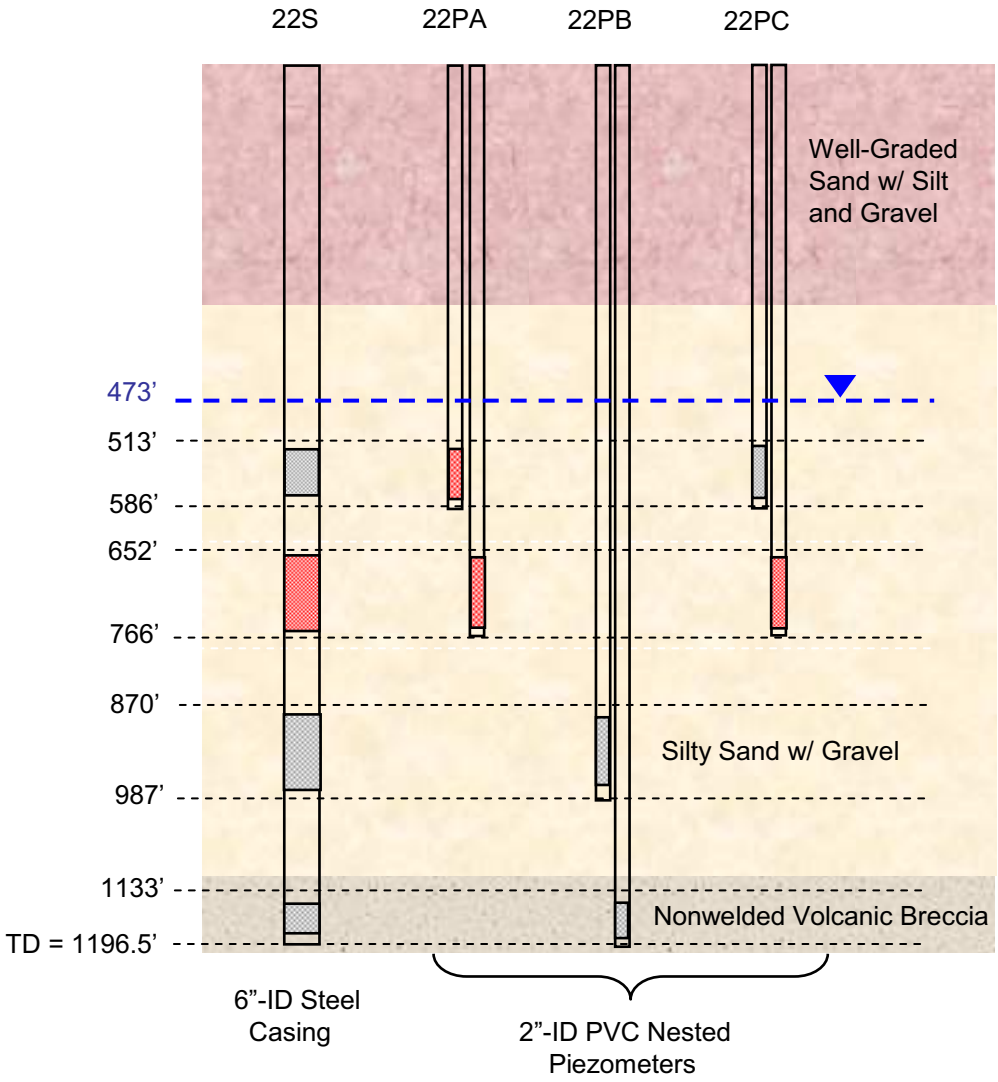

Sources: DTNs: GS030108314211.001 (Stratigraphy) [DIRS 163483], LA0705PR150304.007 (Well Completions) [DIRS 181202].

Figure 6.1-10. Schematic Diagram of NC-EWDP-22S, -22PA, -22PB, and -22PC Completions and Lithology. Red rectangles within wells indicate screens into which tracers were injected during single-well and cross-hole testing. The depths correspond to the tops and bottoms of sand packs (see text for tops and bottoms of screens)

6.1.2 Features, Events, and Processes Supported by This Scientific Analysis

As stipulated in the TWP (BSC 2006 [DIRS 177375]), this analysis report addresses the SZ FEPs pertaining to saturated zone in-situ testing included in TSPA-LA (Table 6.1-3). Table 6.1-3 provides a list of FEPs relevant to this model analysis in accordance with their assignment in the LA FEP list (DTN: MO0706SPAFEPLA.001 [DIRS 181613]). Specific reference to the various sections within this document where issues related to each FEP are addressed is provided in the table.

Table 6.1-3. Features, Events, and Processes Included in TSPA-LA and Relevant to This Report

FEP No.	FEP Name	Sections Where Disposition Is Supported	FEP Topic Addressed in Other SZ Analysis or Model Reports
1.2.02.01.0A	Fractures	Flow in fractures is addressed throughout Section 6.2 and Appendix C. Transport in fractures is addressed throughout Section 6.3 and Appendix D. Also, discussion of lab transport studies in fractures is provided in Appendix E (Section E3.2).	Upstream Feeds[a]–N/A. Expanded Discussion[b] – BSC 2004 [DIRS 170014]. Corroborating[c] – SNL 2007 [DIRS 174109]; SNL 2007 [DIRS 177392]; SNL 2007 [DIRS 177391]; SNL 2007 [DIRS 181650]
1.2.02.02.0A	Faults	The influence of faults (or the potential influence of faults) on flow in the saturated volcanics is discussed in Sections 6.1.1.1, 6.2.3, 6.2.4, 6.2.7, C5, and C6.2.	Upstream Feeds[a]-N/A Expanded Discussion[b] – SNL 2007 [DIRS 174109]Corroborating[c] – SNL 2007 [DIRS 177392]; SNL 2007 [DIRS 181650]
2.2.03.01.0A	Stratigraphy	Hydrologic settings (including stratigraphy) for the hydraulic and tracer tests in the fractured volcanics and in the alluvium are discussed in Sections 6.1.1.1 and 6.1.1.2, respectively.	Upstream Feeds[a]- N/A Expanded Discussion[b] – SNL 2007 [DIRS 174109]; SNL 2007 [DIRS 177391]. Corroborating[c] – SNL 2007 [DIRS 181650]; BSC 2004 [DIRS 170014]
2.2.03.02.0A	Rock properties of host rock and other units	Rock properties as they relate to flow and transport are addressed in many places throughout Sections 6.1.1, 6.2 through 6.5, and in Appendices C through H.	Upstream Feeds[a]-N/A Expanded Discussion[b] – SNL 2007 [DIRS 174109]]; SNL 2007 [DIRS 177391]. Corroborating[c] – SNL 2007 [DIRS 177391]; SNL 2007 [DIRS 181650]
2.2.07.12.0A	Saturated groundwater flow in the geosphere	Saturated groundwater flow in the fractured volcanics is addressed in Section 6.2 and Appendix C. Saturated groundwater flow in the alluvium is addressed in Section 6.4 and Appendix F.	Upstream Feeds[a]-N/A. Expanded Discussion[b] – SNL 2007 [DIRS 177391]. Corroborating[c] – SNL 2007 [DIRS 177391]; BSC 2004 [DIRS 170015]; BSC 2004 [DIRS 170014]; SNL 2007 [DIRS 181650]
2.2.07.13.0A	Water-conducting features in the SZ	Geologic features affecting flow in the fractured volcanics are addressed in Section 6.1.1.1, Section 6.2, and Appendix C. Geologic features affecting flow in the alluvium are addressed in Section 6.1.1.2, Section 6.4 and Appendix F.	Upstream Feeds[a]-N/A. Expanded Discussion[b] – SNL 2007 [DIRS 177391]; SNL 2007 [DIRS 181650]. Corroborating[c] – BSC 2004 [DIRS 170014]

Table 6.1-3. Features, Events, and Processes Included in TSPA-LA and Relevant to This Model Report (Continued)

FEP No.	FEP Name	Sections Where Disposition Is Supported	FEP Topic Addressed in Other SZ Analysis or Model Reports
2.2.07.15.0A	Advection and dispersion in the SZ	Advection and dispersion effects on transport in the fractured volcanics are discussed throughout Section 6.3 and Appendix D, and they are discussed for the alluvium throughout Section 6.5 and Appendix G. Scale dependence of dispersion in the fractured volcanics is addressed in Section E4.1.	Upstream Feeds[a]-N/A Expanded Discussion[b] – SNL 2007 [DIRS 177392]; SNL 2007 [DIRS 181650]. Corroborating[c] – SNL 2007 [DIRS 177391]; BSC 2004 [DIRS 170015]
2.2.07.17.0A	Diffusion in the SZ	Molecular diffusion processes in the volcanics are addressed in Section 6.3 and in several places in Appendices D and E. In Section 6.5 and Appendix G, molecular diffusion is discussed for the alluvium, but it was concluded that it did not have a major effect on transport in the alluvium.	Upstream Feeds[a]-N/A Expanded Discussion[b] – SNL 2007 [DIRS 181650]; SNL 2007 [DIRS 177392]. Corroborating[c] – BSC 2004 [DIRS 170014]; BSC 2004 [DIRS 170006]
2.2.08.08.0A	Matrix diffusion in the SZ	The effects of matrix diffusion on transport in the volcanics are discussed in Section 6.3.2 and in Sections D4. and E4.2. Observations and parameterizations of matrix diffusion in the volcanics are addressed in several places in Section 6.3 and Appendices D and E. Matrix diffusion in the alluvium is discussed in Sections 6.5.2, 6.5.4 and in Appendix G, but it was concluded that matrix diffusion did not have a significant effect on transport in the alluvium.	Upstream Feeds[a]-N/A Expanded Discussion[b] – SNL 2007 [DIRS 181650]; SNL 2007 [DIRS 177392]. Corroborating[c] – BSC 2004 [DIRS 170014]; BSC 2004 [DIRS 170006]
2.2.08.09.0A	Sorption in the SZ	Sorption in the SZ is addressed in Sections 6.3.4, 6.3.5, 6.3.6, and 6.5.6. It is also addressed in detail in the following appendix sections: D4, E1, E3, H1, and H2. The material in Sections 6.3 and D4 address field-scale observations of sorption, and the material in the other sections addresses laboratory observations of sorption of sorbing tracer used in the field tracer tests.	Upstream Feeds[a]-N/A Expanded Discussion[b] – SNL 2007 [DIRS 177392]; SNL 2007 [DIRS 181650]. Corroborating[c] – None (This analysis is corroborating to the two reports above that contain expanded discussions).

Table 6.1-3. Features, Events, and Processes Included in TSPA-LA and Relevant to This Model Report (Continued)

FEP No.	FEP Name	Sections Where Disposition Is Supported	FEP Topic Addressed in Other SZ Analysis or Model Reports
2.2.08.10.0A	Colloidal transport in the SZ	Colloid transport in the volcanics is addressed in Section D4. Colloid detachment rates in the alluvium are addressed in Section G4.6. Colloid-facilitated transport of radionuclides is not directly addressed in this report.	Upstream Feeds[a]-N/A Expanded Discussion[b] – BSC 2004 [DIRS 170006]; SNL 2007 [DIRS 181650]. Corroborating[c] – SNL 2007 [DIRS 177392]
2.2.12.00.0B	Undetected features in the SZ	Undetected features are indirectly addressed in the discussion of anisotropy in horizontal hydraulic conductivity in the fractured volcanics in Sections 6.2.6, C6.2, and C6.3. Flow anisotropy may be the result of undetected features such as fracture sets or faults.	Upstream Feeds[a]-N/A Expanded Discussion[b] – SNL 2007 [DIRS 177391]. Corroborating[c] – BSC 2004 [DIRS 170014]; SNL 2007 [DIRS 181650]

[a] Upstream Feeds – Aspects of the SZ FEP screening position adopted in this report are a result of SZ analyses performed in a directly upstream SZ model or analyses.

[b] Expanded Discussion – The FEP topic is addressed in more detail in an SZ analysis or model report.

[c] Corroborating – Corroborative aspect(s) of the FEP topic is (are) discussed in an SZ analysis or model report.

FEP=feature, event, and process; SZ=saturated zone.

6.2 HYDROLOGIC PROPERTIES OF FRACTURED TUFFS (C-WELLS COMPLEX)

6.2.1 Introduction

This section of the report (1) summarizes the hydraulic tests conducted at the C-wells complex and the interpretive analyses performed on the test data; (2) discusses the implications of the test interpretations, including implications for conceptual understanding of groundwater flow in the fractured volcanics, hydrologic parameter estimates, and horizontal flow anisotropy in the fractured volcanics; and (3) discusses the uncertainties and limitations associated with the hydrologic properties determined from the test analyses.

6.2.2 Summary of C-Wells Hydraulic Testing to Determine Hydrologic Properties

Table 6.2-1 summarizes the hydraulic testing conducted at the C-wells complex over a fifteen-year period. Aquifer storativities and transmissivities were estimated primarily from water-level drawdowns measured in observation wells as a function of pumping time of a production well (i.e., drawdown curves) in the last five tests listed Table 6.2-1. The other tests listed in Table 6.2-1 provided valuable information on flowing intervals within each well; some of this information was used to convert aquifer transmissivity estimates to hydraulic conductivity estimates for flowing intervals. Details of hydraulic testing at the C-wells, especially the tests listed in the last four rows of Table 6.2-1, are provided in Appendix C.

Table 6.3-2. Ratios of Observed Tracer Arrival Times and Distances Squared, as well as Apparent Flow Anisotropy Ratios, for C-Wells Nonsorbing Tracer Tests

Tests (Injection Well)	$Time_{c\#1}$/ $Time_{c\#2\text{-}c\#3}$ [a]	$r_L^2{}_{c\#1}$/ $r_L^2{}_{c\#2\text{-}c\#3}$ [a]	Anisotropy Ratio [a]
Bullfrog: PFBA (c#2) and iodide (c#1)[b]	6	8.5	1.42
Bullfrog: 2,6-DFBA (c#2) and pyridone (c#1)[c]	11	8.5	0.77
Prow Pass: iodide and 2,4,5-TFBA (c#3) and 2,3,4,5-TeFBA (c#1)[d]	10	8.3	0.83

Sources: DTNs: GS010508312315.001 [DIRS 155860]; GS990208312315.001 [DIRS 159238]; LA0007PR831231.001 [DIRS 156043] (data); Borehole separation distances taken from Table 6.1-1.

Output DTN: LA0303PR831231.005.

NOTE: Because the borehole separation distances are unqualified data, the anisotropy ratios are provided for information purposes only. The uncertainties in the anisotropy ratios are quite large because vertical tracer transport distances, which were not accounted for in the calculations, could have been comparable to or even greater than the horizontal travel distances between the boreholes.

NOTE: c#1, c#2, and c#3 are abbreviations for Boreholes UE-25 c#1, UE-25 c#2, and UE-25 c#3. r_L^2 is the distance squared between injection and production wells.

[a] $Time_{c\#1}$ and $r_L^2{}_{c\#1}$ are the time and distance, respectively, between c#1 and the production well (either c#2 or c#3, depending on the test), and $Time_{c\#2\text{-}c\#3}$ and $r_L^2{}_{c\#2\text{-}c\#3}$ are the time and distance, respectively between c#2 and c#3. Columns 2 and 3 give the ratios of these times and distances. Ratio is for c#1 to production well direction divided by c#2 to c#3 direction. For the anisotropy ratio, a value greater than 1.0 indicates that the c#1 to production well direction is the preferred flow orientation.

[b] Both tests conducted with 2.5% to 3.5% recirculation into injection well. Peak tracer arrivals compared.

[c] Both tests conducted with no recirculation. First tracer arrivals compared.

[d] c#3-to-c#2 test conducted with 30% recirculation; c#1-to-c#2 test conducted with no recirculation. Peak tracer arrivals compared.

DFBA= difluorobenzoic acid; PFBA= pentafluorobenzoic acid; TeFBA= tetrafluorobenzoate; TFBA= trifluorobenzoic acid.

The ratios of tracer arrival times and r_L^2 values are in reasonably good agreement in all three cases, with apparent flow anisotropy ratios (c#1 to production well direction divided by c#2-c#3 direction) varying from 0.77 to 1.42. These relatively small ratios suggest that flow anisotropy at the scale of the C-wells may be relatively small despite the apparent orientation of the fracture network in the general direction of c#1 to c#2 (Geldon 1993 [DIRS 101045], pp. 43 to 51). The apparent flow anisotropy ratios deduced from the tracer arrival times should be carefully distinguished from the flow anisotropy ratios discussed in Section 6.2.6, which were based on drawdown observations over much larger scales.

6.3.5 Tracer Test Interpretations: Transport Parameter Estimates at the C-Wells

Estimates of transport parameters that can be used directly in solute transport models were derived from the best-fitting model parameters associated with the model fits shown in Figures 6.3-2 and 6.3-3, as well as from other model fits discussed in Appendix D. The parameter estimates associated with the fits of Figures 6.3-2 and 6.3-3 are presented in Table 6.3-3 as ranges of values consistent with the tracer test interpretation(s). Additional discussion of these ranges and how they were derived is provided in Appendix D. Transport parameter estimates obtained from other tracer tests were generally consistent with the ranges presented in Table 6.3-3 when differences in assumptions regarding tracer residence times in injection intervals were accounted for (Appendix D5.2).

Table 6.3-3. Transport Parameter Estimates Deduced from the Lower Bullfrog and Prow Pass Multiple-Tracer Tests

Parameter	Prow Pass		Bullfrog	
	Lower Bound	Upper Bound	Lower Bound	Upper Bound
Effective flow porosity (Appendix D, Section D4.8.5, Eq. D-6,)	0.003	0.006	0.003[a]	0.031[a]
Longitudinal dispersivity, m[b]	13.0	61.5	3.2	62.5
MTC, $\frac{\phi}{b}\sqrt{D_m}$, for radionuclides ($s^{-1/2}$)[c]	0.00054	0.00095	0.00027	0.0015
Fracture aperture (cm)	0.18	1.05	0.081	1.31
Fracture spacing (cm)	6.4	∞	4.4	∞
Ratio of stagnant to flowing water volumes	3.1	∞	2.1	∞
Colloid filtration rate constant (1/hr)[d]	0.043	0.2	0.04	0.175
Colloid detachment rate constant (1/cm-hr)[d]	0.00015	0.00025	0.0002	1.08

Output DTNs: LA0303PR831231.003, LA0303PR831231.005.

NOTE: These values above are provided as ranges of values; see Appendix D for explanations.

[a] These estimates assume that 75% of the production flow was associated with flow pathways that resulted in the first tracer peak and 25% was associated with the second tracer peak (based on flow survey information (DTN: GS931008312313.016 [DIRS 148173] – qualified for use in Appendix L).

[b] Lower bounds assume Peclet numbers for radial flow and 30-m travel distance; upper bounds assume Peclet numbers for linear flow and interval thicknesses as travel distances (see Table 6.1-1 for actual borehole separations and interval thicknesses.

[c] MTC is the matrix diffusion mass transfer coefficient. It is assumed that bromide and pentafluorobenzoate effectively bound molecular sizes and diffusion coefficients of radionuclide solution species.

[d] Based on interpretations of polystyrene microsphere breakthrough curves; see Appendix D for details.

6.3.6 Laboratory Testing to Support C-Wells Field Tracer Tests

An additional objective of tracer testing at the C-wells complex was to assess the applicability of laboratory-derived tracer transport parameters to field-scale transport predictions. This objective is important because radionuclides cannot be tested in the field, so favorable comparisons of laboratory- and field-scale transport of nonradioactive tracers can lend credibility to the practice of using laboratory-derived radionuclide transport parameters in field-scale predictive simulations. Much of this laboratory testing focused on the sorption characteristics and reactive transport behavior of lithium ion. Comparison of lithium sorption behavior at laboratory and field scales was considered especially important because the TSPA relies heavily on radionuclide sorption parameters determined from laboratory experiments to predict field-scale reactive transport behavior in the saturated zone.

The laboratory experiments also provided information useful in constraining the interpretations of the field tracer tests (e.g., direct estimates of matrix diffusion coefficients), and they provided valuable insights into the scaling behavior of transport processes and parameters in the saturated volcanic tuffs. Laboratory testing conducted in support of C-wells tracer testing included:

- Batch sorption tests to determine lithium sorption parameters associated with various C-wells lithologies (Section E1)

made that the fits are equally plausible. Figure 6.3-5 shows the fits to the iodide and 2,4,5-TFBA data from the Prow Pass tracer test that had the lowest and highest optimized sum-of-squares differences (with the highest still being within a factor of 1.5 of the lowest).

Although there are significant uncertainties in the parameter estimates of Table 6.3-6, the uncertainties are far smaller than when there is only a single tracer breakthrough curve to interpret (i.e., Table 6.3-5). For this reason, transport parameter estimates from multiple-tracer tests should be given more weight in the development of transport parameter distributions than parameter estimates from single-tracer tests. Additional discussion of this examination of nonuniqueness of test interpretations is provided in Appendix D5.3.

The transport parameter ranges of Tables 6.3-3 and 6.3-6, while not necessarily rigorously quantified, are considered to be very effectively captured in the parameter uncertainty distributions specified in *Saturated Zone Flow and Transport Model Abstraction* (SNL 2007 [DIRS 181650]). These transport parameter uncertainty distributions, which are ultimately propagated forward in TSPA, consistently encompass the ranges of estimates in Tables 6.3-3 and 6.3-6. The distributions even tend to be skewed such that the ranges obtained from saturated zone tracer testing often fall in the non-conservative ends of the distributions. For example, the flow porosity estimates of Table 6.3-3 are significantly higher than the lower limit obtained from the distributions of flowing interval spacing and fracture aperture, two parameters that combine to define the effective flow porosity in fractured tuffs in *Saturated Zone Flow and Transport Model Abstraction* (SNL 2007 [DIRS 181650]). Thus, the uncertainties inherent in transport parameter estimates obtained from tracer testing are typically propagated forward in TSPA in a conservative manner.

Table 6.3-5. Transport Parameters Obtained from RELAP Fits to Iodide Data Shown in Figure 6.3-4

Parameter	Fit 1	Fit 2	Fit 3
Mass Fraction	0.23	0.11	0.24
Mean Res. Time, τ, hr (linear flow)	50	700	9,000
Peclet number, *Pe* (linear flow)	17	1.3	0.1
Iodide MTC, $\frac{\phi}{b}\sqrt{D_m}$, $sec^{-1/2}$	0.01	0.0	0.0001

Output DTN: LA0304PR831231.001.

Table 6.3-6. Transport Parameter Ranges from Multiple-Tracer Tests at the C-Wells

Parameter	BF(Peak 1)	BF (Peak 2)	PP (I-TFBA)	PP (Br-PFBA)
Mass Fraction	0.11 to 0.13	0.56 to 0.7	0.17 to 0.3	0.56 to 0.82
Mean Res. Time, τ, hr (linear flow)	320 to 420	700 to 1,800	340 to 1,340	600 to 1,900
Peclet number, *Pe* (linear flow)	5 to 8	0.9 to 2.4	0.6 to 2.6	0.6 to 1.9
Halide MTC, $\frac{\phi}{b}\sqrt{D_m}$, $sec^{-1/2}$	0.000837 to 0.00224	0.000245 to 0.000775	0.000775 to 0.00122	0.000632 to 0.00122

Output DTN: LA0304PR831231.001.

BF=Bullfrog; PFBA=pentafluorobenzoic acid; PP=Prow Pass; TFBA= trifluorobenzoic acid.

hydraulic conductivity assumes an interval thickness of 133 m, which is the total thickness of the saturated alluvium from the water table to the bottom of the deepest screen completed in the alluvium in NC-EWDP-19D. Vertical transmissivity and hydraulic conductivity were not estimated from the test results because the cross-hole hydraulic response conformed to that of a confined aquifer (i.e., no vertical flow) rather than an unconfined aquifer.

Hydraulic parameter estimates from most of the interpretive analyses of the Site 22 hydraulic test data are summarized in Table 6.4-3. The definitions of the parameters are provided at the bottom of this table, and they are also depicted in Figure 6.4-2. In general, the interpretations indicate that the upper ~90 m of saturated alluvium at this location has a horizontal hydraulic conductivity of ~11 to 14 m/day and a vertical anisotropy ratio (K_h/K_z) of about 1.5 to 2. The lower ~75 m of saturated alluvium at this location has a considerably lower horizontal hydraulic conductivity (3.7 m/day for zone 3) and a vertical anisotropy ratio of 12 to 30. Test interval 3 is effectively confined by alluvium layers of low vertical hydraulic conductivity above and below (although the confinement from below could be provided by the top of the underlying volcanic breccia unit). The horizontal hydraulic conductivity of the volcanic breccia underlying the alluvium at Site 22 is about 10 to 11 m/day, which is comparable to that of the upper alluvium.

A short-duration cross-hole pumping test at NC-EWDP-10S (located along Fortymile Wash about 2 miles north–northeast of Site 22 and using borehole 10P as an observation well) indicated a horizontal hydraulic conductivity in the single alluvium zone at this location of about 3 m/day (Swanson 2006 [DIRS 179627]), which is comparable to the horizontal conductivity deduced at both the ATC and in the deepest alluvium zone at Site 22. This test was not analyzed by project staff, so it is not discussed elsewhere in this analysis report.

The entire saturated alluvium section at Site 22 has a composite horizontal hydraulic conductivity of about 5 m/day with a vertical anisotropy ratio of ~13. This composite horizontal hydraulic conductivity is taken to be $K_h = \sum_{i=1,3.5} \frac{K_{hi} b_i}{b_{Total}}$ (Freeze and Cherry 1979 [DIRS 101173], p. 34), where K_{hi} = horizontal hydraulic conductivity of layer i, b_i = thickness of layer i, and I = 1,3.5 indicates that the layers considered are from the top of test zone 1 to the bottom of the confining layer between zones 3 and 4 at Site 22. Similarly, the composite vertical hydraulic conductivity used to estimate the vertical anisotropy ratio is taken to be $K_v = \sum_{i=1,3.5} \frac{b_{Total}}{b_i / K_{vi}}$ (Freeze and Cherry 1979 [DIRS 101173], p. 34). The bases for the equations in the two preceding sentences are discussed in Section F7 of Appendix F. The composite estimates assume that horizontal hydraulic conductivities in the layers between test zones are the same as the estimated vertical hydraulic conductivities of these layers and that the vertical conductivities within the test zones are the same as the estimated horizontal conductivities of these zones (i.e., isotropy is assumed within each layer). These assumptions likely result in underestimation of the composite horizontal hydraulic conductivity and possibly also underestimation of the composite vertical anisotropy ratio because there is likely some vertical anisotropy within each layer. Nevertheless, if the alluvium is lumped as one continuous unit in the SZ flow model, these composite parameter estimates are appropriate values to compare with parameters obtained from calibration of the site-scale flow model (at the Site 22 location). Alternatively, one might consider a conductivity of ~12 to 13 m/day (the largest horizontal conductivity measured in any

Table 6.5-3. Tracer Characteristics, Injection Masses, Injection Concentrations, and Fractional Recoveries in the Two Cross-Hole Tracer Tests at Site 22

Parameter	2,4,5 TFBA	Bromide	Lithium	2,6 DFBA
Solute Tracers – Test 1 [a]				
Free water diffusion coefficient at infinite dilution, D_f (cm^2/s)	7.2×10^{-6} [b]	2.1×10^{-5} [c]	1.0×10^{-5} [c]	7.5×10^{-6} [b]
Expected Sorption	None	None	Weak (ion exchange)	None
Target and directly measured injection mass (kg)	8.500	23.002	18.457 [d]	8.500
Injection mass based on measured injection concentration and volume (kg)	8.232	21.504	18.060	8.116
Approximate injection volume (L)	1,000	1,000	1,000	1,000
Tracer fractional recovery [e]	0.93 to 0.96 (0.06)	0.78 to 0.84 (0.03)	0.092	0.91 (0.14)

CML Microsphere Tracers – Test 1 [f]	
Parameter	**0.2-μm CML microspheres (yellow)**
Calculated free water diffusion coefficient, (cm^2/s)	2.15×10^{-8} [g]
Number of spheres injected	4.65×10^{14}
Injection concentration (number/L)	4.65×10^{11}
Approximate injection volume (L)	1000
Tracer fractional recovery	0.011

Solute Tracers – Test 2		
Parameter	**Iodide**	**Perrhenate**
Free water diffusion coefficient at infinite dilution, D_f (cm^2/s)	2.1×10^{-5} [c]	1.46×10^{-5} [h]
Expected Sorption	None	None or very weak
Target and directly measured injection mass (g)	4,233.13	68.123
Injection mass based on measured injection concentration and volume (g)	3,375.77	59.740
Approximate injection volume (L)	1,000	1,000
Tracer fractional recovery	0.78	0.84

Sources: DTNs:LA0612PR831231.003 [DIRS 178736] (Test 1 solutes), LA0612PR831231.004 [DIRS 178738] (Test 2), LA0612PR831231.005 [DIRS 178739] (Test 1 microspheres).

CML=carboxylate-modified latex; TFBA=trifluorobenzoic acid or trifluorobenzoate; DFBA=difluorobenzoic acid or difluorobenzoate.

[a] 2,5 DFBA was also injected into the uppermost screen of 22PA, but it was never detected in 22S, so it is not listed here.

[b] Benson and Bowman 1994 [DIRS 122788], p. 1125; 1996 [DIRS 153427].

[c] Newman 1973 [DIRS 148719], p. 230, Table 75-1; based on ionic conductances at infinite dilution.

[d] Lithium was injected as 25.0 kg LiBr, 97.0 kg LiCl and 1.99 kg LiOH.

[e] Ranges for TFBA and bromide reflect uncertainty in mass-based vs. concentration-based normalizations. (see Appendix G, Section G5.1, for discussion of these normalizations). Numbers in parentheses indicate the recovery that occurred during the second cross-hole tracer test, which is included in the totals. Lithium concentrations were not measured during the second cross-hole test.

[f] The microsphere injection was initiated 10 days after the solute tracers were injected.

[g] Calculated using Stokes-Einstein equation (Bird et al. 1960 [DIRS 103524]).

[h] Lide 2006 [DIRS 178081].

i.e., travel time = L/(KΔH/L)/η , where L = distance, K = hydraulic conductivity, ΔH = head or drawdown difference, and η = flow porosity, = 20 m / (12 m/day × (0.1/20) m/m / 0.1 = ~33 days. Given the observed horizontal tracer travel time of less than 10 days between wells 22PA and 22S, one would expect the 2,5 DFBA arrival time at 22S to be no more than about 30 + 10 = 40 days in a homogeneous, isotropic system. The fact that there was no 2,5 DFBA arrival at 22S in over 60 days of pumping (and also no arrival in another ~45 days of pumping during the second cross-hole tracer test) indicates that the flow system must have a lower effective vertical hydraulic conductivity relative to horizontal hydraulic conductivity. If the vertical travel distance were 20 m (the distance from the bottom of zone 1 to the top of zone 2), a lower bound estimate of the horizontal-to-vertical hydraulic conductivity ratio would be about 3:1 based on the fact that there was no arrival in over 100 days of pumping. However, if the vertical travel distance were greater than the minimum distance of 20 m, then the lower bound estimate of the conductivity ratio would be smaller. Also, the possibility that the 2,5 DFBA arrived at 22S in concentrations too low to detect cannot be discounted given that the 2,5 DFBA injection mass was only about 18% of the injection mass of the 2,4,5 TFBA and 2,6 DFBA and that peak tracer concentrations tend to decrease approximately as 1/travel time.

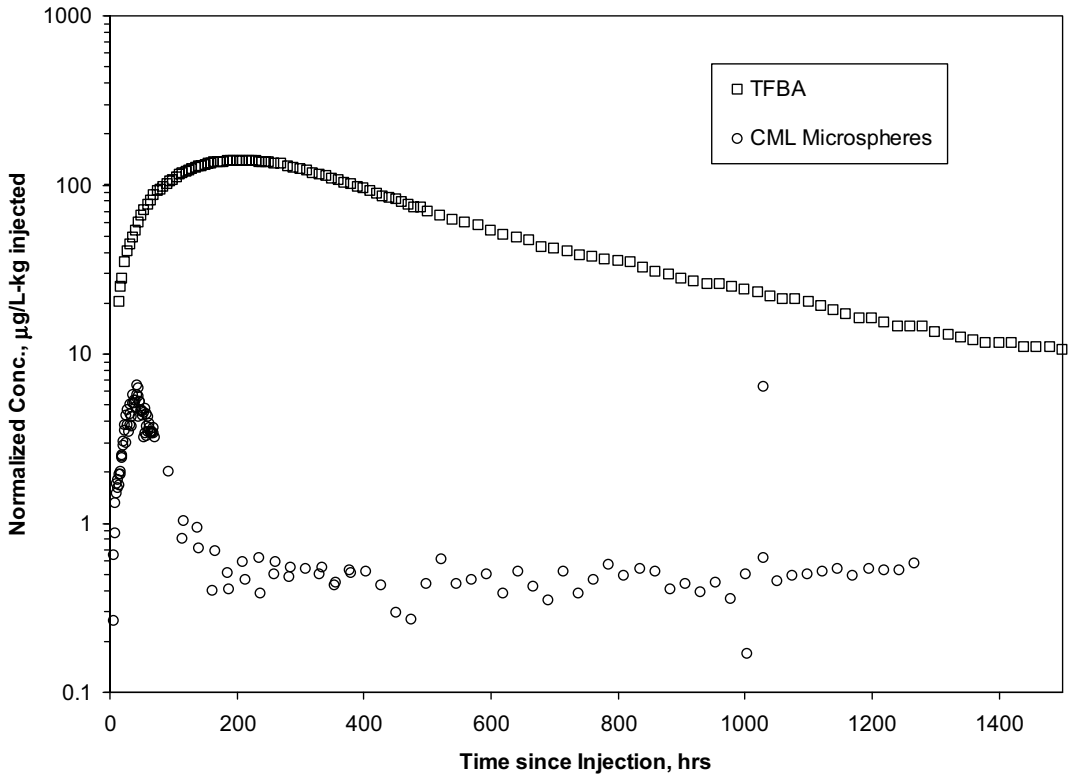

DTN: LA0612PR831231.005 [DIRS 178739] (microspheres); LA0612PR831231.003 [DIRS 178736] (TFBA) .

NOTE: Note the log normalized concentration scale. The very high microsphere data point at about 1,050 hours was reanalyzed and verified to be valid; this high concentration may have been the result of an undocumented flow perturbation.

Figure 6.5-6. Mass-Based Normalized Breakthrough Curves of 2,4,5 TFBA and CML Microspheres in the First Cross-Hole Tracer Test at Site 22

6.5.5 Tracer Test Interpretations: Estimates of Ambient Flow Velocity in Alluvium

Four methods were used to obtain groundwater velocity estimates from the single-well tracer tests at the ATC, and three of these were also used to estimate groundwater velocities from single-well tracer tests at Site 22. The three methods used at both locations involved relatively simple spreadsheet calculations that, given various simplifying assumptions, solve for groundwater velocities consistent with the observed differences in the following:

1. Peak tracer concentration arrival times

2. "Late" tracer arrival times, defined as the times in each test when the fractional tracer mass recovery was equal to the final recovery in the test having the lowest overall mass recovery.

3. "Mean" arrival times of tracer mass recovered at the same arbitrarily selected high fractional recovery in each test.

Note that these three times also correspond to volumes pumped, and the latter can provide a more meaningful basis of comparison between tests when pumping rates vary in different tests. The peak, late, and mean arrival times (and corresponding volumes) for each test are listed in Table 6.5-4. The points on the tracer breakthrough curves corresponding to the mean and late arrival times in each test are identified in the right-hand plots of Figures 6.5-2 and 6.5-4.

The fourth method of estimating ambient groundwater velocity, which was applied only to the ATC tracer test data, involved detailed analytical calculations of tracer migration during the tests by linking together solute transport solutions for the injection, rest, and pumping phases that assume a two-dimensional homogeneous and isotropic aquifer. This method also provided estimates of effective flow porosity and longitudinal dispersivity in the alluvium, although these estimates are not well constrained.

The details of the calculations associated with four estimation methods are provided in Appendix G. Table 6.5-5 lists the results obtained for both the groundwater velocity, v_{GW}, and the specific discharge, v_S (= $\eta\, v_{GW}$), as a function of assumed flow porosity (η) by all four methods of estimation for the ATC. Table 6.5-6 lists the same estimates obtained from the first three methods for Site 22. Of the first three methods, the peak analysis method offers the smallest estimates, and the analysis of late-arriving mass (high recovery) offers the largest estimate at both locations. The range of the estimates from the three methods used at both sites spans about a factor of three for a given assumed value of flow porosity. The velocity estimate from the linked analytical solutions is in good agreement with the peak analysis method at the ATC.

An additional estimate of ambient flow velocity at Site 22 was obtained by analyzing the responses of nonsorbing tracers in 22S after a 159-day stoppage of flow between the two cross-hole tracer tests that were conducted at this location. This analysis, which is described in detail in Section G5.3, yielded a seepage velocity estimate of 9.25 m/yr. The corresponding specific discharge estimates for different assumed flow porosities are listed at the bottom of Table 6.5-6.

Table 6.5-4. Times and Pumped Volumes Associated with Each of the Single-Well Tracer Test Arrival Times Used in the Different Methods of Estimating Groundwater Velocities

	Arrival Time (hr)/Volume (L [gal])		
19D Rest Period:	**0.5 hr**	**2 days**	**30 days**
Peak arrival	24 / 76,000 [20,000]	30.5 / 76,000 [20,000]	12.2 / 38,600 [10,200]
Late arrival [a]	168 / 511,000 [135,000]	225 / 556,000 [147,000]	639 / 1,780,000 [471,000]
Mean arrival [b]	52 / 161,000 [42,500]	71 / 178,000 [46,500]	109 / 344,000 [91,000]
Alternate mean arrival [c]	61.5 / 189,000 [50,000]	81 / 201,000 [53,000]	149 / 469,000 [124,000]
22S Rest Period:	**3 days**	**30 days**	
Peak arrival	5.6 / 60,000 [15,900]	3.8 / 41,000 [10,800]	
Late arrival [d]	57 / 611,000 [161,400]	169 / 1,820,000 [481,700]	
Mean arrival [e]	12.6 / 135,000 [35,700]	20.9 / 225,500 [59,600]	

Sources: DTNs:UN0109SPA008IF.006 [DIRS 162442] (19D, 0.5 hr); UN0102SPA008KS.003 [DIRS 162614] (19D, 2 days); UN0109SPA008KS.007 [DIRS 162615] (19D, 30 days); LA0612PR831231.001 (22S, 3 days) [DIRS 178733]; LA0612PR831231.002 (22S, 30 days) [DIRS 178735].

Output DTNs: LA0303PR831231.002 (19D); LA0701PR150304.001 (22S).

[a] Time/volume associated with approximately 86.4% mass recovery in each test at 19D (the final recovery in the 0.5-hr rest period test, which had the lowest final recovery of any test).

[b] Mean arrival time calculated by truncating all tracer response curves at approximately 86.4% recovery in each test.

[c] Alternate mean arrival time calculated by extrapolating the tracer response curves in the 0.5-hr rest period test to 91.3% and truncating the response curves in the 2-day rest period test to 91.3% recovery (the final recovery in the 30-day rest period test).

[d] Time/volume associated with approximately 96.7% mass recovery in each test at 22S.

[e] Mean arrival time calculated by truncating all tracer response curves at 96.7% recovery in each test at 22S.

Table 6.5-5. Groundwater Specific Discharges and Seepage Velocities Estimated from the Different Ambient Flow Velocity Analysis Methods as a Function of Assumed Flow Porosity at 19D

	Specific Discharge (m/yr) / Seepage Velocity (m/yr)		
Assumed Flow Porosity[a]	**0.05**	**0.18**	**0.3**
Peak Arrival Analysis	1.2 / 24.5	2.4 / 13.1	3.0 / 9.9
Late Arrival Analysis [b]	3.9 / 77.1	7.3 / 40.4	9.4 / 31.3
Mean Arrival Analysis [c]	2.0 / 40.3	3.8 / 20.9	4.9 / 16.4
Mean Arrival Analysis [d]	2.5 / 49.1	4.6 / 25.8	6.0 / 20.2
Linked Analytical Solutions	1.5 / 15 with a flow porosity of 0.10 and a longitudinal dispersivity of 5 m.		

Output DTN: LA0303PR831231.002.

[a] The three values are approximately the lowest, expected, and highest values of the alluvium flow porosity used in the *SZ Flow and Transport Model Abstraction* (SNL 2007 [DIRS 181650]).

[b] Time/Volume associated with approximately 86.4% recovery in each test (the final recovery in the 0.5-hr rest period test, which had the lowest final recovery of any test).

[c] Mean arrival time calculated by truncating all tracer response curves at approximately 86.4% recovery in each test.

[d] Alternative mean arrival time calculated by extrapolating the tracer response curves in the 0.5-hr rest period test to 91.3% and truncating the response curves in the 2-day rest-period test to 91.3% recovery (the final recovery in the 30-day rest-period test).

Table 6.5-6. Groundwater Specific Discharges and Seepage Velocities at 22S Estimated from Different Drift Analysis Methods as a Function of Assumed Flow Porosity

	Specific Discharge (m/yr) / Seepage Velocity (m/yr)		
Assumed Flow Porosity[a]	**0.05**	**0.18**	**0.3**
Single-Well Peak Arrival Analysis	0.47 / 9.5	0.89 / 5.0	1.2 / 3.9
Single-Well Late Arrival Analysis[b]	2.2 / 43.8	4.2 / 23.1	5.4 / 17.9
Single-Well Mean Arrival Analysis[c]	0.82 / 16.4	1.6 / 8.6	2.0 / 6.7
Analysis of Cross-Hole Tracer Responses after 159-day Flow Interruption	0.46 / 9.25	1.7 / 9.25	2.8 / 9.25

Output DTNs: LA0701PR150304.001 (single-well tests); LA0701PR150304.004 (cross-hole test).

[a] The three values are approximately the lowest, expected, and highest values of the alluvium flow porosity used in *SZ Flow and Transport Model Abstraction* (SNL 2007 [DIRS 181650]).

[b] Time/Volume associated with approximately 96.7% recovery in each test.

[c] Mean arrival time calculated by truncating the two tracer response curves at 96.7% recovery in each test.

6.5.5 Tracer Test Interpretations: Conceptual Transport Model Implications

As with the C-wells tracer tests, the alluvium tracer tests at Site 22 were interpreted using a combination of the RELAP V2.0 (STN: 10551-2.0-00 [DIRS 159065]) and MULTRAN V 1.0 (STN: 10666-1.0-00 [DIRS 159068]) computer codes. The single-well tracer tests were interpreted using MULTRAN, and the cross-hole tracer tests were interpreted using RELAP. The MULTRAN interpretations of the single-well tracer tests were conducted to estimate parameters describing diffusion between flowing and stagnant water in the alluvial flow system. Figure 6.5-8 shows simultaneous MULTRAN fits to the tracer test responses in the two single-well tests at Site 22 using the same diffusive mass transfer parameters for each test. The single-well tests at the ATC were not quantitatively interpreted because they showed no evidence of dual-porosity behavior, so test interpretations were limited to the ambient flow velocity estimates discussed in the previous section. The RELAP interpretations of the Site 22 cross-hole tests were conducted to provide estimates of diffusion parameters, flow porosities, flow anisotropy, colloid (microsphere) filtration and detachment parameters, and retardation/sorption parameters for lithium and perrhenate in the alluvium. Details of the analyses are provided in Section G5.

The cross-hole tracer responses between 22PA and 22S were interpreted assuming multiple flow pathways contributed to the observed breakthrough curves. This assumption was supported by inflections in the time derivatives of the nonsorbing tracer breakthrough curves (see Figure G-41) and by the inability to fit the early portion of the breakthrough curves assuming a single flow pathway. Figure 6.5-9 shows a simultaneous multi-pathway RELAP fit to the nonsorbing tracer responses between 22PA and 22S in the first cross-hole tracer test. Figure 6.5-10 shows a simultaneous RELAP fit to the iodide and perrhenate responses in the second tracer test. The two flow pathways providing good fits to the responses in the second test corresponded very closely to the first two pathways in the first tracer test, suggesting that the third pathway was not accessed by tracers in the second test. It is suspected that the third pathway was activated in the first test but not in the second test because of the very high density of the tracer solution in the first test (specific gravity of greater than 1.12).

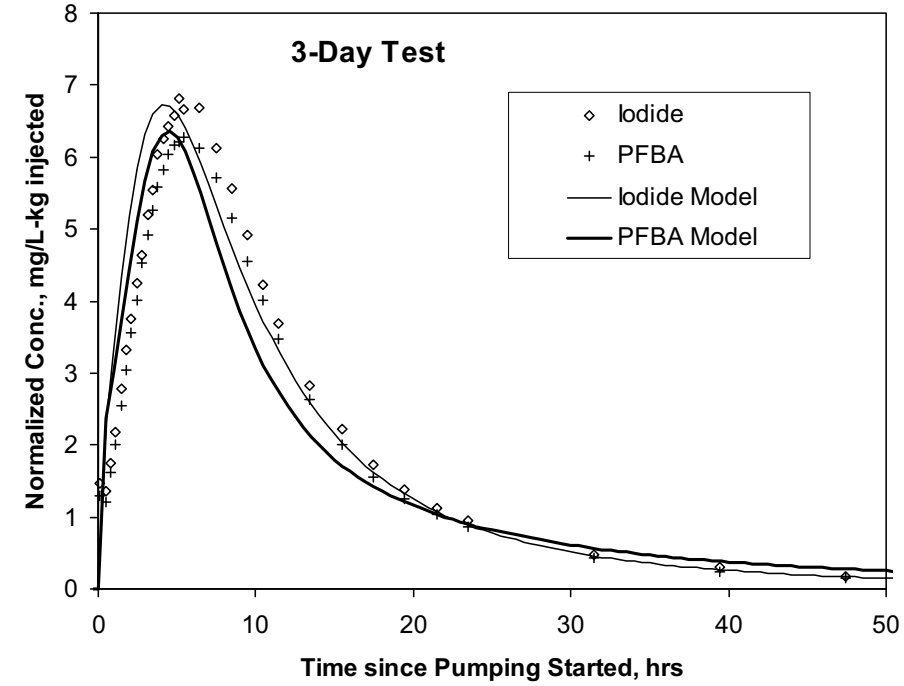

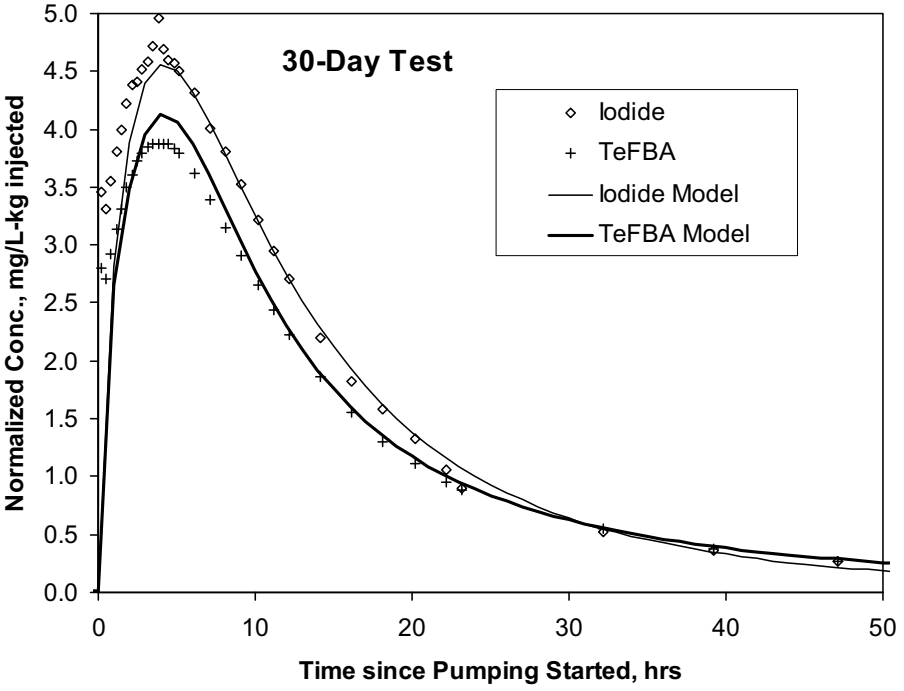

Sources: DTNs: LA0612PR831231.001 [DIRS 178733] (3-day test data), LA0612PR831231.002 [DIRS 178735] (30-day test data), and LA0701PR150304.007 (output).

NOTE: Details of the fitting procedure are provided in Appendix G, and model parameters are listed in Table G-11.

Figure 6.5-8. MULTRAN Model Matches to the 22S Single-Well Tracer Test Breakthrough Curves

The large contrast in density between the tracer solution and the groundwater probably resulted in density-driven flow in the vicinity of the injection wellbore that did not occur in the second test.

This density-driven flow likely caused some of the tracer solution to "sink" into pathways that were not accessed in the second test. RELAP fits to the lithium and microsphere responses between 22PA and 22S and to the 2,6 DFBA response between 22PC and 22S in the first cross-hole test are presented and discussed in Section G5 of Appendix G. The microsphere filtration and detachment parameters deduced from RELAP are listed in Table 6.5-7. The deduced retardation factors and partition coefficients (K_d values) for lithium are discussed and compared with laboratory-derived K_d estimates in Section G5.4.3. The conclusion from this comparison is that the laboratory K_d values would probably result in underestimation of field-scale sorption/retardation in the alluvium if used in large-scale predictive transport models.

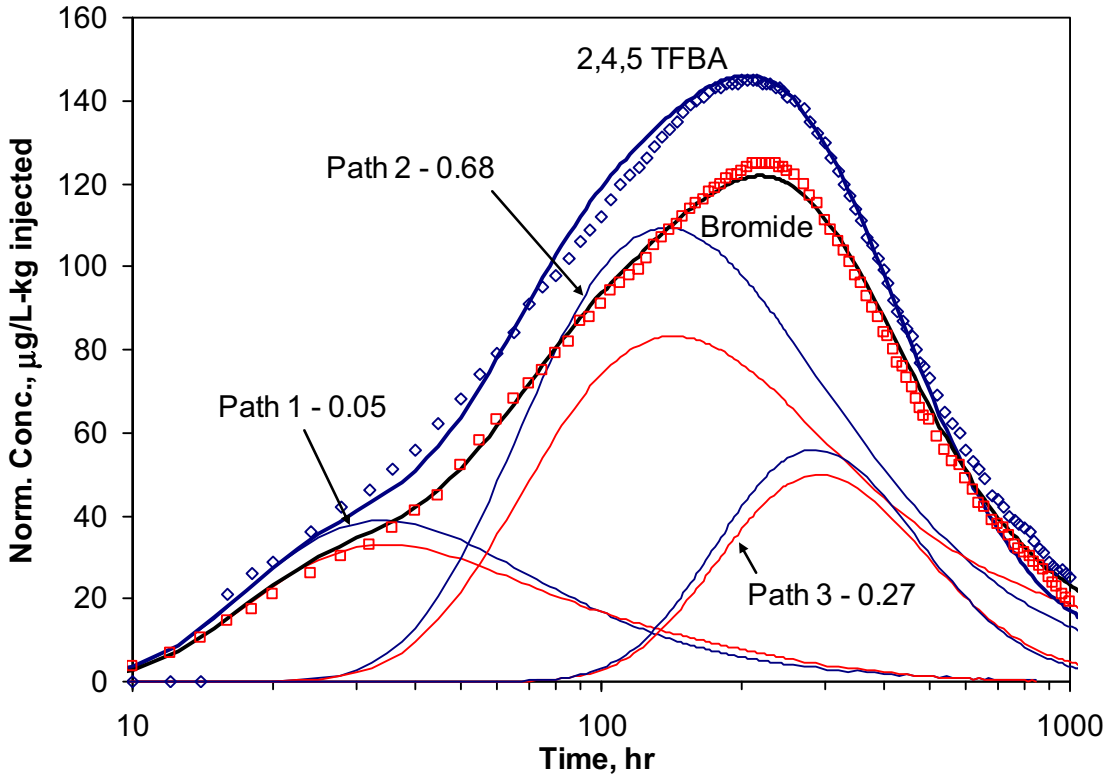

Output DTN: LA0701PR150304.006.

NOTE: These normalizations yield the maximum possible difference between the TFBA and bromide breakthrough curves – as opposed to the minimum possible differences in Figure 6.5-5. The tracer mass fractions in each pathway are indicated on the plot. All pathways have dual-porosity behavior. The bold black curves are the sums of the three individual model pathway curves. Model parameters are listed in Table G-15. The simulated tracer responses associated with the individual pathways are indicated by the thin colored lines.

Figure 6.5-9. Composite Three-Pathway RELAP Fits to the First 1,000 Hours of the 2,4,5 TFBA (Concentration-Based Normalizations) and Bromide (mass-based normalization) Breakthrough Curves at Site 22

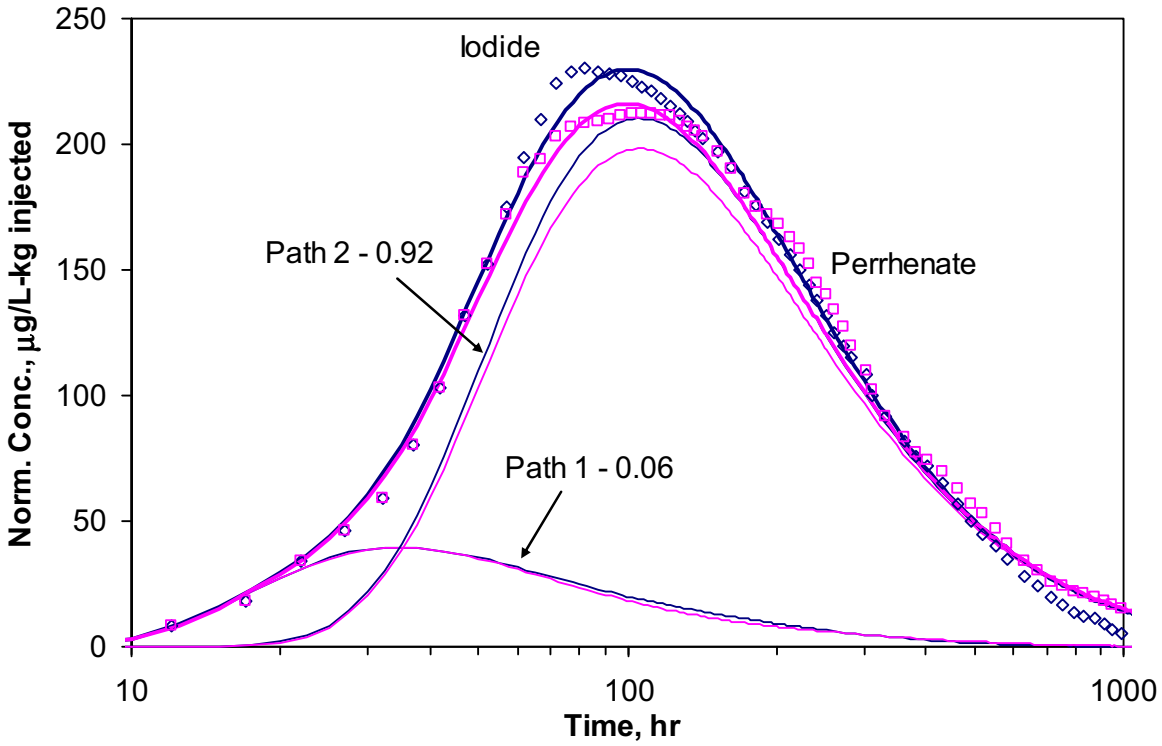

Output DTN: LA0701PR150304.003.

NOTE: The bold curves are the sum of the two individual model pathway curves. Model parameters are listed in Table G-18 of Appendix G.

Figure 6.5-10. Two-Pathway RELAP Fits to the Iodide and Perrhenate (mass-based normalization) Breakthrough Curves in the Second Cross-Hole Tracer Test at Site 22

Although there was no apparent diffusion between flowing and stagnant water in the single-well tracer tests at the ATC, the single-well and cross-hole tracer test results and interpretations at Site 22 collectively indicate dual-porosity transport behavior in the alluvium at this location. However, the diffusion time and length scales are relatively short compared to those of the fractured volcanics, and an important conclusion is that, over the time and distance scales of importance for performance assessment calculations, the tracer test interpretations suggest that the alluvium will behave as a single-porosity transport system with an effective porosity equal to the sum of the flowing and stagnant porosities deduced from the tracer tests. The short diffusion time and distance scales are more consistent with a diffusion-into-grains (or blocks) conceptual model than a diffusion-into-layers conceptual model. However, longer diffusion time scales cannot be ruled out in the alluvium because of the short time and distance scales of the tracer tests relative to performance assessment time scales. It is possible that the tests were strongly influenced by diffusion into grains within flow pathways, but the flow pathways were large enough in thickness or diameter (i.e., channels) that longer-time-scale diffusion into stagnant water surrounding the pathways was not observed. Estimates of transport parameters that can be used directly in solute transport models derived from the best-fitting model parameters associated with the MULTRAN and RELAP model fits are listed in Table 6.5-8. Additional discussion of these ranges and how they were derived is provided in Appendix G.

the lithium transport behavior are both consistent with dual-porosity transport regardless of the uncertainties in the normalizations of the tracer breakthrough curves.

Another uncertainty associated with the alluvium tracer test interpretations is the inherent and unquantifiable uncertainty associated with the conclusion that diffusion time and distance scales are quite small and that the alluvium should therefore behave as a single-porosity transport system over much larger time and distance scales than the tracer tests. The possibility exists that the time and distance scales of the tracer tests may have been too short to observe significant diffusion out of flowing pathways and into relatively extensive layers or grains of stagnant or near-stagnant alluvium in the flow system. Furthermore, the uncertainties associated with the tracer injection masses (above) make any assessment of larger diffusion time and length scales essentially impossible using the available data from Site 22. However, it should be noted that the mass-fraction-weighted sum of the flowing and stagnant porosities from the two pathways between 22PA and 22S in the second cross-hole tracer test (the test without density-driven flow issues) is slightly greater than 0.2, which is probably quite close to the total porosity of the alluvium (considered to have a maximum value of around 0.3). Thus, while we cannot rule out the possibility of longer diffusion time and distance scales in the alluvium than the tracer tests indicated, the tracer test interpretations are consistent with tracers accessing the majority of the total porosity in the flow system.

- Section 7.4 lists specific locations in Section 6 and in the appendices where the reader can find discussions of uncertainties associated with hydrologic and transport parameters derived from SZ in situ testing. These uncertainties are incorporated into probability distributions for parameters documented primarily in *SZ Flow and Transport Model Abstraction* (SNL 2007 [DIRS 181650]).

The SZ included FEPs supported by this scientific analysis are listed in Section 6.1.2 of this report, which also indicates where in the report the FEPs are addressed.

The specific acceptance criteria that relate to this report are discussed in Section 4.2.

7.2 APPLICABLE ACCEPTANCE CRITERIA

The following information describes how this analysis addresses the acceptance criteria in *Yucca Mountain Review Plan, Final Report* (NRC 2003 [DIRS 163274], Sections 2.2.1.3.8.3 and 2.2.1.3.9.3). Only those acceptance criteria applicable to this report (Section 4.2) are discussed. In most cases, the applicable acceptance criteria are not addressed solely by this report; rather, the acceptance criteria are fully addressed when this report is considered in conjunction with other analysis and model reports that describe flow and transport in the saturated zone.

7.2.1 Acceptance Criteria from Section 2.2.1.3.8.3, *Flow Paths in the Saturated Zone*

Acceptance Criterion 1: ***System Description and Model Integration Are Adequate***

- **Subcriterion (2)**—Sections 6.2 and 6.4 (and Appendices C and F) adequately describe and identify aspects of hydrology, geology, physical phenomena, and couplings, that may affect flow paths in the saturated zone. Conditions and assumptions supporting the abstraction of flow paths in the saturated zone are readily identified and supported in these two sections. Section 6.2 and Appendix C describe the hydraulic tests conducted and analyses performed on the test data, and extrapolates test results to estimate hydrogeologic properties of the volcanic rocks. Section 6.4 and Appendix F present hydrogeologic properties of the alluvium through interpretation of test results. Volcanic and alluvium hydrogeologic properties affect flow paths in the saturated zone.

- **Subcriterion (3)**—The assumptions, technical bases, data, and models incorporated in this report are appropriate and consistent with those supporting other abstractions because they are derived from tests and experiments directly applicable to the saturated zone at Yucca Mountain as described in Sections 6.2 and 6.4 (and Appendices C and F). Descriptions and technical bases provided in Sections 6.2 and 6.4, and in Appendices C and F) are transparent and traceable (Section 4.1 for data references) for items that support the total system performance assessment and abstraction for flow paths in the saturated zone.

- **Subcriterion (10)**—This document has been developed under *Quality Assurance Requirements and Description* (QARD) (DOE 2006 [DIRS 177092]).

Acceptance Criterion 4: ***Model Uncertainty Is Characterized and Propagated Through the Model Abstraction***

- **Subcriterion (1)**—Alternative modeling approaches of features, events, and processes are considered in Sections 6.3 and 6.5 (and in Appendices D and G) and are consistent with available data and current scientific understanding, and the results and limitations are appropriately considered in the abstraction. Appendix D Sections D3, D5, and Appendix G, Section G1 particularly, discuss conceptual models considered and justify the selection of the appropriate models.

- **Subcriterion (2)**—Conceptual model uncertainties are adequately defined and documented, and effects on conclusions regarding performance are properly assessed in Sections 6.3.7, 6.5.7, Appendices D, Sections D1, D3, D4, D5; E, Sections E2 and E4; G, Sections G3 and G4.

- **Subcriterion (3)**—Consideration of conceptual model uncertainty is consistent with available site characterization data, laboratory experiments, field measurements, and process-level modeling studies shown throughout Sections 6.3 and 6.5 (and Appendices D and G).

- **Subcriterion (4)**—Appropriate alternative modeling approaches discussed in Sections 6.3 and 6.5 and, more specifically, in Appendix D, Sections D3, D5, and Appendix G, Section G1, are consistent with available data and current scientific knowledge, and appropriately consider their results and limitations using tests and analyses that are sensitive to the processes modeled. For example, for radionuclide transport through fractures in volcanic rocks and porous media in alluvium, the report adequately considers alternative modeling approaches to develop its understanding of distributions and ranges of transport properties in the saturated zone.

7.3 OUTPUTS

Table 7-1 lists the output data for this scientific report. The data will be used primarily to support the development of CDFs for various flow and transport parameters used in TSPA simulations. These CDFs are documented in *SZ Flow and Transport Model Abstraction* (SNL 2007 [DIRS 181650]). The horizontal hydraulic conductivity anisotropy ratio described in Section 6.2.6 is used to support flow model calibrations described in *Saturated Zone Site-Scale Flow Model* (SNL 2007 [DIRS 177391]). Also, transport parameters and tracer breakthrough curves from C-wells tracer testing (Sections 6.3 and Appendix D) are used in the model validation section of *Site-Scale Saturated Zone Transport Model* (SNL 2007 [DIRS 177392]) and in the development of colloid transport parameter distributions in *Saturated Zone Colloid Transport* (BSC 2004 [DIRS 170006]).

The steps involved in processing the input data listed in Table 4-1 to arrive at the output data listed in Table 7-1 is often quite involved and is unique to each output DTN. Appendix I lists all the steps associated with this process for Figure C-21 (an example for a hydraulic test interpretation) and for Figure 6.3-3 (an example for a tracer test interpretation). Additionally, Appendix F, section F6, contains a thorough description of the process of interpreting the hydraulic tests at Nye County Site 22. The examples of Appendix I and the description in

Table 7-1. Output Data (Continued)

Data Description	Data Tracking Number	Location of Output DTNs in This Report
C-wells tracer test sensitivity calculations	LA0304PR831231.001	Figures 6.3-4, 6.3-5 and D-31 to D-38 Tables 6.3-5, 6.3-6 and D-13 to D-14

NOTE: ATC=Alluvial Testing Complex; DTN=data tracking number; STN=software tracking number.

7.4 UNCERTAINTIES

Discussions of uncertainties associated with the flow and transport parameters presented in this report can be found in the following sections:

- Hydraulic testing and test interpretations in saturated fractured volcanics at the C-wells are discussed in detail in Section 6.2.7 (also Appendix C, Section C5).
- Anisotropy of horizontal hydraulic conductivity in the fractured volcanics are discussed in Section 6.2.6.
- Tracer testing and test interpretations at the C-wells are discussed in detail in Section 6.3.7 (also Appendix D, Section D5).
- Hydraulic testing and test interpretations in the saturated alluvium at the ATC and Nye County Site 22 are discussed in Section 6.4.6 (also Appendix F, Section F4 for the ATC, and Sections F7 and F8 for general discussion that applies to both locations).
- Tracer testing and test interpretations at the ATC and Nye County Site 22 are summarized in Section 6.5.6 and discussed in detail in Appendix G, Section G4.4 (for groundwater velocity or specific discharge estimates) and in Section G8.

Uncertainty distributions for SZ flow and transport parameters are provided in *SZ Flow and Transport Model Abstraction* (SNL 2007 [DIRS 181650]). The rationale for documenting the uncertainty distributions in the model abstraction report rather than in this scientific analysis is that the distributions are based only in part on the parameters (and their uncertainties) presented in this report. The only exception is that the uncertainty distribution for the north-south and east-west anisotropy ratio of horizontal hydraulic conductivity in the fractured volcanics is derived entirely from the information presented in this scientific analysis (Section 6.2.6 and Appendix C, Section C6).

Literature data, expert elicitation input, and peer review input were considered in the development of parameter distributions because of the limited spatial representation of the SZ offered by the C-wells and alluvium hydraulic and tracer tests. Also, the time and distance scales of the C-wells and alluvium tests were relatively small compared to time and distance scales of performance assessment calculations. One exception is the long-term C-wells hydraulic test that led to the uncertainty distribution for hydraulic conductivity anisotropy ratio over an approximately 21-km^2 area. Thus, the flow and transport parameters derived from the C-wells and alluvium in-situ tests represent only discrete points in continuous distributions of parameter values spatially distributed throughout the SZ, and that potentially have scale dependencies that

would not be revealed by C-wells and alluvium in-situ testing. The parameter uncertainty distributions in *SZ Flow and Transport Model Abstraction* (SNL 2007 [DIRS 181650]) are consistent with and supported by the parameters presented in this report, but they generally consist of a much wider range of potential values because of representativeness and scale of the field tests.

170014 BSC 2004. *Probability Distribution for Flowing Interval Spacing.* ANL-NBS-MD-000003 REV 01. Las Vegas, Nevada: Bechtel SAIC Company. ACC: DOC.20040923.0003.

168361 BSC 2004. *Q-List.* 000-30R-MGR0-00500-000-000 REV 00. Las Vegas, Nevada: Bechtel SAIC Company. ACC: ENG.20040721.0007.

170015 BSC 2004. *Recharge and Lateral Groundwater Flow Boundary Conditions for the Saturated Zone Site-Scale Flow and Transport Model.* ANL-NBS-MD-000010 REV 01. Las Vegas, Nevada: Bechtel SAIC Company. ACC: DOC.20041008.0004.

170006 BSC 2004. *Saturated Zone Colloid Transport.* ANL-NBS-HS-000031 REV 02. Las Vegas, Nevada: Bechtel SAIC Company. ACC: DOC.20041008.0007.

178672 BSC 2006. *Impacts of Solubility and Other Geochemical Processes on Radionuclide Retardation in the Natural System – Rev 01*. Las Vegas, Nevada: Bechtel SAIC Company. ACC: MOL.20060105.0022.

177375 BSC 2006. *Technical Work Plan for Saturated Zone Flow and Transport Modeling*. TWP-NBS-MD-000006 REV 02. Las Vegas, Nevada: Bechtel SAIC Company. ACC: DOC.20060519.0002.

165281 Bussod, G. 2001. LA-EES-1-NBK-98-005, UZ Transport Test Notebook 2. Scientific Notebook SN-LANL-SCI-038-V1. ACC: MOL.20010830.0382.

165123 Callahan, T. 2001. LA-CST-NMTECHA-NBK-96-001, Laboratory Investigation YMP C-Wells Reactive Tracers Test. Scientific Notebook SN-LANL-SCI-028-V1. ACC: MOL.20010830.0385.

156649 Callahan, T.J. 2001. *Laboratory Investigations and Analytical and Numerical Modeling of the Transport of Dissolved Solutes Through Saturated Fractured Rock.* Ph.D. dissertation. Socorro, New Mexico: New Mexico Institute of Mining and Technology. TIC: 251010.

156648 Callahan, T.J.; Reimus, P.W.; Bowman, R.S.; and Haga, M.J. 2000. "Using Multiple Experimental Methods to Determine Fracture/Matrix Interactions and Dispersion of Nonreactive Solutes in Saturated Volcanic Tuff." *Water Resources Research, 36,* (12), 3547-3558. Washington, D.C.: American Geophysical Union. TIC: 250760.

107944 Rush, F.E.; Thordarson, W.; and Bruckheimer, L. 1983. *Geohydrologic and Drill-Hole Data for Test Well USW H-1, Adjacent to Nevada Test Site, Nye County, Nevada*. Open-File Report 83-141. Denver, Colorado: U.S. Geological Survey. ACC: HQS.19880517.1835.

100075 Sawyer, D.A.; Fleck, R.J.; Lanphere, M.A.; Warren, R.G.; Broxton, D.E.; and Hudson, M.R. 1994. "Episodic Caldera Volcanism in the Miocene Southwestern Nevada Volcanic Field: Revised Stratigraphic Framework, $^{40}Ar/^{39}Ar$ Geochronology, and Implications for Magmatism and Extension." *Geological Society of America Bulletin, 106,* (10), 1304-1318. Boulder, Colorado: Geological Society of America. TIC: 222523.

101291 Scott, R.B. and Castellanos, M. 1984. Stratigraphic and Structural Relations of Volcanic Rocks in Drill Holes USW GU-3 and USW G-3, Yucca Mountain, Nye County, Nevada. Open-File Report 84-491. Denver, Colorado: U.S. Geological Survey. ACC: NNA.19870519.0095.

156862 Skagius, K. and Neretnieks, I. 1986. "Porosities and Diffusivities of Some Nonsorbing Species in Crystalline Rocks." *Water Resources Research, 22,* (3), 389-398. Washington, D.C.: American Geophysical Union. TIC: 225291.

174109 SNL (Sandia National Laboratories) 2007. *Hydrogeologic Framework Model for the Saturated Zone Site-Scale Flow and Transport Model.* MDL-NBS-HS-000024 REV 01. Las Vegas, Nevada: Sandia National Laboratories. ACC: DOC.20070411.0003.

177396 SNL 2007. *Radionuclide Transport Models Under Ambient Conditions.* MDL-NBS-HS-000008 REV 03. Las Vegas, Nevada: Sandia National Laboratories.

181650 SNL 2007. *Saturated Zone Flow and Transport Model Abstraction*. MDL-NBS-HS-000021 REV 03 AD 01. Las Vegas, Nevada: Sandia National Laboratories.

177391 SNL 2007. *Saturated Zone Site-Scale Flow Model.* MDL-NBS-HS-000011 REV 03. Las Vegas, Nevada: Sandia National Laboratories.

177392 SNL 2007. *Site-Scale Saturated Zone Transport.* MDL-NBS-HS-000010 REV 03. Las Vegas, Nevada: Sandia National Laboratories.

181006 SNL 2007. *Particle Tracking Model and Abstraction of Transport Processes.* MDL-NBS-HS-000020 REV 02 AD 01. Las Vegas, Nevada: Sandia National Laboratories.

101297 Spengler, R.W.; Byers, F.M., Jr.; and Warner, J.B. 1981. *Stratigraphy and Structure of Volcanic Rocks in Drill Hole USW-G1, Yucca Mountain, Nye County, Nevada*. Open-File Report 81-1349. Denver, Colorado: U.S. Geological Survey. ACC: NNA.19870406.0222.

180315 Spiegel, M. R. 1968. *Mathematical Handbook of Formulas and Tables*. Schuam's Outline Series in Mathematics. New York, New York: McGraw-Hill. On Order

168378 MO0206GSC02074.000. As-Built Survey of Nye County Early Warning Drilling Program (EWDP) Phase III Boreholes, Second Set. Submittal date: 06/03/2002.

161274 MO0212SPANYESJ.149. Nye County Well ONC-1 Temperature and Pressure Data 03/01/1996 through 12/22/1997. Submittal date: 12/09/2002.

165876 MO0306NYE05259.165. Revised NC-EWDP-19IM1 Well Completion Diagram. Submittal date: 07/02/2003.

179376 MO0306NYE05264.170. Revised NC-EWDP-22S Well Completion Diagram. Submittal date: 07/03/2003.

179377 MO0306NYE05265.171. Revised NC-EWDP-22PA Well Completion Diagram. Submittal date: 07/03/2003.

179378 MO0306NYE05266.172. Revised NC-EWDP-22PB Well Completion Diagram. Submittal date: 07/03/2003.

164821 MO0308SPATRCRC.000. Concentration Data for "2,3,4,5-Tetrafluorobenzoic Acid" Used for Tracer Testing at the C-Well Complex. Submittal date: 08/19/2003.

168534 MO0401COV03168.000. Coverage: NCEWDPS. Submittal date: 01/27/2004.

171464 MO0408NYE05474.217. UE-25 ONC#1 Pressure and Temperature Data, April 1995 - November 1999. Submittal date: 08/30/2004.

177373 MO0411NYE06360.302. EWDP Manual Water Level Measurements through June 2004. Submittal date: 11/08/2004.

175275 MO0503GSC05025.000. As-Built Location of Nye County Early Warning Drilling Program (EWDP) Phase V Borehole Number NC-EWDP-22PC. Submittal date: 03/10/2005.

179599 MO0505NYE06464.314. NC-EWDP-22PC Well Completion Diagram. Submittal date: 05/16/2005.

181613 MO0706SPAFEPLA.001. FY 2007 LA FEP List and Screening. Submittal date: 06/20/2007.

180070 MO0703U25CHPTL.000. Borehole U-25 C-Hole Complex Packer and Transducer Locations. Submittal date: 03/21/2007.

172179 TMUE25C3000095.001. Geophysical Logs for UE-25 C#3. Submittal date: 11/14/1995.

162614 UN0102SPA008KS.003. Concentration Dataset for Tracers (2, 6-Difluorobenzoic Acid and Iodide) Used for 48 Hour Shut in Tracer Test at the Alluvial Tracer Complex in Nye County. Submittal date: 06/11/2001.

Table B-1. Wells Discussed in This Report and Their Abbreviations

Name	Abbreviation
NC-EWDP-4PA, NC-EWDP-4PB	NA
NC-EWDP-10S, NC-EWDP-10P	10S, 10P
NC-EWDP-15P	NA
NC-EWDP-19D	19D
NC-EWDP-19IM1, NC-EWDP-19IM2	19IM1, 19IM2
NC-EWDP-19P	19P
NC-EWDP-19PB	19PB
NC-EWDP-22PA	22PA
NC-EWDP-22PB	22PB
NC-EWDP-22PC	22PC
NC-EWDP-22S	22S
UE-25 b#1	b#1
UE-25 c#1	c#1
UE-25 c#2	c#2
UE-25 c#3	c#3
UE-25 ONC-1	ONC-1
UE-25 p#1	p#1
UE-25 J-13	J-13
UE-25 WT#3	WT#3
UE-25 WT#12	WT#12
UE-25 WT#13	WT#13
UE-25 WT#14	WT#14
UE-25 WT#17	WT#17
USW G-1	G-1
USW G-2	G-2
USW G-3 and GU-3	G-3 and GU-3
USW G-4	G-4
USW H-1	H-1
USW H-3	H-3
USW H-4	H-4
USW H-5	H-5
USW H-6	H-6
USW WT-1	WT#1
USW WT-10	WT-10
Washburn-1X	NA

NOTE: NA means that an abbreviation is not used for that well in this report.

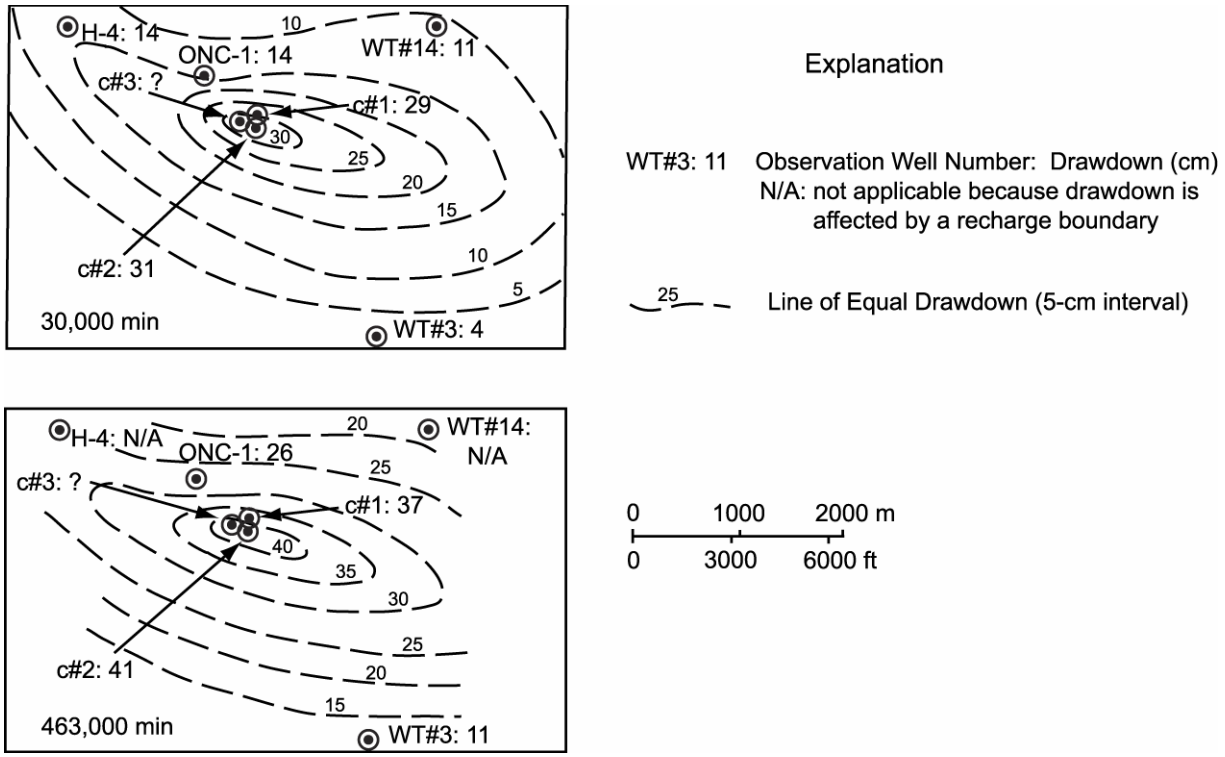

Sources: DTNs: GS970308312314.001 [DIRS 159240], GS970708312314.005 [DIRS 159241], GS981008312314.002 [DIRS 147068], GS981008312314.003 [DIRS 144464], GS010608312314.001 [DIRS 179647], GS970308312314.002 [DIRS 161273], GS970708312314.006 [DIRS 144468], MO0212SPANYESJ.149 [DIRS 161274].

Output DTN: GS031008312314.004.

NOTE: The upper panel shows the drawdown distribution 30,000 minutes (20.8 days) after pumping started; the lower panel shows the distribution 463,000 minutes (321.5 days) after pumping started.

The reason for the question mark in the figure is that the drawdown in the aquifer at the location of the pumped well, c#3, is unknown; only the apparent drawdown in the well, which consists largely of friction head loss, is known.

Figure C-38. Distribution of Drawdown in Observation Wells at Two Times after Pumping Started in UE-25 c#3 on May 8, 1996

In addition, all the analytical methods used in this study, except for the Neuman (1975 [DIRS 150321]) method, assume radial flow to the pumping well, and, therefore, ignore vertical flow (application of the Neuman fully penetrating-well solution, as was done in this report, to cases where pumping was in one interval and the analyzed drawdown response was in another, also ignores vertical flow). The flow from intervals other than the one being pumped that was detected during hydraulic tests in February 1996 and May 1996 to November 1997 indicates that flow during those tests actually was three-dimensional. To obtain hydrologic parameter estimates in nonpumped intervals, it was necessary to assume an equivalent radial volumetric flow rate in these intervals. These estimates of equivalent radial flow were quite uncertain, and they could have resulted in significant errors in hydrologic parameter estimates in nonpumped intervals. However, parameter estimates based on an assumed radial flow in nonpumped intervals were generally in good agreement with estimates obtained from open-hole pumping of c#3 in May through June 1995, and also from later pumping of the intervals when they were isolated (e.g., estimates for the Prow Pass interval when the Lower Bullfrog was pumped in 1996 to 1997 were in good agreement with estimates obtained when the Prow Pass interval was pumped directly in 1998). Thus, the approach taken seems to have yielded reasonable hydrologic parameter estimates in the cases in which it could be verified with a more direct measurement.

All the analytical techniques used in this study required input parameters that had to be determined or approximated for hydrogeologic intervals or boreholes in which drawdown was monitored. Included in those parameters are the distance of the interval or borehole from the pumping well, the transmissive thickness of the interval or borehole, the barometric efficiency of the interval or borehole, the proportion of flow from a given hydrogeologic interval, and the fracture spacing within a hydrogeologic interval. Errors in deriving any of those input parameters could have changed calculated hydrologic properties considerably.

Uncertainties and nonuniqueness in estimates of storativity, transmissivity, and hydraulic conductivity were not quantitatively analyzed because these parameter estimates were not used directly in the SZ site-scale flow model (SNL 2007 [DIRS 177391], Sections 6.6, 6.7, and 7); they were used only qualitatively/corroboratively in the flow model. Based on the ranges of transmissivity estimates obtained for a given hydrogeologic interval by different methods using either the drawdown or recovery data from the C-wells hydraulic tests (Tables C-6 and C-7) or the drawdown data from distant wells that responded to pumping c#3 in 1996 to 1997 (see Section C6.2, Tables C-10 and C-11), the transmissivity estimates determined in this analysis can be considered accurate to within about a factor of 1.5 for high-transmissivity intervals (lower Bullfrog and upper Tram Tuffs) and within a factor of 2.5 for low transmissivity intervals (Calico Hills, Prow Pass, and upper Bullfrog Tuffs). The factor of 2.5 also applies to the assemblage of volcanic tuffs between the C-wells and distant wells. Storativity estimates can be considered accurate to only within an order of magnitude or so. These ranges of transmissivity and storativity estimates are a result of the use of different theoretical models to fit the data (confined porous medium, confined/fissure block, unconfined), and also the data set analyzed (different tests, drawdown vs. recovery curves). However, relative values of transmissivity estimates (that is, the ratios of transmissivities of different flow intervals) can be considered more accurate because errors and biases should be reasonably consistent for estimates obtained by the same analyst using similar assumptions and methods (as is the case here). Estimates of hydraulic conductivity are more uncertain than transmissivity estimates because hydraulic

- Volume of water in which the mass of tracer is dissolved prior to entering the aquifer, V (L)
- Time for the tracer slug to enter the aquifer, t_{inj} (s)
- Flow porosity, ϕ_f, and matrix porosity, ϕ' (matrix porosity is also referred to, interchangeably, as "storage porosity" in Appendix B)
- Longitudinal dispersivity, α_L, in the form of a Peclet number ($Pe = r_L/\alpha_L$) (m)
- Retardation coefficients representing linear, reversible adsorption R in the fractures and R' in the matrix (always assumed to be 1.0 for conservative tracers)
- Dimensionless diffusion coefficient, gamma, which is a function of the effective coefficient of diffusion from the fractures into the matrix, D', and of h, ϕ_f, R, q_o, and the radius, b', of theoretical sphere-shaped matrix blocks of the dual-porosity aquifer
- Dimensionless storage parameter, sigma, which is a function of ϕ_f, ϕ', R, and R'
- Dimensionless skin parameter, SK, which is a function of the mass transfer coefficient, k_s, representing the continuity of diffusive flux across the "skin" (such as mineral fracture-surface coatings separating fractures from matrix blocks), and of D' and b'.

In a radially convergent flow field, the volume of interest is a cylinder centered at the production borehole and extending to the injection borehole. Moench (1989 [DIRS 101146]) assumes that the injection borehole is well mixed and that the tracer is distributed over a specified fraction of the borehole interval length (i.e., the "mixing length").

Radially convergent, flow-type curves were generated for a range of Peclet numbers. These single-porosity and dual-porosity type curves are in the form of log—log plots of dimensionless concentration, C_D = C/Ci, where Ci = average concentration in injection borehole after tracer injection, versus dimensionless time, $t_D = t/(\pi h \phi (r_L^2 - r_w^2)/q_o)$, where the denominator is referred to as the advective transport time, t_a. The observed field tracer breakthrough data are presented in the form of log−log plots of normalized concentration, C/C_{max} (where the concentration is normalized by the maximum observed concentration), versus time since injection. By overlaying the type curve and dimensionless breakthrough curve and matching the rising portions of the two curves, an estimate of the advective transport time, t_a, is obtained when the match point ($C_D = 1$, $t_D = 1$) is projected onto the log-time axis of the dimensionless field breakthrough curve (e.g., Figure D-1, which shows this process for the tracer test described in Section D1.1.1). In addition, because dimensionless time is defined as the ratio of time since injection to the advective transport time, the value of t_a is equal to the time since injection, indicated on the time axis of the breakthrough curve, corresponding to $t_D = 1$. The Peclet number is also estimated based on the type curve match. In the dual-porosity solution, diffusion is minimal on the rising limb of the breakthrough curve, but it was calculated on the falling limb. The tail of the observed data was matched to a theoretical dual-porosity breakthrough curve with diffusion processes in which the controlling parameters include the gamma and sigma terms. The physical parameters that are estimated are the matrix porosity, ϕ', and the dimensionless diffusion coefficient, gamma.

D1.2.1.1 Single-Porosity, Purely Convergent Interpretation

The single-porosity, purely convergent solution is obtained directly from the Moench (1989 [DIRS 101146]) solution to the advection-dispersion equation. A best visually matching single-porosity solution corresponding to flow porosity and longitudinal dispersivity values of 0.0007 and 1.45 m, respectively, is presented in Figure D-12, along with the iodide and 2,4,5 TFBA breakthrough curves. All breakthrough curves, such as the ones in Figure D-12, were normalized by dividing the measured concentrations by the maximum concentration, C_{max}, rather than by the concentration of the injected mass slug, C_0. Longitudinal dispersivity is a measure of the media's ability to disperse a solute along streamlines. Transverse dispersivity, which represents the media's ability to disperse a solute in a direction perpendicular to streamlines, is not obtainable from this analysis method and flow geometry. The longitudinal dispersivity of 1.45 m and the 29-m flow length correspond to a Peclet number of 20. Only one curve fit is shown in Figure D-12 because a single-porosity solution is capable of simulating only a single breakthrough curve for tracers with different diffusion coefficients.

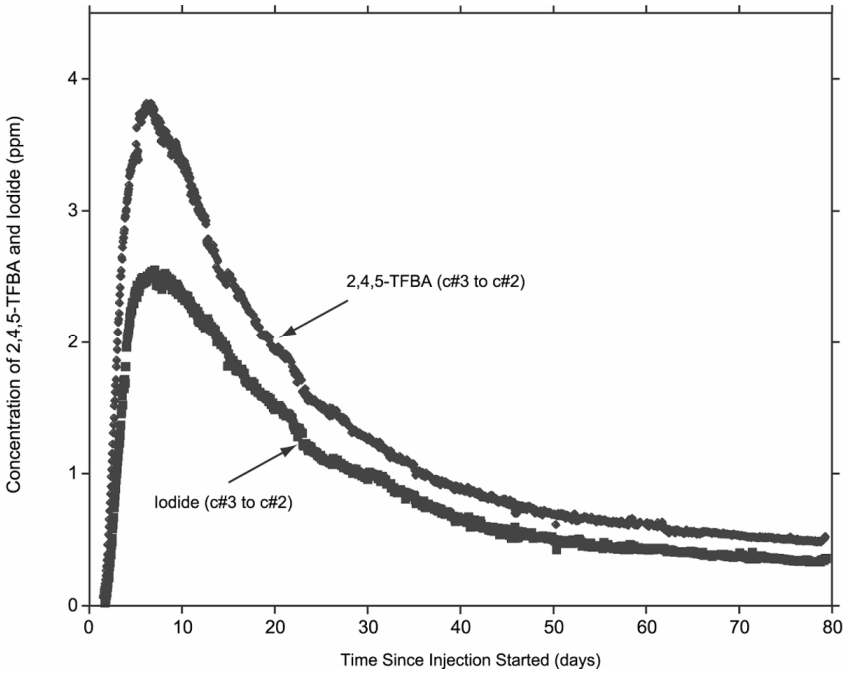

Source: DTN: GS990208312315.001 [DIRS 159238] (data).
NOTE: c#2 and c#3 refer to UE-25 c#2 and UE-25 c#3, respectively.

Figure D-11. Breakthrough Curves for 2,4,5 TFBA and Iodide Tracer Test from UE-25 c#3 to UE-25 c#2

hand, if the ratio of arrival times is greater than the ratio of distances squared, then the direction from c#2 to c#3 is a preferred flow orientation. Furthermore, the ratio of arrival times divided by the ratio of distances squared can be taken as a measure of the flow anisotropy ratio for the two different directions relative to the production well (note that these two directions are not strictly orthogonal). The ratios of tracer arrival times and r_L^2 values are in reasonably good agreement in all three cases, with apparent flow anisotropy ratios (c#1 to production well direction divided by c#2-c#3 direction) varying from 0.77 to 1.42. These relatively small ratios suggest that flow anisotropy at the scale of the C-wells may be relatively small despite the apparent orientation of the fracture network in the general direction of c#1 to c#2 (Geldon 1993 [DIRS 101045], pp. 43 to 51). The apparent flow anisotropy ratios deduced from the tracer arrival times should be carefully distinguished from the flow anisotropy ratios derived in Section A6, which were based on drawdown observations over much larger scales.

Table D-1. Ratios of Observed Tracer Arrival Times and Distances Squared, as well as Apparent Flow Anisotropy Ratios, for C-Wells Nonsorbing Tracer Tests

Tests (Injection Well)	$Time_{c\#1}$/ $Time_{c\#2\text{-}c\#3}$ [a]	$r_L^2{}_{c\#1}$/ $r_L^2{}_{c\#2\text{-}c\#3}$ [a]	Anisotropy Ratio [a]
Bullfrog: PFBA (c#2) and iodide (c#1)[b]	6	8.5	1.42
Bullfrog: 2,6-DFBA (c#2) and pyridone (c#1)[c]	11	8.5	0.77
Prow Pass: iodide and 2,4,5-TFBA (c#3) and 2,3,4,5-TeFBA (c#1)[d]	10	8.3	0.83

Sources: DTNs: GS010508312315.001 [DIRS 155860]; GS990208312315.001 [DIRS 159238]; LA0007PR831231.001 [DIRS 156043] (data); Borehole separation distances taken from Table 6.1-1.

Output DTN: LA0303PR831231.005.

NOTES: Because the borehole separation distances are unqualified data, the anisotropy ratios are provided for information purposes only. The uncertainties in the anisotropy ratios are quite large because vertical tracer transport distances, which were not accounted for in the calculations, could have been comparable to or even greater than the horizontal travel distances between the boreholes. c#1, c#2, and c#3 are abbreviations for Boreholes UE-25 c#1, UE-25 c#2, and UE-25 c#3. r_L^2 is the distance squared between injection and production wells.

[a] $Time_{c\#1}$ and $r_L^2{}_{c\#1}$ are the time and distance, respectively, between c#1 and the production well (either c#2 or c#3, depending on the test), and $Time_{c\#2\text{-}c\#3}$ and $r_L^2{}_{c\#2\text{-}c\#3}$ are the time and distance, respectively between c#2 and c#3. Columns 2 and 3 give the ratios of these times and distances. Ratio is for c#1 to production well direction divided by c#2 to c#3 direction. For the anisotropy ratio, a value greater than 1.0 indicates that the c#1 to production well direction is the preferred flow orientation.
[b] Both tests conducted with 2.5% to 3.5% recirculation into injection well. Peak tracer arrivals compared.
[c] Both tests conducted with no recirculation. First tracer arrivals compared.
[d] c#3-to-c#2 test conducted with 30% recirculation; c#1-to-c#2 test conducted with no recirculation. Peak tracer arrivals compared.

DFBA= difluorobenzoic acid or difluorobenzoate; PFBA= pentafluorobenzoic acid or pentafluorobenzoate; TFBA= trifluorobenzoic acid.

D3. SUMMARY OF CONCEPTUAL MODELS AND PARAMETERS FROM NONSORBING TRACER TESTS AT THE C-WELLS

Uncertainty in the values of longitudinal dispersivity, flow porosity, and matrix (or storage) porosity result from physical processes, such as the scale-dependence of dispersivity (when comparing tracer tests conducted from Borehole c#1 to those conducted between Boreholes c#2 and c#3), as well as from variability in the transport characteristics of the tracer materials. However, there is good agreement in dispersivity values obtained from tracer tests conducted

between Boreholes c#2 and c#3 in the Bullfrog and Tram intervals. Peclet numbers range from 11 to 15; therefore, the longitudinal dispersivities are similar (Table D-2).

The breakthrough times are identical for the iodide and the DFBA tracer tests (Table D-2), and the advective transport times are within 10%. Therefore, the inferred flow porosities are similar, which implies that similar flow pathways are used by the tracers in those tests. These differences can be explained by the different thicknesses of the zones tested: the iodide tracer test was conducted in the combined Bullfrog-Tram zone, and the DFBA tracer test was conducted in the Lower Bullfrog zone.

The parameter estimates are robust because the visual-graphic match is close to the PEST fit (which is based on the dual-porosity analytical solution.) The differences are less than 5% for all parameters except matrix porosity, and these estimates vary by only 0.03.

The estimated flow porosities suggest that the pathways between Boreholes c#2 and c#3 in the Bullfrog and Tram intervals are not well-connected. This possibility is supported by the interpretation of the higher-than-expected flow porosities for the Bullfrog and Tram Tuffs. The microsphere responses (Section D4) are consistent with this interpretation. The arrival of the microspheres at the recovery borehole indicates the existence of a connected pathway, somewhere, with an aperture at least 0.36 μm (the diameter of the spheres).

Table D-2. Summary of Results and Transport Properties for the Bullfrog and Tram Tuffs from Nonsorbing Tracer Tests

	Iodide Test from c#2 to c#3 in Bullfrog-Tram	DFBA Test from c#2 to c#3 in Lower Bullfrog	Pyridone Test from c#1 to c#3 in Lower Bullfrog
Breakthrough (days)	5.07	5.07	56.3
Peak concentration (μg/L)	99.5	251	0.210 (final value)
Peclet number	11	12 to 15	11
Dispersivity (m)	2.6	2.4 to 1.9	6.2
Flow porosity, ϕ_f (%)	8.6	9.9 to 7.2	Not Estimated
Matrix (or storage) porosity, ϕ (%)	19	8.8 to 13.2	Not Estimated

Sources: DTNs: GS960808312315.001 [DIRS 159235] (Iodide data) and GS010508312315.001 [DIRS 155860] (DFBA and Pyridone data).

Output DTN: GS031008312315.002 (analysis).

NOTES: c#1, c#2, and c#3 are abbreviations for Boreholes UE-25 c#1, UE-25 c#2, and UE-25 c#3, respectively.

DFBA= difluorobenzoic acid or difluorobenzoate.

This report presents the first unequivocal tracer testing from Borehole c#1 to c#3 in the Lower Bullfrog test and from c#1 to c#2 in the Prow Pass test. The preliminary results suggest that the arrival time from c#1 to c#3, 56.3 days, is consistent with the arrival time from c#2 to c#3, 5.07 days, because, as implemented in the Moench (1989 [DIRS 101146]) solution, the arrival time is directly proportional to the square of the distance between injection and production wells (Section D2).

Table D-3. Summary of Results and Transport Properties in a Partly Recirculating Tracer Test from Borehole c#3 to c#2 and from Borehole c#1 to c#2, Prow Pass Tuff

Parameter	2,4,5 TFBA & Iodide: c#3 to c#2		2,3,4,5 TeFBA: c#1 to c#2
Breakthrough (days)	1.67		17
Peak concentration (ppm)	TFBA : 3.7 Iodide : 2.7		0.09
	Single-Porosity, Partial Recirculating Solution	Dual–Porosity, Partial Recirculating Solution	
Longitudinal dispersivity (m)	0.27	0.27	Not Estimated
Peclet number	107.4	107.4	Not Estimated
Flow porosity, ϕf	0.00045	0.00045	Not Estimated
Gamma (dimensionless matrix diffusion coefficient)	N/A	0.000444, 0.001(TFBA and Iodide, respectively)	Not Estimated
Storage porosity, ϕ'	N/A	0.01	Not Estimated

Sources: DTNs: GS990208312315.001 [DIRS 159238] and MO0308SPATRCRC.000 [DIRS 164821] (data).

Output DTN: GS031008312315.002 (analysis).

NOTE: c#1, c#2, and c#3 are abbreviations for Boreholes UE-25 c#1, UE-25 c#2, and UE-25 c#3, respectively. Borehole mixing length was assumed to be 30.5 m.

N/A = Not Applicable. TFBA = trifluorobenzoic acid.

D4. MULTIPLE TRACER TESTS WITH SORBING SOLUTES AND COLLOID TRACERS AT THE C-WELLS

D4.1 INTRODUCTION AND OBJECTIVES

This section describes the conduct and interpretation of two cross-hole tracer tests between c#2 and c#3 in which multiple solute tracers and colloid tracers (carboxylate-modified latex (CML) microspheres) were simultaneously injected. One test was conducted in the Lower Bullfrog Tuff and the other was conducted in the Prow Pass Tuff (referred to as the Bullfrog test and the Prow Pass test, respectively). The objectives of the multiple-tracer tests in the fractured tuffs at the C-wells included the following:

- Testing/validating the applicability of a dual-porosity conceptual transport model (Section D4.2) in the saturated, fractured volcanic tuffs that underlie Yucca Mountain
- Obtaining estimates of key transport parameters in the flow system, including parameters for colloid transport
- Assessing the applicability of laboratory-derived tracer transport parameters to field-scale transport predictions.

The latter objective is important because radionuclides cannot be tested in the field, so favorable comparisons of laboratory- and field-scale transport of nonradioactive tracers can lend credibility to the practice of using laboratory-derived radionuclide transport parameters in field-scale predictive simulations.

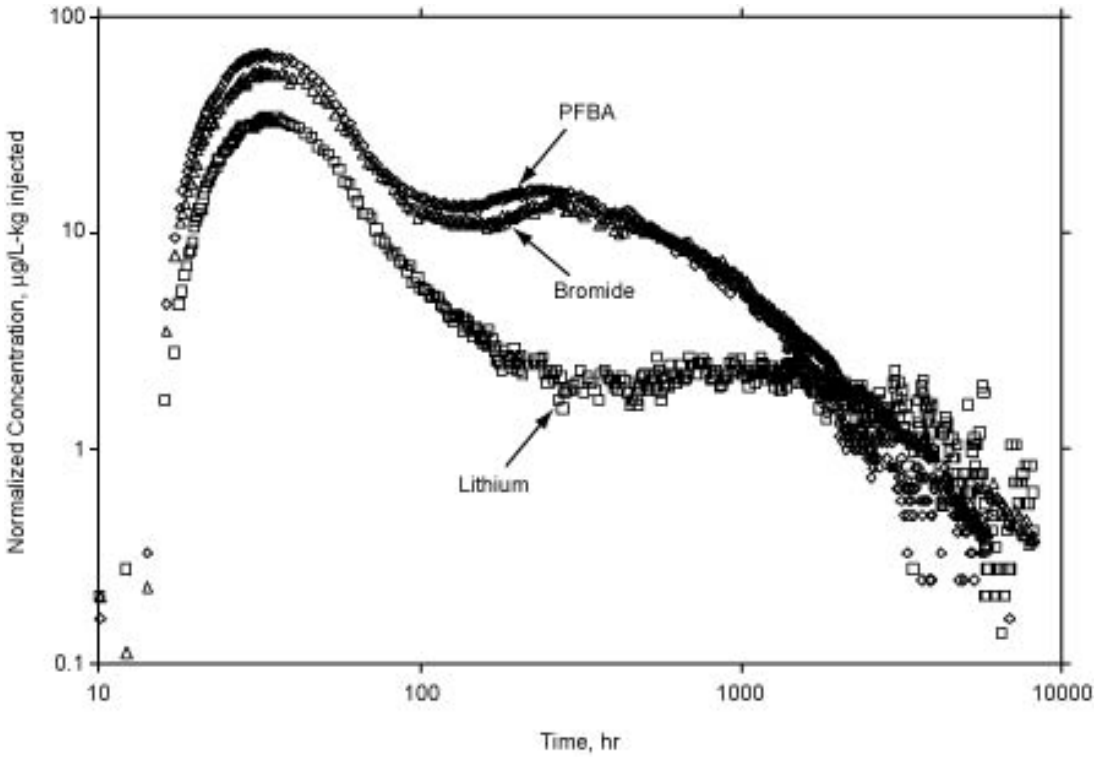

Sources: DTNs: LA0007PR831231.001 [DIRS 156043] (raw data), LA0410PR831231.001 [DIRS 171899] (normalized concentrations).

NOTE: Log−log scales are used for the axes so that the bimodal nature of the tracer responses can be seen more clearly.

Figure D-19. Normalized Tracer Concentrations Versus Time in the Bullfrog Tuff Tracer Test Conducted from October 1996 to September 1997

PFBA concentrations in the earlier test were monitored for just over 3,000 hr with a total fractional recovery of 0.72; at 3,000 hr into the second test, the total PFBA fractional recovery was 0.60 (DTN: LA0410PR831231.001 [DIRS 171899]). Thus, the tracer recovery in the former test was actually higher than in the latter test despite the early tracer arrival in the latter test. This observation, plus the fact that the shapes of the common peaks of the two tests are different, suggest that a considerable fraction of the mass injected in the latter test followed additional pathways not accessed in the first test. Although the possibility of additional recovery of PFBA from the first test in the second test cannot be ruled out, it is not plausible that the PFBA from the first test could have caused either the first or second PFBA peak in the second test because all of the other tracers used in the second test (which were not injected in the first test) exhibited a bimodal response.

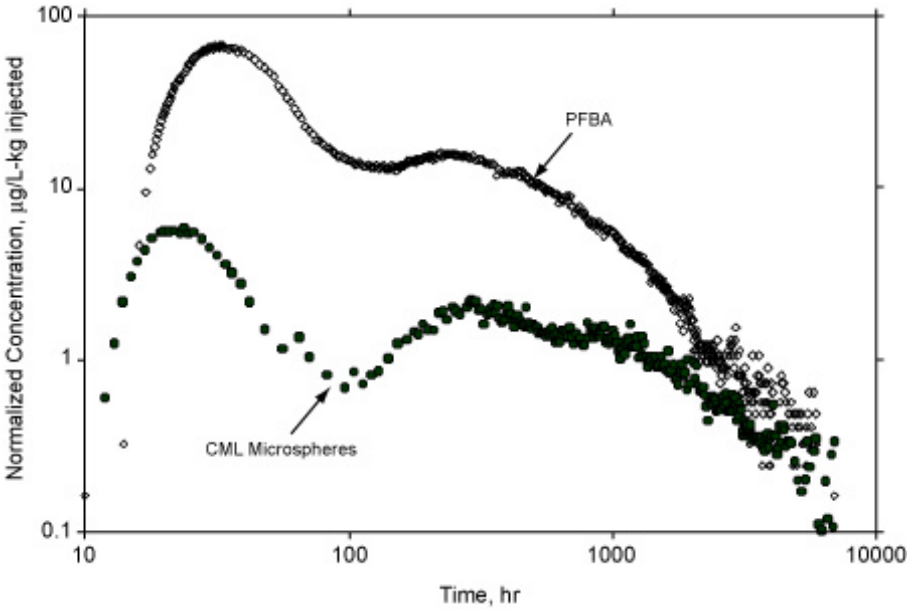

Sources: DTNs: LA0007PR831231.001 [DIRS 156043] (raw data), LA0410PR831231.001 [DIRS 171899] (normalized concentrations).

NOTE: Log−log scales are used for the axes so that the bimodal nature of the tracer responses can be seen more clearly.

Figure D-20. Normalized Concentrations of PFBA and 360-nm-Diameter Carboxylate-Modified Polystyrene Latex Microspheres in the Bullfrog Tuff Tracer Test

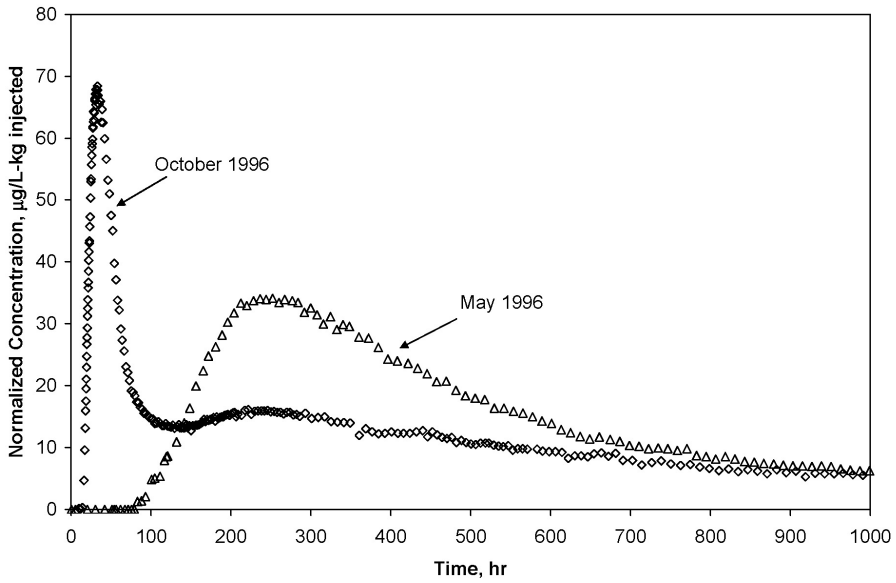

Sources: DTNs: LA0007PR831231.001 [DIRS 156043] (raw data), LA0410PR831231.001 [DIRS 171899] (normalized concentrations).

NOTE: The test conditions were the same in both tests, but the injection solution volume was approximately 1,000 L in the May test and approximately 12,000 L in the October test.

Figure D-21. Comparison of Normalized PFBA Responses in the Bullfrog Tuff Resulting from Tracer Injections in May 1996 and October 1996

η = porosity within fractures

ϕ = matrix porosity

b = fracture half aperture, cm

L = spacing between centerlines of adjacent fractures, cm.

The transformation of Equations D-1 and D-2 to the Laplace domain and their subsequent solution in the Laplace domain and inversion of the solution back to the time domain are described by Reimus and Haga (1999 [DIRS 154705], Appendix B). Equations D-1 and D-2 reduce to a single-porosity system if the matrix porosity, ϕ, (or the matrix diffusion coefficient, D_m) is set equal to zero. RELAP V 2.0 (STN: 10551-2.0-00 [DIRS 159065]) provides a simultaneous least-squares fit to up to four tracer data sets by automatically adjusting the following parameters (which arise from the dimensionless forms of the governing equations):

- Mean fluid residence time in fractures (τ)
- Peclet number ($Pe = r_L/\alpha$, where r_L = distance between wells, m, and α = dispersivity in fractures, m)
- Mass fraction of tracers participating in the test (f)
- Matrix diffusion mass-transfer coefficient, $\frac{\phi}{b}\sqrt{D_m}$, which is obtained from the Laplace transformations of Equations D-1 and D-2
- Characteristic fracture spacing, L
- Fracture retardation factor, R_f
- Matrix retardation factor, R_m.

The fractional mass participation (f) is used as an adjustable parameter because low mass recoveries are frequently observed in field tracer tests in fractured rock (e.g., Reimus and Haga 1999 [DIRS 154705], Appendix B), presumably due to (1) dense tracer solutions "sinking" out of the zone of influence of pumping, (2) a significant volumetric flow of tracer solution into the matrix within the injection wellbore (this tracer mass will not make it to the production well during the tracer test because of the very low flow velocities in the matrix), or (3) the loss of tracer mass due to stagnation points induced either by recirculation or by the superposition of the induced flow field on the ambient flow field. Although these phenomena can affect absolute tracer responses, they should not, in principle, affect the relative responses of different tracers that are injected simultaneously.

The interpretation of the tracer responses in each test involved first fitting the two nonsorbing tracer responses by simultaneously adjusting all of the parameters listed above with the constraint that the matrix diffusion coefficient, D_m, for bromide was three times that of PFBA

(and therefore the matrix diffusion mass transfer coefficient, $\frac{\phi}{b}\sqrt{D_{\mathrm{m}}}$, was approximately 1.7 times that of PFBA). This factor-of-three difference is based on the experimental diffusion

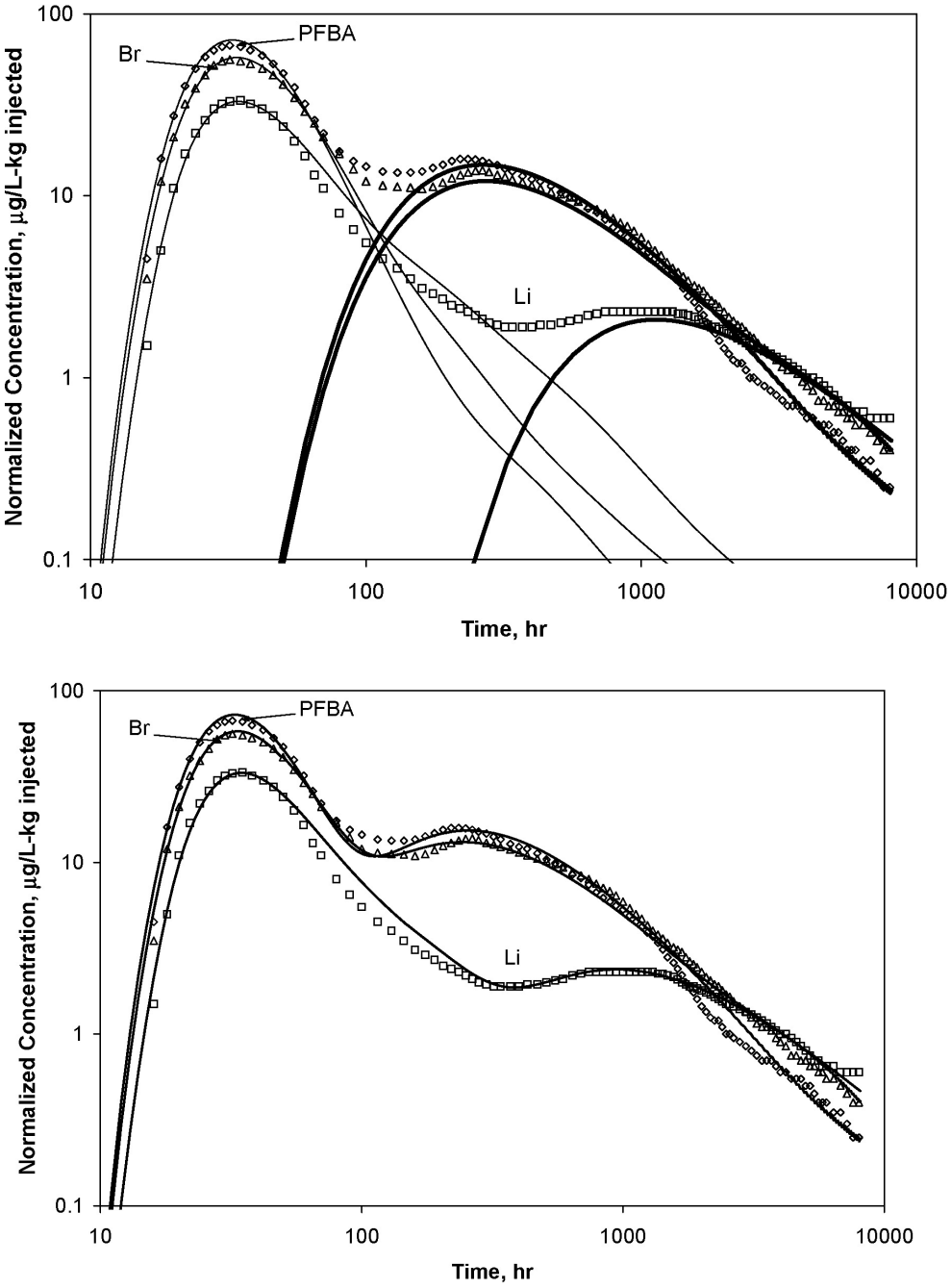

Sources: DTNs: LA0007PR831231.001 [DIRS 156043] (data), LA0410PR831231.001 [DIRS 171899] (normalized concentrations).

Output DTN: LA0303PR831231.003 (interpretive fits).

NOTE: The upper plot shows individual fits to first and second tracer peaks (MULTRAN V 1.0 (STN: 10666-1.0-00 [DIRS 159068]) and RELAP V 2.0 (STN: 10551-2.0-00 [DIRS 159065]), respectively, and the lower plot shows composite fits. For clarity, the data points shown are a subset of the actual data. The best-fitting model parameters are provided in Table D-6.

Figure D-26. RELAP and MULTRAN Fits to the Tracer Response Curves in the Bullfrog Tuff Tracer Test

The quantitative estimates of the lumped mass transfer parameter, $\frac{\phi}{b}\sqrt{D_m}$ for bromide in Tables D-6 and D-7 are based on the assumption that bromide has a diffusion coefficient a factor of three greater than PFBA. This assumption is based on matrix diffusion coefficients measured in laboratory diffusion cell tests, which are discussed in Section E2. It is worth noting that RELAP V 2.0 (STN: 10551-2.0-00 [DIRS 159065]) simulations in which a finite matrix was assumed (i.e., a finite spacing between fractures) offered a slightly better fit to the tracer responses associated with the second peak of the Bullfrog test than simulations assuming an infinite matrix. This result suggests that tracer molecules may have diffused far enough into the matrix to begin encountering molecules from neighboring fractures, which implies a relatively small fracture spacing. Alternatively, the tracers may have encountered diffusion boundaries (no-flux boundaries) within the matrix, which implies a significant increase in tortuosity or a decrease in interconnected porosity at some distance into the matrix from fracture surfaces. For the first peak in the Bullfrog test and for the Prow Pass test, a finite matrix offered no better fits to the tracer data than an infinite matrix. In these cases, it can only be stated that the fracture spacing must have exceeded some threshold value below which the tracer responses would have been significantly different than observed. The applicable threshold values for the first Bullfrog test peak and for the Prow Pass test were estimated by adjusting the fracture spacing in RELAP until the simulated tracer responses began to differ significantly from the simulated responses assuming an infinite matrix. The results are presented in Table D-10 as lower bounds for fracture spacing.

The tracer responses and the qualitative and quantitative conclusions about matrix diffusion that can be drawn from them illustrate very clearly the advantages of using multiple nonsorbing tracers with different diffusion coefficients in tracer tests to distinguish between alternative conceptual transport models. The individual responses of either bromide or PFBA could have been fit reasonably well assuming no matrix diffusion at all. Only when the responses of these tracers are considered together is it obvious that diffusive mass transfer must be invoked to explain the test results. Even long tails that plot linearly on log−log plots of tracer responses (power-law behavior), which are often said to infer matrix diffusion when single tracer responses are analyzed (Haggerty et al. 2000 [DIRS 156832], pp. 3,467 to 3,469), do not unequivocally substantiate diffusive mass transfer. Such responses can also be attributed to hydrodynamic dispersion that scales with residence time (due to the recirculating flow field or effects of density-driven flow), stagnation points, and/or source-term effects (e.g., the slow release of tracers from the injection borehole). Furthermore, the fact that the lithium responses were significantly attenuated in concentration but not in time supports the concept that a significant amount of diffusion occurred into the matrix pores and not simply into stagnant water within the fracture network. This conclusion is very important for Yucca Mountain performance assessment because mass transfer between flowing fractures and the true matrix implies that a large amount of surface area will be available for sorption of radionuclides in the saturated, fractured tuffs.

D4.8.2 Fracture Apertures

An estimate of the average fracture aperture ($2b$) experienced by the tracers in the Bullfrog and Prow Pass tests can be obtained from the estimate of the lumped, diffusive, mass-transfer parameter, $\frac{\phi}{b}\sqrt{D_m}$ provided independent estimates of matrix porosity, ϕ, and matrix diffusion coefficients, D_m, are available. Using estimates of ϕ determined from laboratory measurements and D_m for bromide and PFBA from diffusion cell tests (Section E2), estimates of 2b range from 0.081 to 1.31 cm in the Bullfrog Tuff and from 0.18 to 1.05 cm in the Prow Pass Tuff, as listed in Table D-10. Because the long tracer test intervals in each test both included more than one major lithology (Figure 6.1-2), it was necessary to estimate $2b$ for each major lithologic unit in each interval. The fact that there is a positive correlation between matrix porosity and matrix diffusion coefficient results in a relatively large range of aperture estimates. If it is assumed that the flow pathways associated with the first tracer peak in the Bullfrog test were in the central Bullfrog unit and the pathways associated with the second tracer peak were in the lower Bullfrog unit, then the aperture estimates in these two units correspond to the two extremes listed in Table D-10. These aperture estimates based on tracer responses should be distinguished from friction loss or cubic-law aperture estimates obtained from hydraulic responses (Tsang 1992 [DIRS 113901], pp. 1,451 to 1,455), although they should be the most appropriate aperture estimates to use for transport calculations.

D4.8.3 Ratios of Stagnant Water to Flowing Water Volumes

Estimates of the ratio of stagnant water volume to flowing water volume in the flow system(s) can be calculated from estimates of fracture spacings obtained from RELAP V 2.0 (STN: 10551-2.0-00 [DIRS 159065]) simulations and the matrix porosities and fracture apertures used in the RELAP simulations (ratio = $\phi(L/2b - 1)$). Ranges of these estimates are listed in Table D-10. The upper-bound ratios for both tracer tests are listed as infinite because all tracer responses could be fitted reasonably well, assuming infinite fracture spacing. The lower bounds in Table D-10 were obtained using fracture spacings that yielded slightly better fits to the tracer responses than the fits obtained assuming an infinite fracture spacing. These ratios plus one can be considered physical retardation factors for nonsorbing species in the flow system when flow rates are low enough that there is ample time for solutes to diffuse throughout the stagnant water in the system (Robinson 1994 [DIRS 101154]).

D4.8.4 Lithium Sorption Behavior

Tables D-6 and D-7 list the best-fitting values of the lithium fracture and matrix retardation factors (R_f and R_m, respectively) for the Bullfrog and Prow Pass tests. The $R_f$values are 1 for both the Prow Pass test and for the first peak in the Bullfrog test, implying negligible retardation within the fractures and sorption only in the matrix. A fracture retardation factor of 1 does not necessarily imply that sorption did not occur on fracture surfaces; it merely suggests that the majority of the lithium sorption occurred after a diffusive mass-transfer step to sorptive surfaces in the matrix. For the second peak in the Bullfrog test, the lithium response was best fitted with $R_f = 4$ and $R_m = 20$, implying some sorption in fractures and a large amount of sorption in the matrix.

(Moench 1989 [DIRS 101146]). Using these input parameters, along with a Peclet number of 100 (i.e., a longitudinal dispersivity of 0.29 m), the RELAP code yields the fits shown in Figure D-31 (the mean residence time and mass fraction were adjusted to obtain these fits). The longitudinal dispersivity reported in Section D1.2.1 was 0.27 m. The tracer responses and fits in Figure D-31 are adjusted so that they all have the same maximum concentration, which is consistent with the analysis used in Section D1.2.1. A comparison of Figure D-31 and Figure D-16 shows that the two methods yield almost indistinguishable results when the same input parameters are used.

The injection borehole time constant of 0.0023 hr^{-1} used in the above analysis translates to a mean tracer residence time in the borehole of 1/0.0023, or approximately 435 hr. This residence time is at odds with the tracer concentration measurements in the injection borehole described in Section D1.2.1.1, where it is stated that the borehole was effectively flushed of tracer in approximately 8.5 hr. The fact that the tracer was flushed from the borehole in such a short time is not surprising given that there was a continuous injection of approximately 1.5 gpm (approximately 5.7 L/min) of groundwater into the injection zone following the injection of tracers. A mean residence time of approximately 9 hrs is calculated by dividing the volume of the injection interval (approximately 3,000 L) by the 5.7 L/min flow rate. For these reasons, a second RELAP simulation was conducted in which it was assumed that the injection borehole time constant was 0.11 hr^{-1} ((5.7)(60)/3,000). This is the same time constant value that was used in the analysis of the PFBA and bromide tracer test conducted in the Prow Pass Tuff described in Section D4.7.1. The resulting RELAP fits to the tracer data are shown in Figure D-32, where in this case the tracer concentrations are normalized to tracer injection mass, as in Section D4. The RELAP transport parameters for the simulations of Figures D-31 and D-32 are listed in Table D-12. Also listed in this table are the parameters obtained from RELAP fits to the PFBA and bromide data in the Prow Pass Tuff, discussed in Section D4.7. This test was conducted in the same configuration and with the same flow rates as the iodide and 2,4,5-TFBA test, although the volume of the tracer solution injected was considerably larger. Clearly, there is a very large difference in the mean residence times and Peclet numbers of the simulations with significantly different borehole time constants, although the iodide mass transfer coefficients, $\frac{\phi}{b}\sqrt{D_m}$, are in reasonably good agreement in all simulations.

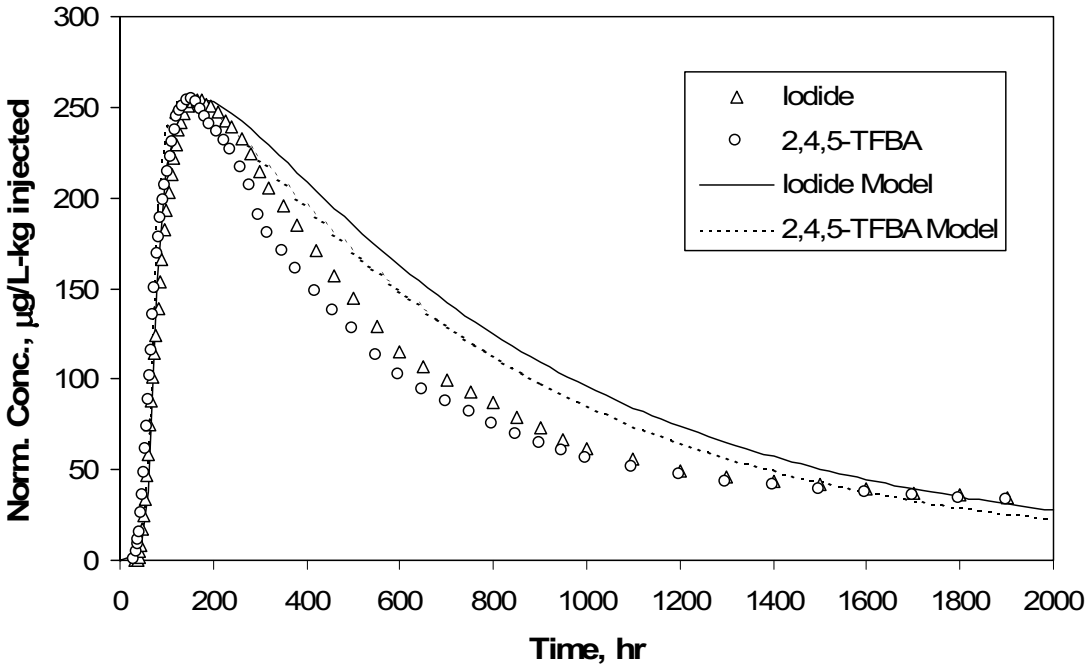

Output DTN: LA0304PR831231.001.

NOTE: Data points represent a subset of the actual data. Data and curves are adjusted so that they all have the same maximum normalized concentration (see Figure D-16 for comparison). The same parameters obtained from the Moench solution in Section D1.2.1 were used. "Model" refers to a fit generated by the RELAP code.

Figure D-31. RELAP Fits to the Iodide and 2,4,5-TFBA Responses in the Prow Pass Tuff Tracer Test Assuming an Injection Zone Time Constant of 0.0023 hr^{-1}

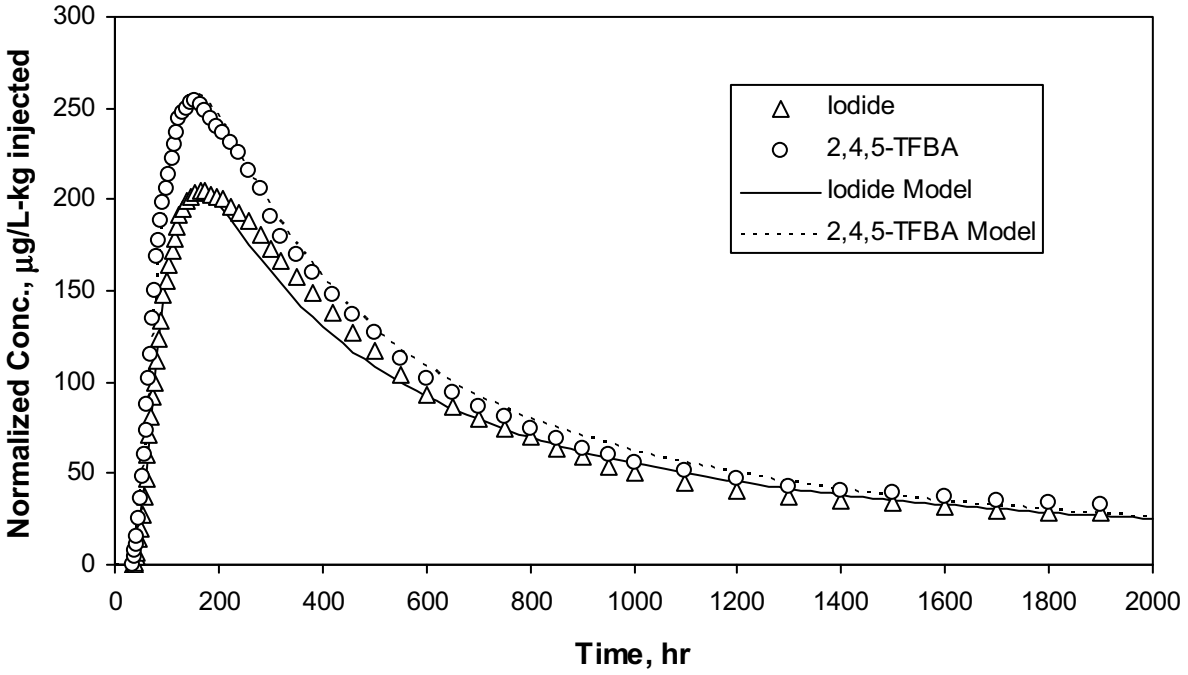

Output DTN: LA0304PR831231.001.

NOTE: Data points represent a subset of the actual data. "Model" refers to a fit generated by the RELAP code.

Figure D-32. RELAP Fits to the Iodide and 2,4,5-TFBA Responses in the Prow Pass Tuff Tracer Test Assuming an Injection Borehole Time Constant of 0.11 hr^{-1}

The reason for the large differences in mean residence times and Peclet numbers in Table D-12, particularly between the two interpretations of the iodide and 2,4,5-TFBA test, becomes clear when one considers the implications of the different borehole mixing assumptions. Figure D-33 shows tracer responses calculated by RELAP V 2.0 (STN: 10551-2.0-00 [DIRS 159065]) in a hypothetical system with a mean residence time in the aquifer (not the injection borehole) of 1 hr, a Peclet number of 100, and no matrix diffusion. With this choice of parameters, the responses are due almost entirely to tracer residence time in the injection borehole. The tails of the responses are linear on a semi-log plot because tracer concentrations in a well-mixed region decay exponentially. The curve with the largest time constant corresponds to the tracer residence time distribution in the borehole for the RELAP fits of Figure D-32, and the curve with the smallest time constant shows the residence time distribution associated with the fits of Figure D-31. The iodide response in the Prow Pass tracer test is also shown in Figure D-33. It is apparent that the curve with the smallest time constant has a tail that matches the tracer data quite well. Thus, to match the entire breakthrough curve, it is only necessary to impose a lag on the borehole response (accounted for by a finite residence time in the flow system), with only a very small amount of additional dispersion or matrix diffusion in the flow system necessary to optimize the fit. However, as the borehole time constants get larger, it becomes necessary to impose a greater lag and account for more dispersion or matrix diffusion in the flow system to achieve a match to the data.

It is important to note that the ranges of parameter values in Table D-14 are not completely independent of each other. That is, when one parameter value is taken from the high end of its range, another may have to be taken from near the low end of its range to achieve a good fit. This is especially true of the mean residence time and Peclet number, which have a very strong inverse correlation. Figure D-37 shows the relationship between best-fitting values of Peclet number and mean residence time for the four multiple-tracer tests at the C-wells. All of the points plotted in this figure are associated with equally good fits to the data according to the criterion stated in the previous paragraph. The range of mean residence times is significantly lower for the data set with the largest Peclet numbers compared to the three data sets with smaller Peclet numbers. This result was found to be true in general (i.e., the range of mean residence times was smaller for hypothetical tracer responses with less longitudinal dispersion).

Figure D-38 shows that the best-fitting mass fractions are positively correlated with the best-fitting mean residence times for the iodide and 2,4,5-TFBA responses in the Prow Pass Tuff. This result and Figure D-37 imply a negative correlation of mass fraction with Peclet number. These same trends were obtained for all other multiple-tracer tests. Interestingly, the MTC, $\frac{\phi}{b}\sqrt{D_{\mathrm{m}}}$, was poorly correlated with any of the other transport parameters. In fact, the extremes of MTC values were generally associated with values of other parameters not near the ends of their respective ranges. Also, the range of MTC values never included zero, which indicates that a dual-porosity system is always implied from the fits.

The parameter ranges in Table D-14 reflect considerable uncertainty associated with the nonuniqueness of interpretive fits for multiple tracer tests. These ranges, in general, are comparable in magnitude to the ranges of derived parameter values provided in Table D-10, which were based on uncertainties in tracer travel distances and radionuclide diffusion coefficients, as well as the range of parameter values obtained from different tests in the same interval. The ranges in Table D-10 would have to be expanded somewhat to account for the additional uncertainty associated with the nonuniqueness of fits. Expanding these ranges by multiplying the lower value of any parameter in Table D-10 by 0.5 and the upper value by 2 would effectively capture this additional uncertainty.

A few points are worthy of mention regarding uncertainty associated with nonuniqueness of the semi-analytical solution fits to obtain transport parameter estimates:

1. Although there is considerable uncertainty associated with model fits to multiple-tracer data sets, the uncertainty is far less than the uncertainty associated with fits to single-tracer data sets (compare Tables D-13 and D-14). Also, all the fits to multiple-tracer data sets indicated a dual-porosity system (in which flow occurs primarily through fractures but with a significant volume of stagnant or near-stagnant water in the matrix that is in diffusive communication with the flowing water), while fits to single-tracer data sets cannot effectively distinguish between a single- and dual-porosity transport system.

2. This uncertainty analysis and discussion is by no means complete. Other factors must be considered when doing a rigorous uncertainty analysis. A couple of additional considerations that go beyond the scope of this report are:

   - When fitting multiple data sets, one must be careful to not inadvertently give one set more weight than the others in the fitting procedure. Inappropriate weighting can occur, for instance, when one data set has significantly more data points than the other(s) or when one set has much larger numerical values than the other(s). Approaches to dealing with this problem include (1) various weighting schemes, (2) making the number of data points the same for all data sets (by dropping some data from the larger data sets), or (3) normalizing the sum-of-squares errors for each data set by dividing by the number of points fitted for each set. Each of these approaches introduces some arbitrary bias into the fitting procedure, which introduces bias into the errors associated with the parameter estimates. In this report, we use approach (3).

   - The fitting criteria (or objective function) are very important and can have a significant influence on both parameter estimates and error estimates. For instance, one will obtain different answers if the sum-of-squares differences between semi-analytical solution and data are minimized vs. minimizing the sum-of-squares differences between the log of the data and the solution. In this report, it was chosen to minimize the straight sums-of-squares differences rather than the differences in any transformations of the data and solution values.

   Although the transport parameter uncertainty analysis is not necessarily complete or entirely quantitative, it is important to point out that the uncertainties in the parameter estimates obtained from tracer testing are considered to be very effectively, and even conservatively, captured in *Saturated Zone Flow and Transport Model Abstraction* (SNL 2007 [DIRS 181650]). Thus, conservatism is ultimately built into the downstream propagation of transport parameter uncertainties in the TSPA.

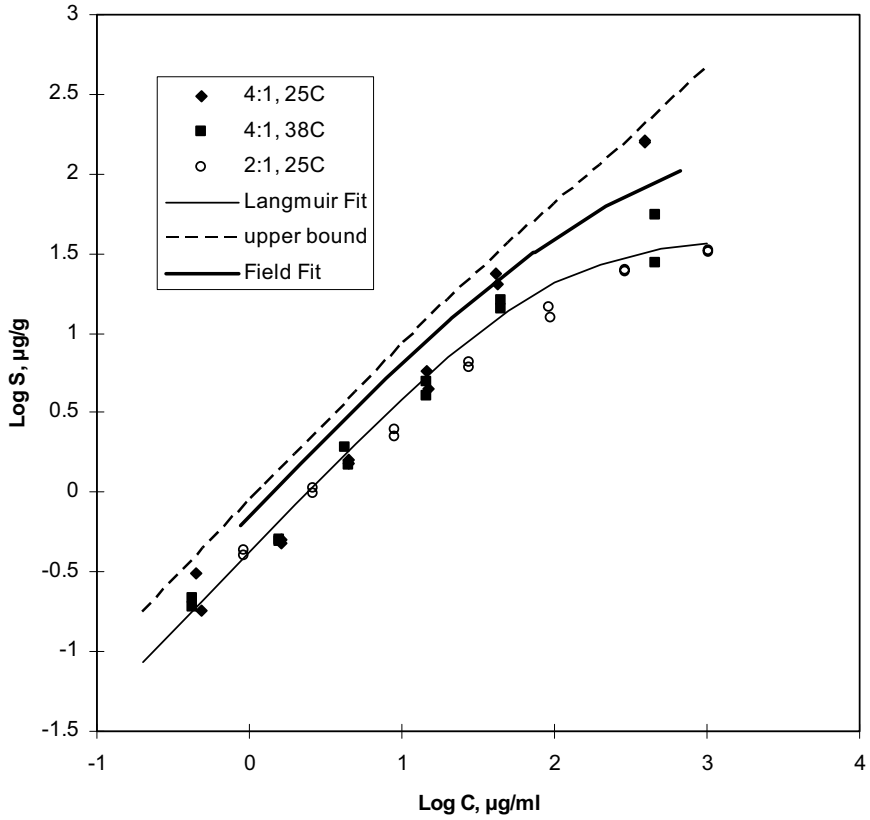

Source: DTN: MO0012SORBCHOL.000 [DIRS 153375] (data).

Output DTN: LA0303PR831341.003 (isotherm fits).

NOTE: The legend indicates the solution:solid ratio (mL:g) and the temperature of the experiments. The dashed line is an upper error bars associated with a 10% experimental error (this error bar is plotted relative to the Langmuir isotherm line – lower error bound is off-scale over entire range of data). The method for calculating the error bars is by Reimus (2003 [DIRS 165129], p. 126). J-13 well water was used in all experiments. The lithium concentration in the Prow Pass Tuff field test ranged from less than 0.1 µg/mL up to 2,700 µg/mL. The line labeled "Field Fit" is the isotherm corresponding to the MULTRAN V 1.0 (STN: 1066-1.0-00 [DIRS 159068]) "fit" to the lithium data in the Prow Pass Tuff field tracer test (Figure D-27).

Figure E-6. Lithium Sorption Data and Fitted Langmuir Isotherm for the Lower Prow Pass Tuff (c#1, 573 m Below Land Surface)

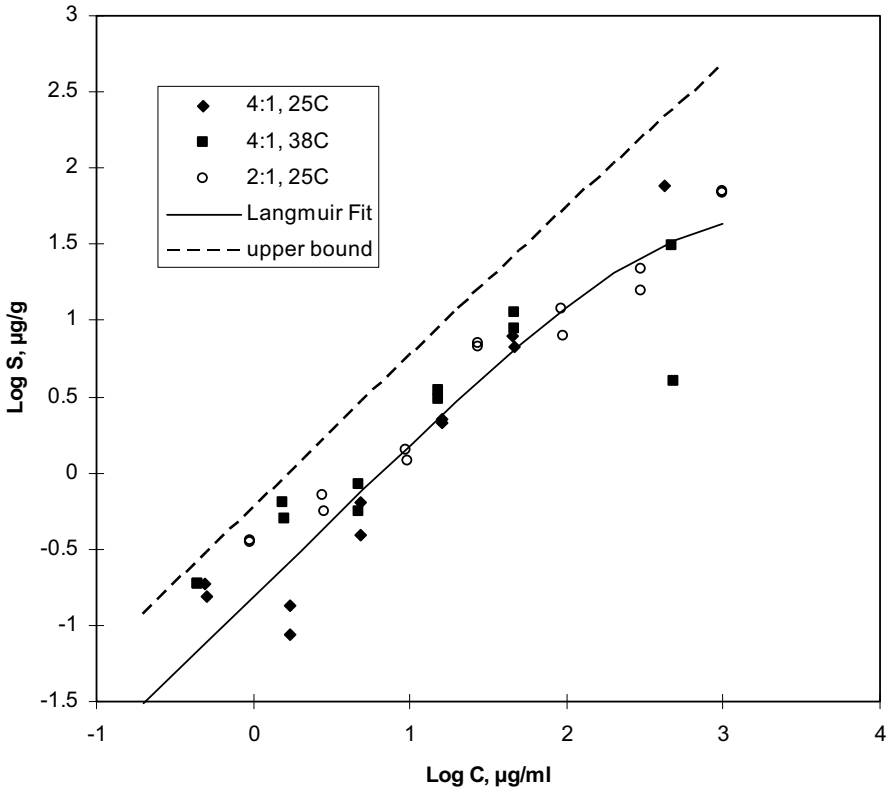

Source: DTN: MO0012SORBCHOL.000 [DIRS 153375] (data).

Output DTN: LA0303PR831341.003 (isotherm fits).

NOTE: The legend indicates the solution:solid ratio (mL:g) and the temperature of the experiments. The dashed line is an upper error bar associated with a 10% experimental error (these error bars are plotted relative to the Langmuir isotherm line - lower error bound is off-scale over entire range of data). The method for calculating the error bars is described by Reimus (2003 [DIRS 165129], p. 126). J-13 well water was used in all experiments.

Figure E-8. Lithium Sorption Data and Fitted Langmuir Isotherm for the Upper Tram Tuff (c#2, 839 m Below Land Surface)

Output DTN: LA0303PR831341.003.

NOTE: The lithium concentration range in the field test in the central and lower Bullfrog Tuff spanned from less than 0.1 µg/mL up to 1,200 µg/mL. The concentration range in the Prow Pass Tuff field test ranged from less than 0.1 µg/mL up to 2,700 µg/mL.

Figure E-9. Fitted Langmuir Isotherms for the Seven C-Wells Tuffs

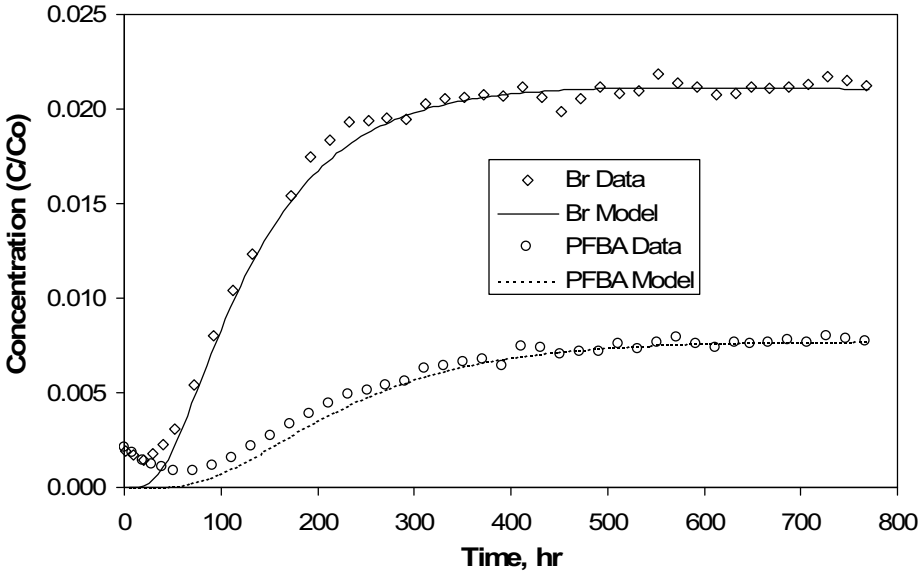

Source: DTN: MO0012DIFFCHOL.000 [DIRS 159243] (data).

Output DTN: LA0303PR831362.001 (DIFFCELL fits).

NOTE: Diffusion coefficients are given in Table E-6.

Figure E-17. Second Diffusion Cell Data (Tracer Concentrations in Outlet Reservoir Normalized to Starting Concentrations in Inlet Reservoir, C_o) and DIFFCELL Fits for Bromide and PFBA in the Lower Prow Pass Tuff

Table E-6. Measured Porosities, Permeabilities, and Matrix Diffusion Coefficients of Bromide and PFBA in C-wells Tuffs

Tuff[a]	Porosity	Permeability (mDarcy)	Thickness[b] (cm)	Diffusion Coefficient ($cm^2/s \times 10^6$)[c]		Br/PFBA (Ratio)
				Br	PFBA	
Central Bullfrog (1)	0.094	0.00107	1.12	0.42	0.12	3.5
Lower Bullfrog (3)	0.298	0.0949	0.79	1.0	0.35	2.86
Upper Prow Pass (4)	0.272	4.72	0.98	6.2	2.0	3.1
Central Prow Pass (5)	0.138	0.000786	1.23	0.38	0.13	2.92
Lower Prow-1 (6)[d]	0.288	0.455	2.27	3.0	1.1	2.73
Lower Prow-2 (6)[d]	0.288	0.455	1.82	2.8	1.0	2.8

Sources: DTNs: MO0012POROCHOL.000 [DIRS 153376] (porosity); MO0012PERMCHOL.000 [DIRS 153368] (permeability); MO0012DIFFCHOL.000 [DIRS 159243] (diffusion cells).

Output DTN: LA0303PR831362.001 (DIFFCELL results – diffusion coefficients).

NOTE: Synthetic J-13 well water was used for the experiments involving the first three tuffs. Filtered J-13 well water was used in the other three experiments.

[a]Numbers in parentheses correspond to numbers in Figure E-1 (locations where core was collected from the C-wells) and in Table E-2 (where actual depths associated with the cores are listed).

[b]Thickness, *L*, of tuff pellet.

[c] Measured matrix diffusion coefficients are equal to values in these columns multiplied by 10^{-6}.

[d]Experiments were conducted using two separate tuff pellets from the Lower Prow Pass Tuff.

PFBA=pentafluorobenzoic acid or pentafluorobenzoate.

Table E-7. Results of RELAP Fits to Rising Limbs of Lithium and Bromide Breakthrough Curves in Crushed Tuff Columns

Column	Figure	Flow Rate (mL/hr)	Lithium Conc. (mg/L)	τ (hr)	*Pe*	R_F	k_f (1/hr)	Da
1[a]	E-20	2.2	23.5	7.6	250	2.0 (2.0)	3.1	24
1	E-21	1.6	23.5	10.3	260	2.0 (2.0)	3.7	38
1[a]	E-22	9.7	20.1	1.8	580	1.8 (1.7)	8.8	16
2[a]	E-23	2.2	5.9	7.7	870	2.3 (2.3)	22	169
2	E-24	1.6	5.9	10.4	750	2.3 (2.25)	4.6	48

Source: DTN: LA0301PR831231.001 [DIRS 162603] (for flow rates and concentrations).

Output DTN: LA0303PR831361.003 (RELAP results).

NOTE: τ = residence time; *Pe* = Peclet number; R_f = retardation factor; k_f = rate constant for sorption onto the column material; and *Da* = Damkohler number (= $k_f\tau$), which represents the ratio of reaction rate to advection rate in the columns. R_f values in parentheses indicate the best-fitting retardation factors when equilibrium sorption was assumed (i.e., very fast sorption kinetics).

[a]Denotes experiments in which tracer concentrations were monitored until background levels were reached.

E3.1.2 Interpretive Methods

The bromide responses in the experiments were interpreted using the RELAP V 2.0 computer code (STN: 10551-2.0-00 [DIRS 159065]) to obtain estimates of mean residence times and dispersivities/Peclet numbers in the columns. RELAP was also used to fit the rising limbs of the lithium responses in each experiment to obtain an estimate of the lithium retardation factor in the columns. The rate-limited sorption features of RELAP were also used to obtain an estimate of the rate constant (k_f) describing lithium sorption onto the column packing material. The rate constants were obtained by relaxing the equilibrium sorption assumption and adjusting the rate constants for each data set until the RELAP fits were optimized. Damkohler numbers ($k_f\tau$), which represent the ratio of reaction rate to advection rate in the columns, were calculated for each experiment. Damkohler numbers significantly greater than one indicate a system that can be treated as being at equilibrium locally (Valocchi 1985 [DIRS 144579], pp. 808 to 820).

It was apparent that while RELAP V 2.0 (STN: 10551-2.0-00 [DIRS 159065]) could fit the arrival of lithium, it could not fit the tails of the lithium responses when concentrations were monitored until they returned to background levels. The tails exhibited a behavior suggesting that a portion of the lithium eluted with the bromide as if it were a nonsorbing tracer. This behavior can occur when an ion-exchanging cation such as lithium comprises the majority of the cation equivalents in the tracer solution, which was certainly the case in the higher-concentration LiBr experiments. Essentially, if the CEC of the tuff and the exchange equilibria are not sufficient to exchange all of the lithium injected into a column, then some of the lithium must elute with the bromide to maintain charge balance in the solution exiting the column. Thus, for the tests in which the lithium was fully eluted from the columns, the MULTRAN V 1.0 computer code (STN: 10666-1.0-00 [DIRS 159068]), which is capable of explicitly modeling cation exchange and maintaining solution charge balance, was used to interpret the lithium responses (see Section E3.2.2 for description of the code).

three cores. The flow rate in at least one of the multiple-tracer experiment in each core was approximately an order of magnitude lower than the flow rate(s) in the other multiple-tracer experiment(s). Flow rates were varied over this large range so that the effect of experiment time scale on matrix diffusion processes could be assessed in fracture systems of constant geometry. The fractures were thoroughly flushed after each experiment so that residual tracer concentrations were minimized in subsequent experiments.

A steady-state flow field was established in each core by continuously injecting degassed, filtered groundwater obtained from well J-13. A pulse of tracer solution (tracers dissolved in J-13 well water) was then injected. After injection of the tracer pulse, continuous injection of tracer-free J-13 well water was resumed. The effluent was monitored for the tracer ions as well as for Na^+ and Ca^{2+} using ion chromatography for $Br^-$and PFBA and ICP-AES for analysis of Li^+, Na^+, and Ca^{2+}. Iodide was analyzed either using an ion-selective electrode or ion chromatography. The quantitative detection limits were 0.05 mg/L for Li^+, Na^+, and Ca^{2+}; 0.04 mg/L for Br^-; 0.02 mg/L for I^-; and 0.02 mg L^{-1} for PFBA. Na^+ and Ca^{2+} were analyzed so that cation-exchange equilibria could be more rigorously quantified than in the crushed-tuff column experiments described in Section E3.1. Copper complexed with ethylenediamine tetraacetic acid was used as a tracer in some of the experiments to determine its potential to serve as a weakly sorbing tracer in field tests. In some of the tests (Tables E-9 through E-13), flow was interrupted for a time after the tracer concentrations had been tailing to verify diffusive mass transfer in the cores (Brusseau et al. 1997 [DIRS 156647], pp. 205 to 219; Callahan et al. 2000 [DIRS 156648]). This strategy was similar to that used in the Prow Pass multiple-tracer field test (Section D4.4).

Table E-8. Experimental Conditions for the Iodide Fracture Transport Tests, Upper Prow Pass Tuff Core (Core 1)

Experimental Parameters			
Core length, L (m)	0.161		
Core width, w (m)	0.095		
Matrix porosity, nm	0.272		
Hydraulic aperture, B_h (m)[a]	0.14×10^{-3}		
Iodide tests:	**Test 1**	**Test 2**	**Test 3**
Volumetric flow rate, Q (mL/hr)	2.2	19.6	8.7
Injection duration, t_p (hr)	28.02	3.08	7.23
Injection concentration, C_o (mg/L)	1,000	1,000	1,000
Flow interruption period, time since start of injection (hr)	N/A[b]	N/A[b]	N/A[b]
Flow rate after restart, Q (mL/hr)	N/A[b]	N/A[b]	N/A[b]
Mass recovery (%)	86	96	94

Source: Reimus 2003 [DIRS 163760], Attachment B1.

[a] Determined from a constant head permeameter method.

[b] N/A: Not applicable; flow was not interrupted during these tests.

Table E-13. Experimental Conditions for the Multiple-Tracer Fracture Transport Tests, Lower Bullfrog Tuff Core (Core 4)

Experimental Parameters	Test 1	Test 2
Volumetric flow rate, Q (mL/hr)	5.0	0.47
Injection duration, t_p (hr)	34.0	335.0
Injection concentration, C_o (mg/L)	165 (Li^+) 342 (Na^+) 0 (Ca^{2+}) 1930 (Br^-) 299 (I^-) 681 (PFBA) 150 (Cu^{2+}) 699 (EDTA)	192 (Li^+) 0 (Na^+) 0 (Ca^{2+}) 1728 (Br^-) 300 (I^-) 635 (PFBA)
Background groundwater concentration, C_i (mg/L)	0.04 (Li^+) 51.1 (Na^+) 11.0 (Ca^{2+}) 0.14 (Br^-) 0.07 (I^-) 0.14 (PFBA)	4.41 (Li^+) 67.2 (Na^+) 16.4 (Ca^{2+}) 60.1 (Br^-) 9.49 (I^-) 16.2 (PFBA)
Flow interruption period, time since start of injection (hr)	67.2 to 87.2	79 to 992
Flow rate after restart, Q (mL/hr)	5.05	0.47
Mass recovery (%)	57 (Li^+) 96 (Br^-) 86 (I^-) 99 (PFBA)	85 (Li^+) 103 (Br^-) 86 (I^-) 91 (PFBA)

Source: Reimus 2003 [DIRS 163760], Attachment B2.

EDTA=ethylenediamine tetraacetic acid; PFBA=pentafluorobenzoic acid.

E3.2.2 Interpretive Methods

The RELAP V 2.0 (STN: 10551-2.0-00 [DIRS 159065]) code was used to interpret the nonsorbing iodide, bromide, and PFBA tracer responses. For the iodide-only experiments conducted in cores 1 and 2, the responses at the three different flow rates were simultaneously fitted, assuming the same Peclet number and matrix diffusion mass transfer coefficient (mass transfer coefficient [MTC] = $\frac{\phi}{b}\sqrt{D_m}$) in each test, and a mean residence time (τ) that was inversely proportional to flow rate. This procedure assumes that the *MTC* and Peclet number have no flow rate or time scale dependence.

For the multiple-tracer tests, the bromide and PFBA responses were simultaneously fitted, assuming that bromide had a matrix diffusion coefficient a factor of three greater than PFBA (this same assumption was used in the field tracer-test interpretations). However, because of the difficulties encountered in fitting the lithium responses in the crushed-tuff column experiments,

and the fact that Na^+ and Ca^{2+} were analyzed in addition to Li^+ in the fractured-core experiments, it was decided to use MULTRAN V 1.0 (STN: 10666-1.0-00 [DIRS 159068]).

Table E-16. Best-Fit Model Parameters for the Multiple-Tracer Tests Conducted in Cores 1 and 2

Modeling Parameters	Core 1, Test 1	Core 1, Test 3	Core 2, Test 1	Core 2, Test 1
Porosity of matrix	0.27	0.27	0.14	0.14
Solute mean residence time, τ (hr) [a]	5.4	40.2	1.95	26.1
Peclet number, *Pe* [a]	4.0	4.0	3.5	3.5
Dispersivity in fracture, $\alpha = \frac{L}{Pe}$ (cm)	4.0	4.0	5.0	5.0
Li^+ Matrix retardation factor, *R* [a]	2.25	1.1	4.2	5.9
Li^+ Matrix partition coefficient, K_d (L/kg)	0.17	0.014	0.19	0.30
Mass transfer coefficient [a], $MTC = \frac{\phi}{b}\sqrt{D_m}$ ($hr^{-0.5}$)	0.80 (Br^-) 0.46 (PFBA)	0.80 (Br^-) 0.46 (PFBA)	0.21 (Br^-) 0.12 (PFBA)	0.21 (Br^-) 0.12 (PFBA)
Fracture aperture, 2*b* (cm) [b]	0.134	0.134	0.07	0.07
Distance to diffusion boundary (fracture half spacing), (cm)	1.9	1.9	0.9	0.9
Matrix diffusion coefficient[c], D_m ($\times 10^{-10}$ m^2/s)	11.0 (Br^-) 3.7 (PFBA)	11.0 (Br^-) 3.7 (PFBA)	0.8 (Br^-) 0.27 (PFBA)	0.8 (Br^-) 0.27 (PFBA)
CEC (meq/kg), Measured	19.9	19.9	43.2	43.2
Q_1 [d]	0.05	0.025	10.2	6.0
Q_2 [d]	0.079	0.04	3.0	0.45

Source: DTN: MO00012POROCHOL.000 [DIRS 153376] (for porosity).

Output DTNs: LA0303PR831361.004 (model results); LA0303PR831231.005.

NOTE: Cores 1 and 2 are shown in Figures E-31 through E-34.

[a] Parameters obtained using RELAP to fit simultaneously the Br^- and PFBA data from the two tests for a given core with the constraint that the D_m ratio for Br^-:PFBA was 3:1. The matrix diffusion coefficient for Li^+ was assumed to be two-thirds the value for Br^-.

[b] Based on the relationship $b = \frac{Q\tau}{Lw}$, where τ is the solute mean residence time.

[c] Determined from the *MTC* using the measured ϕ and the calculated *b*.

[d] Equilibrium ion-exchange coefficients, obtained using MULTRAN to manually "fit" the Li^+, Na^+, and Ca^{2+} data for each test.

MTC = mass transfer coefficient; PFBA = pentafluorobenzoic acid or pentafluorobenzoate.

Table E-17. Best-Fit Transport Parameters for the Multiple-Tracer Tests Conducted in Cores 3 and 4

Transport Parameters	Core 3, Test 1	Core 3, Test 2	Core 4, Test 1	Core 4[a], Test 2
Porosity of matrix	0.29	0.29	0.30	0.30
Solute mean residence time, τ (hr)[b]	0.55	13.6	2.0	21.3
Peclet number, *Pe*[b]	4.5	4.5	130	130
Dispersivity in fracture, $\alpha = \frac{L}{Pe}$ (cm)	2.6	2.6	0.09	0.09
Li^+ Matrix retardation factor, *R*[b]	1.3	1.6	9.2	8.2
Li^+ Matrix partition coefficient, K_d (L/kg)	0.046	0.092	1.33	1.16
Mass transfer coefficient[b], $MTC = \frac{\phi}{b}\sqrt{D_m}$ ($hr^{-0.5}$)	1.32 (Br^-) 0.76 (PFBA)	1.32 (Br^-) 0.76 (PFBA)	1.45 (Br^-) 0.84 (PFBA)	1.45 (Br^-) 0.84 (PFBA)
Fracture aperture, 2*b* (cm)[c]	0.057	0.057	0.049	0.049
Distance to diffusion boundary (fracture half spacing), (cm)	4.4	4.4	4.6	4.6
Matrix diffusion coefficient[d], D_m ($\times 10^{-10}$ m^2/s)	4.6 (Br^-) 1.5 (PFBA)	4.6 (Br^-) 1.5 (PFBA)	3.8 (Br^-) 1.3 (PFBA)	3.8 (Br^-) 1.3 (PFBA)
CEC (meq/kg), Measured	31.9	31.9	179.7	179.7
Q_1[e]	0.1	0.085	6.0	0.2[e]
Q_2[e]	0.08	0.035	0.3	0.12[e]

Source: DTN: MO00012POROCHOL.000 [DIRS 153376] (for porosity).

Output DTNs: LA0303PR831361.004 (simulation results), LA0303PR831231.005.

NOTE: Cores 3 and 4 are shown in Figures E-35 and E-36.

[a] The MULTRAN V 1.0 (STN: 10666-1.0-00 [DIRS 159068]) "fit" shown for Core 4, Test 2 in Figure E-36 was actually obtained assuming sorption in both the fracture and the matrix. The fracture was assumed to have a porosity of 0.9, a CEC of 200 meq/kg, K_1 = 5.0, and K_2 = 50.0. The matrix had a CEC of 179.7 meq/kg, and $K_1 = K_2$ = 0.0223. The resulting fit was somewhat better than the fit assuming sorption only in the matrix.

[b] Parameters obtained using RELAP V 2.0 (STN: 10551-2.0-00 [DIRS 159065]) to simultaneously fit the Br^- and PFBA data from the two tests for a given core with the constraint that the D_m ratio for Br^-:PFBA was 3:1. The matrix diffusion coefficient for Li^+ was assumed to be 2/3 the value for Br^-.

[c] Based on the relationship $b = \frac{Q\tau}{Lw}$, where τ is the solute mean residence time.

[d] Determined from the *MTC* using the measured ϕ and the calculated *b*.

[e] Equilibrium ion exchange coefficients, obtained using MULTRAN V 1.0 (STN: 10666-1.0-00 [DIRS 159068]) to manually "fit" the Li^+, Na^+, and Ca^{2+} data for each test.

MTC=mass transfer coefficient;PFBA=pentafluorobenzoic acid or pentafluorobenzoate.

All of the test results discussed here are consistent with diffusive mass transfer having a strong influence on the migration of solutes in fractured volcanic tuffs. However, at short time and distance scales, there may be a significant influence of diffusion into stagnant free water within fractures in addition to "true" matrix diffusion. Thus, matrix diffusion parameters obtained from laboratory tracer experiments should be used cautiously when predicting contaminant migration at larger scales in fractured media.

Table E-18. Comparison of Matrix Diffusion Coefficients Calculated from Fractured-Core Tracer Tests and from Diffusion-Cell Experiments

Core	Fractured Core D_m (Br^-) (m^2/s)[a]	Diffusion Cell D_m (Br^-) (m^2/s)
Upper Prow Pass (1)	11.0×10^{-10}	6.2×10^{-10}
Central Prow Pass (2)	0.8×10^{-10}	0.38×10^{-10}
Lower Prow Pass (3)	4.6×10^{-10}	2.9×10^{-10} [b]
Lower Bullfrog (4)	3.8×10^{-10}	1.0×10^{-10}

Output DTNs: LA0303PR831362.001 (diffusion cells); LA0303PR831361.004 (fractured cores).

[a] Determined from MTC using the measured matrix porosity and b determined from $b = Q\tau$ (see Tables E-16 and E-17).

[b] Average of two measurements.

MTC=mass transfer coefficient.

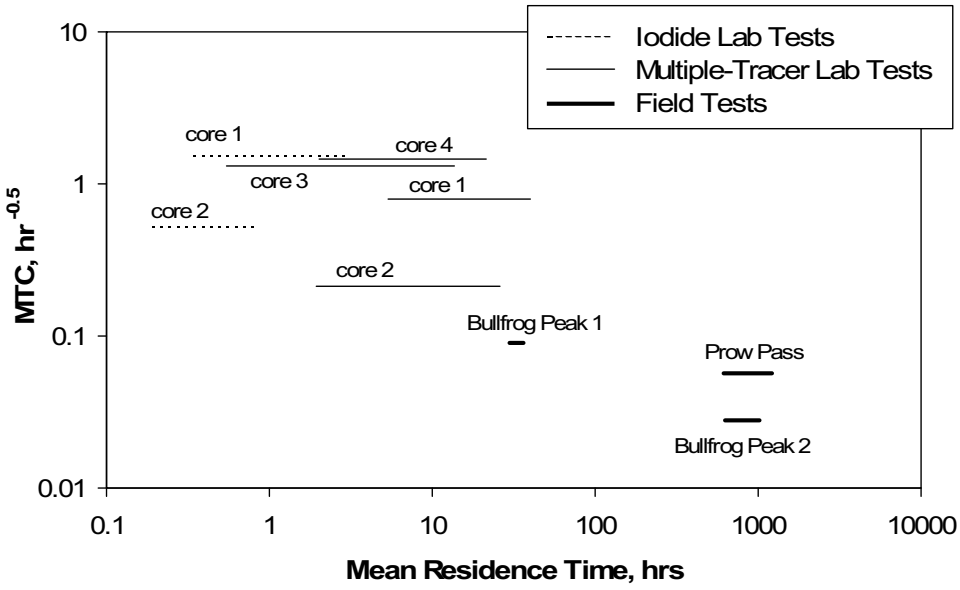

Output DTNs: LA0303PR831231.003 (field data); LA0303PR831361.004 (lab data); LA0303PR831231.005.

NOTE: The lines represent the field tests; endpoints of the lines reflect the uncertainty in the mean residence time depending on whether radial or linear flow is assumed.

The matrix diffusion mass transfer coefficient, MTC, is defined as $\frac{\phi}{b}\sqrt{D_m}$.

The experimental time scale here is the mean residence time.

Figure E-41. Matrix Diffusion Mass Transfer Coefficient as a Function of Experimental Time Scale in All C-Wells Laboratory and Field Multiple Tracer Tests

APPENDIX F

DETAILS OF HYDRAULIC TESTING AND HYDRAULIC TEST INTERPRETATIONS IN SATURATED ALLUVIUM SOUTH OF YUCCA MOUNTAIN

Hydrologic properties of the alluvium have been determined from single-well and cross-hole hydraulic tests at the Alluvial Testing Complex (ATC), which is centered around well NC-EWDP-19D, located just outside the southwest corner of the Nevada Test Site (see Figure 6.1-6) and also at Nye County Site 22, located approximately 4.5 km northeast of the ATC and just east of Fortymile Wash. The ATC tests, which are described in detail in Sections F1 and F2, were interpreted using analytical methods similar to those used for interpretation of the hydraulic tests in fractured tuffs at the C-wells (Section 6.2 and Appendix C). Specifically, the unconfined aquifer solution of Neuman (1975 [DIRS 150321]) and the confined aquifer solution of Theis (1935 [DIRS 150327]) were used to interpret the single-well and cross-hole hydraulic responses, respectively. Although other analytical solutions were considered, the test responses appeared to conform most closely to these two solutions, so they were used for the analyses. The hydraulic tests at Site 22 were interpreted using a multiple-aquifer variation of the confined leaky aquifer solution presented by Hantush (1960 [DIRS 178665]). These tests and their interpretation(s) are discussed in detail in Section F6.

The analytic solutions provide first-order estimates of hydrologic parameters consistent with both the limited knowledge of the nature and extent of subsurface heterogeneities in the alluvium at the scale of the ATC and Site 22 and the manner in which hydrologic parameter estimates are used in the site-scale saturated zone (SZ) flow model. The analytical methods assume that the test interval has one average transmissivity and storativity value. Similarly, the SZ flow model assumes that single average intrinsic hydrologic property (i.e., permeability, porosity) values apply to the alluvium over large spatial areas in the SZ flow system. Furthermore, the hydrologic parameters derived from ATC and Site 22 testing are not used as direct inputs in the site-scale SZ flow model, but rather they are used primarily for qualitative/corroborative consistency checks with the hydrologic parameters derived from calibrations of the SZ flow model. Because of this qualitative end use of the parameter estimates, detailed analyses of the uncertainty and nonuniqueness of the estimates were not conducted.

F1. ATC SINGLE-WELL HYDRAULIC TESTS

Single-well hydraulic testing of the saturated alluvium in well NC-EWDP-19D was conducted between July 2000 and November 2000. This section presents the results and interpretations of those tests. Detailed documentation of the tests is reported by Umari et al. (2003 [DIRS 164573]). The single-well test results are presented here primarily to provide some indication of the variability in hydraulic conductivity that occurs with depth at the ATC location and also to provide information on the alluvium aquifer characteristics (e.g., confined, unconfined). Analyses of single-well step-drawdown tests (Section F1.4), calculations of leakage between screens 4 and 5 in NC-EWDP-19D (Section F1.5), and interpretations of subsequent cross-hole hydraulic tests (Section F2) all indicate that hydraulic conductivity estimates derived from single-well testing in NC-EWDP-19D are biased low because of significant near-wellbore head losses and/or artificial near-wellbore leakage between adjacent intervals. However, it is assumed that the relative values of hydraulic conductivities obtained from different intervals in the single-well tests are valid for comparison purposes, which implicitly assumes that the near-wellbore head losses in each interval (as a fraction of total drawdown) are comparable.

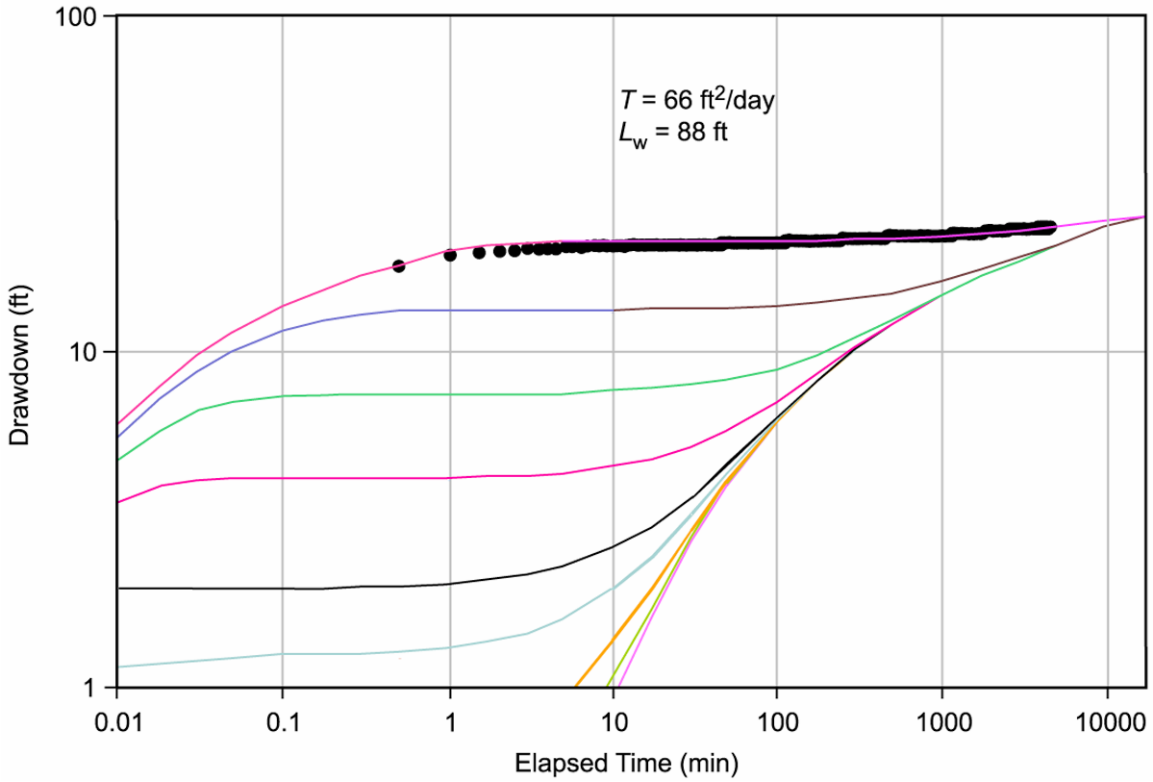

Source: DTN: GS020708312316.001 [DIRS 162678] (data).

Output DTN: GS031008312316.002 (analysis).

NOTE: The chosen type curve fits early- and late-time data simultaneously. L_w is defined in Section F1.3. English units are shown in the figure because the analysis was conducted in English units. However, parameter estimates are reported in metric units to downstream users.

Figure F-4. Drawdown versus Elapsed Time for the Hydraulic Test in Screen #1 of NC-EWDP-19D Overlaid with the Neuman Unconfined Aquifer Type Curves

On October 31, 2000, a hydraulic test in the second interval from the top in the alluvium, screen #2, was started in 19D. Pumping continued at a nominal rate of 17 L/min (19 gpm) until November 6, 2000. Recovery was monitored until November 9, 2000. Figure F-5 presents the drawdown data from the test. It is apparent that, unlike the other isolated interval hydraulic tests in 19D, the drawdown in screen #2 increased at a relatively constant rate. This interval was completed just below a clay-rich layer in the alluvium, and there is a possibility (unconfirmed) that the screen and gravel pack may have been gradually clogging with fines during the test. Figure F-6 presents a fit of the Neuman (1975 [DIRS 150321]) (Neuman.vi V 1.0, STN: 10972-1.0-00 [DIRS 162754]) fully penetrating unconfined aquifer analytic solution to the drawdown data from screen #2, which was obtained following the same procedure of matching the early- and late-time drawdown responses as in the combined-interval test, but with no horizontal shift required. The fully penetrating Neuman solution gives a transmissivity value of 0.70 m^2/day (7.5 ft^2/day) (Output DTN: GS031008312316.002) (see Section F1.3 for correction needed because screen #2 only partially penetrates the total saturated alluvium section).

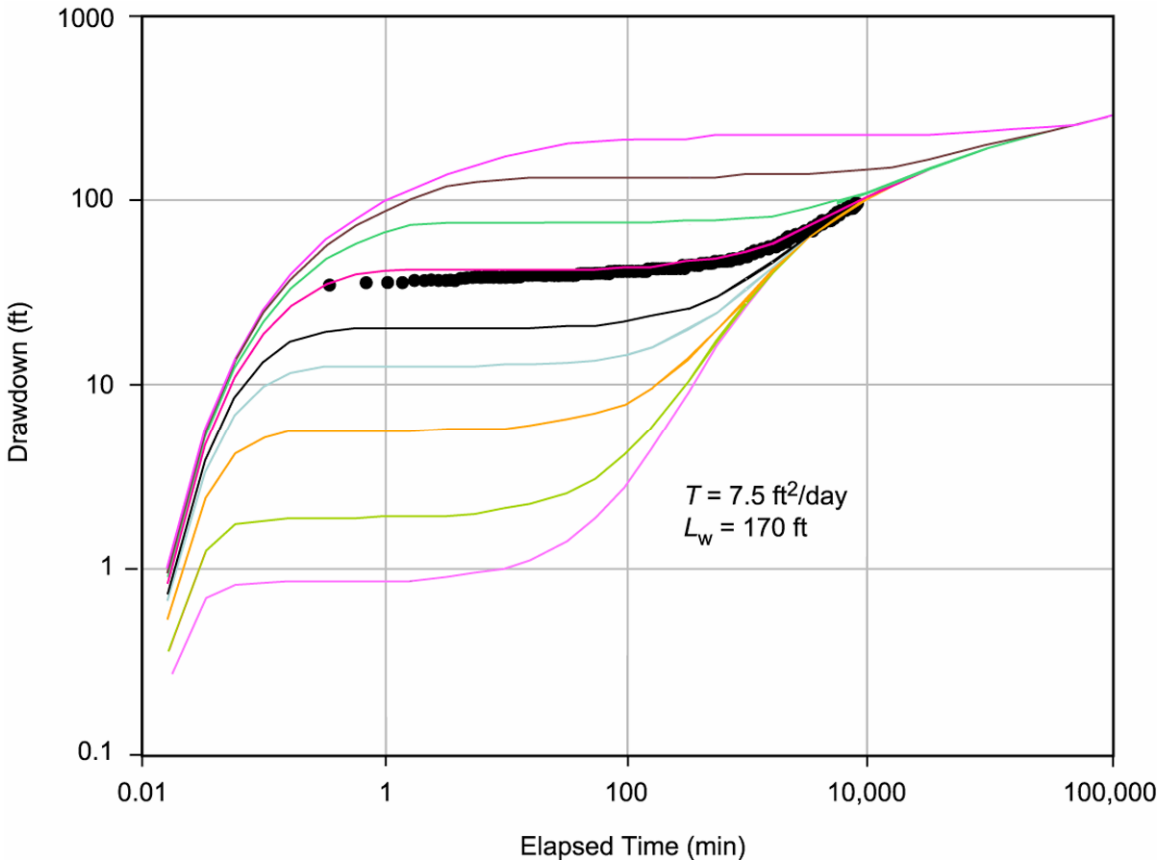

Source: DTN: GS020708312316.001 [DIRS 162678] (data).

Output DTN: GS031008312316.002 (analysis).

NOTE: The chosen type curve fits early- and late-time data simultaneously. L_w is defined in Section F1.3. English units are shown in the figure because the analysis was conducted in English units. However, parameter estimates are reported in metric units to downstream users.

Figure F-6. Drawdown as a Function of Time during the Hydraulic Test in Screen #2, NC-EWDP-19D, Overlaid with the Neuman Unconfined Aquifer Type Curves

On September 9, 2000, a hydraulic test in the second interval from the bottom in the alluvium, screen #3, was started in 19D. Pumping continued at a nominal rate of 314 L/min (83 gpm), with an average of 309.3 L/min (81.7 gpm), until September 16, 2000. Recovery was monitored until September 21, 2000. Figure F-7 presents the drawdown data from this test. The stair-step shape of the drawdown versus time curve suggests that the gravel pack was compacting at discrete times during this test, thus causing nearly instantaneous jumps in the drawdown. Figure F-8 presents a fit of the Neuman (1975 [DIRS 150321]) (Neuman.vi V 1.0, STN: 10972-1.0-00 [DIRS 162754]) fully penetrating unconfined aquifer analytic solution to the drawdown data from screen #3, which was obtained following the same procedure of matching the early- and late-time drawdown responses as in the combined-interval test, but with no horizontal shift required. The fully penetrating Neuman (1975 [DIRS 150321]) solution gives a transmissivity value of 20.7 m^2/day (223 ft^2/day) (see Section F1.3 for correction needed because screen #3 only partially penetrates the total saturated alluvium section).

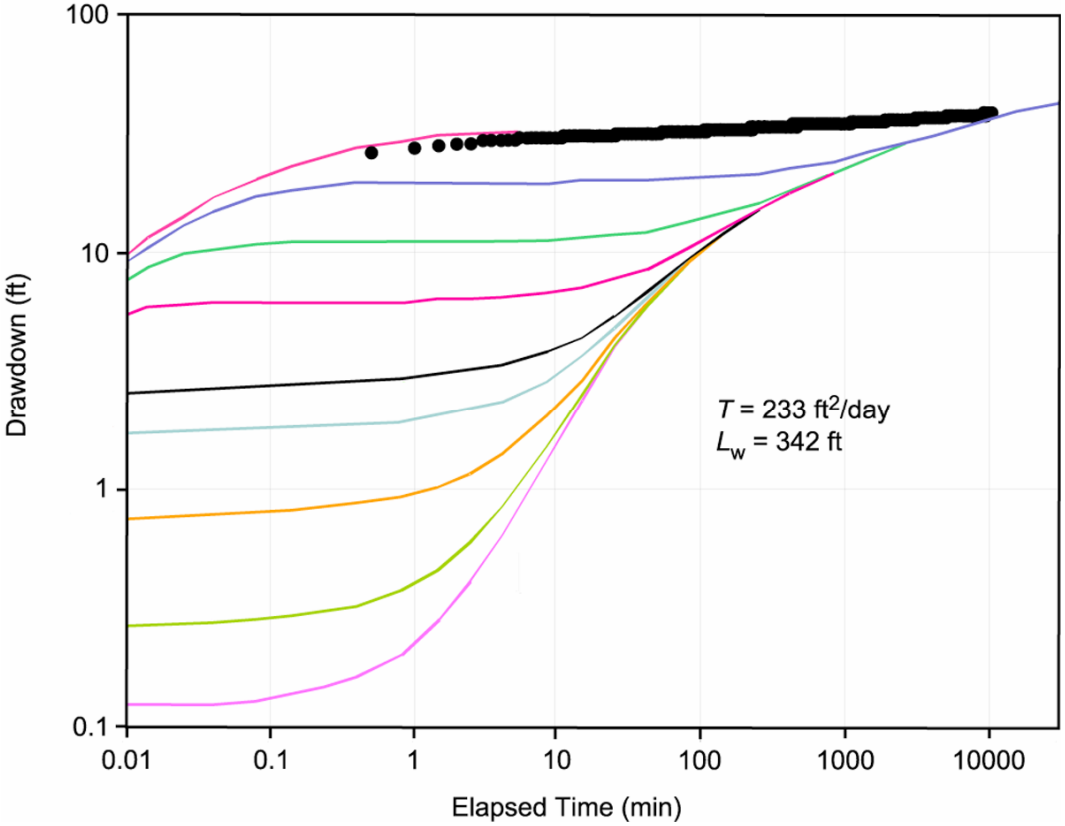

Source: DTN: GS020708312316.001 [DIRS 162678] (data).

Output DTN: GS031008312316.002 (analysis).

NOTE: The chosen type curve fits early- and late-time data simultaneously. L_w is defined in Section F1.3. English units are shown in the figure because the analysis was conducted in English units. However, parameter estimates are reported in metric units to downstream users.

Figure F-8. Drawdown as a Function of Time during the Hydraulic Test in Screen #3, NC-EWDP-19D, Overlaid with the Neuman Unconfined Aquifer Type Curves

On August 24, 2000, a hydraulic test in the lower-most screen in the alluvium section of 19D, screen #4, was started. Pumping continued at the nominal rate of 299 L/min (79 gpm) until August 31, 2000, with an average of 299.8 L/min (79.2 gpm). Recovery was monitored from August 31, 2000, to September 7, 2000. Figure F-9 presents the drawdown data from this test, including both the pumping and recovery periods. Figure F-10 presents a fit of the Neuman (1975 [DIRS 150321]) (Neuman.vi V 1.0, STN: 10972-1.0-00 [DIRS 162754]) fully penetrating unconfined aquifer analytic solution to the drawdown data from screen #4, which was obtained following the same procedure of matching the early- and late-time drawdown responses as in the combined-interval test. The fully penetrating Neuman solution gives a transmissivity value of 28 m^2/day (300 ft^2/day) (Output DTN: GS031008312316.002) (see Section F1.3 for correction needed because screen #4 only partially penetrates the total saturated alluvium section).

The drawdown in the combined screens #5, #6, and #7 interval as a function of elapsed time during the above test in screen #4 beginning on August 24, 2000, is presented in Figure F-19 in Section F1.5, where it is used to calculate the rate of leakage from below the alluvium into the screen #4 interval.

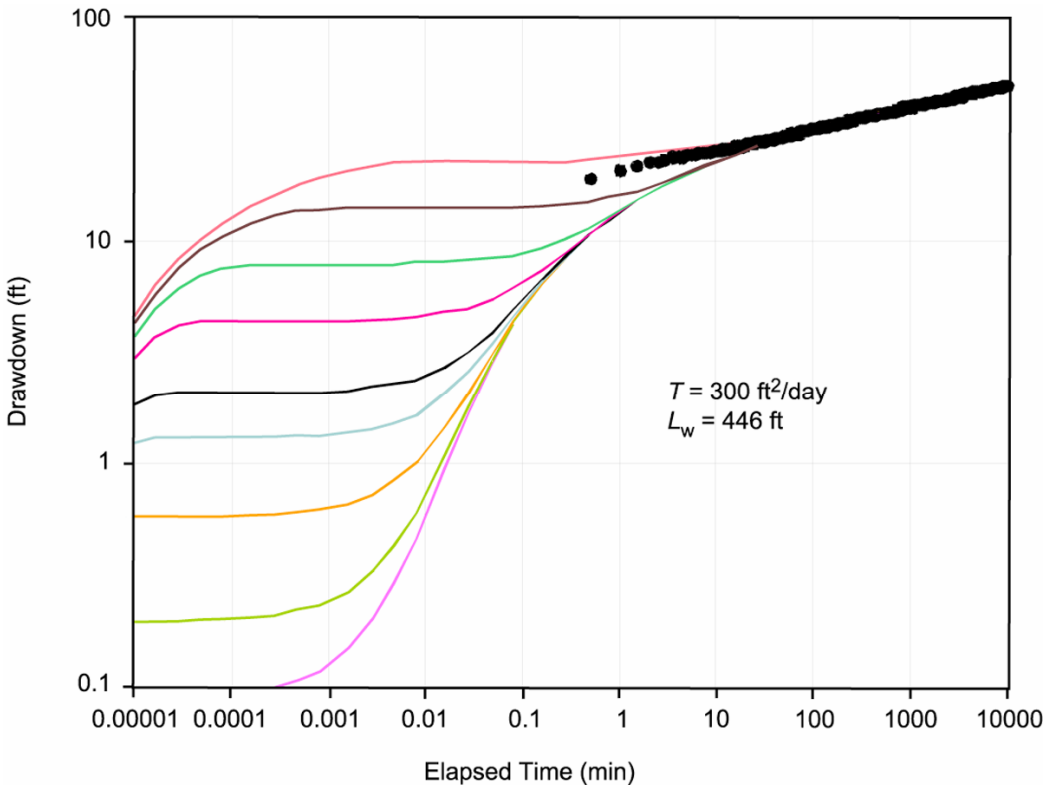

Source: DTN: GS020708312316.001 [DIRS 162678] (data).

Output DTN: GS031008312316.002 (analysis).

NOTE: The matching type curve has been shifted horizontally to emphasize the match to the late-time data. The early time data were also matched by this type curve, although, unlike in Figure F-2, the early-time and late-time type curve (Neuman 1975 [DIRS 150321]) matches are not "spliced" together to show a single composite fit. L_w is defined in Section F1.3. English units are shown in the figure because the analysis was conducted in English units. However, parameter estimates are reported in metric units to downstream users.

Figure F-10. Drawdown as a Function of Time during the Hydraulic Test in Screen #4, NC-EWDP-19D, Overlaid with the Neuman Unconfined Aquifer Type Curves

F1.3 SUMMARY OF SINGLE-WELL HYDRAULIC TESTS IN ALLUVIUM IN NC-EWDP-19D

The hydraulic tests in 19D, screens 1 through 4, were analyzed using the fully penetrating Neuman (1975 [DIRS 150321]) (Neuman.vi V 1.0, STN: 10972-1.0-00 [DIRS 162754]) unconfined aquifer solution because all four individual screens, as well as the combined intervals, exhibited characteristic unconfined aquifer responses. Because each of the screens did not fully penetrate the unconfined alluvial aquifer, they should be analyzed by the partially penetrating Neuman solution. However, there is no Yucca Mountain Project–qualified software to perform this analysis, so the transmissivity, T, values resulting from the Neuman fully penetrating solution should be corrected to account for the length of the screen, L_e, and the depth from the water table to the bottom of the screen being tested, L_w (see, for example, Bouwer 1978 [DIRS 162675], pp. 79 to 82, 114 to 117). An empirical relationship was sought between transmissivity and each of L_e and L_w by plotting transmissivity versus L_e (Figure F-11) and transmissivity versus L_w/b in Figure F-12, where b is the total unconfined alluvial aquifer

F5. SUMMARY OF HYDROLOGIC PARAMETERS IN ALLUVIUM FROM HYDRAULIC TESTING AT THE ATC

The single-hole testing indicated an overall transmissivity for the alluvium of 28 m^2/day (300 ft^2/day) with an associated hydraulic conductivity of 0.20 m/day (0.67 ft/day) (Output DTN: GS031008312316.002). This is a horizontal hydraulic conductivity value with no directional dependence. The transmissivity and hydraulic conductivity estimates were also estimated without assuming any near-wellbore head losses, which apparently were very significant, possibly because of the narrow slots in the well screens and the relatively small particle size of the sand packs in 19D, among other reasons (well efficiency is determined to be 9.1% [Output DTN: GS031008312316.002]; see Section F1.4, Equation F-7). Thus, the true transmissivity and hydraulic conductivity are believed to be approximately an order-of-magnitude higher than the single-hole *apparent* values.

Vertical hydraulic conductivities could not be estimated from the single-well testing, although they were presumably small, because none of the intervals above or below the isolated intervals in the hydraulic tests showed any pressure response during pumping (with the exception of interval #5 in the tuffs, which responded slightly to pumping interval #4). Also, there was minimal response in 19P when pumping any of the intervals in 19D except for screen #1 and the combined-interval test.

Estimates of transmissivity and horizontal hydraulic conductivity were greatly improved after cross-hole hydraulic testing was conducted at the 19D location (Section F2). The cross-hole tests indicated a transmissivity of 306 m^2/day (3,300 ft^2/day) (hydraulic conductivity of 2.0 m/day [6.7 ft/day]), which is about an order of magnitude higher than the transmissivity and hydraulic conductivity values obtained from single-well hydraulic tests. Because of well losses in 19D (well efficiency of 9.1%), the cross-hole transmissivity value of 306 m^2/day (3,300 ft^2/day) is considered to be much more representative of the saturated alluvium in the vicinity of 19D than the single-well transmissivity values of approximately 28 m^2/day (approximately 300 ft^2/day). The cross-hole tests also provided storativity estimates as well as qualitative information on horizontal anisotropy of hydraulic conductivity in the saturated alluvium.

F.6 RESULTS AND ANALYSES OF THE HYDRAULIC TEST DATA AT NYE COUNTY SITE 22

F6.1 INTRODUCTION

This section documents the analysis of the pumping tests at the Nye County Site 22 complex located just east of Fortymile Wash approximately 5 miles north–northwest of Amargosa Valley and about 3 miles northeast of the ATC site (see Figure 6.1-6; Amargosa Valley is labeled "Lathrop Wells" in this figure). Five pumping tests were conducted at this site, and the data from all five tests were analyzed to produce estimates of transmissivity and storativity of the different intervals of the alluvium and underlying volcanic breccia, as well as the leakage parameters between these intervals. The estimated transmissivity and leakage parameter values were used to calculate horizontal and vertical hydraulic conductivities within the different

Table F-1. Zones and Screen Depths in Site 22 Wells

Well Name	Well Zone	Sand Pack Depth Interval, m bgs	Sand Pack Height, m	Screen Top to Bottom Depth, m bgs	Screen Height, m
22S	1	156.5-178.7	22.2	159.0-177.2	18.2
	2	198.7-233.6	35.0	201.5-231.8	30.2
	3	265.3-300.8	35.5	268.3-298.7	30.4
	4	345.4-364.7	19.3	347.5-359.7	12.2
22PA	1	155.1-178.9	23.9	158.7-176.7	18.0
	2	198.0-237.7	39.7	201.6-231.6	30.0
22PB	3	265.4-301.5	36.1	268.6-298.6	30.0
	4	343.0-365.7	22.7	347.6-359.6	12.0

Source: DTN: LA0705PR150304.007 [DIRS 181202].
bgs = below ground surface.

The first pumping test was conducted in March of 2002. All four zones in well 22S were simultaneously pumped in this test. The test was preceded by spinner tests and background observations. The test began on March 19, 2002. It was interrupted once for about 1 hour after 19 hours of pumping due to a pump shut down and was resumed for another 5 hours after that. Recovery was observed for about 15 hours. The pumping rate was apportioned to the four screened intervals in 22S in accordance with the spinner test results (see Table F-2). The MOSDAX™ pressure sensor readings recorded during this test are available from DTN: LA0705PR150304.008 [DIRS 181203].

The data in DTN LA0705PR150304.008 [DIRS 181203] are unqualified. The data qualification is described in Appendix N. The data are qualified for use in this analysis only. The pumping test interpretation was conducted for the Nye County Department of Natural Resources and Federal Facilities Nuclear Waste Repository Project Office under Grant # DE-FC28-02RW12163 by Questa Engineering Corporation. The field data, analyses, and interpretation are documented in *Preliminary Analysis of Pump-Spinner Tests and Pump Test in Well NC-EWDP-22S, Near Yucca Mountain, Nevada* (Questa Engineering Corporation 2003 [DIRS 178565]).

The 4 subsequent pumping tests were conducted in August to September of 2003. Only one zone in the well 22S was pumped in each test. Each test was preceded by background observations. The pumping was conducted for about 11 hours and was followed by observation of the recovery. The MOSDAX™ pressure sensor readings recorded during these tests are available from DTNs: LA0705PR150304.009 [DIRS 181204], LA0705PR150304.010 [DIRS 181205], LA0705PR150304.011 [DIRS 181207], and LA0705PR150304.012 [DIRS 181208]. The data in these DTNs are unqualified. The data qualification is described in Appendix N. These data are qualified for use in this analysis only.

The pumping test interpretation was conducted for the Nye County Department of Natural Resources and Federal Facilities Nuclear Waste Repository Project Office under Grant # DE-FC28-02RW12163 by Questa Engineering Corporation. The field data, analyses, and interpretation are documented in *Analysis of Aquifer Pump Tests in Individual Well Zones at Site 22 Near Yucca Mountain, Nevada* (Questa Engineering Corporation 2004 [DIRS 178566]). The

first pumping test in the series of isolated interval tests began on August 5, 2003, with Zone 1 in 22 S pumped at the rate of 43.5 gpm. The second test began on August 12, 2003, with Zone 2 in

22 S pumped at the rate of 44.1 gpm. The third test began on September 9, 2003 with Zone 3 in 22 S pumped at the rate of 27.1 gpm, and the last test began on September 23 of 2003 with Zone 4 in 22 S pumped at the rate of 20.5 gpm.

Table F-2. Summary of the Pumping Test Duration and Rates

Test Date	Pumping Period Duration (hrs)	Recovery Period Duration (hrs)	Pumping Rate in m^3/day (gpm)			
			Zone 1	Zone 2	Zone 3	Zone 4
03-19-02 8:40:00 AM	19.33*	–	240.39 (44)	288.90 (53)	125.37 (23)	70.86 (13)
08-05-03 5:24:00 AM	11.06	45.42	237.12 (43.5)	–	–	–
08-12-03 5:21:20 AM	11.14	37.47	–	240.39 (44.1)	–	–
09-09-03 5:48:50 AM	10.73	14.62	–	–	147.72 (27.1)	–
09-23-03 5:36:30 AM	10.86	15.13	–	–	–	111.75 (20.5)

Output DTN LA0701EK150304.001

NOTE: *The pump was shut down for an hour after 19.33 hrs of pumping and the pumping period data after the pumping was resumed were not used as well as the recovery period data.

The analysis presented in this section is based on the same input data (pressure readings, pumping rates, and well information) as the analyses presented in *Preliminary Analysis of Pump-Spinner Tests and Pump Test in Well NC-EWDP-22S, Near Yucca Mountain, Nevada* (Questa Engineering Corporation 2003 [DIRS 178565]) and in *Analysis of Aquifer Pump Tests in Individual Well Zones at Site 22 Near Yucca Mountain, Nevada* (Questa Engineering Corporation 2004 [DIRS 178566]). However, the processing of the input data was conducted independently and the data interpretation methods are different, as will be discussed below. The results obtained in this analysis are compared to the results obtained in *Preliminary Analysis of Pump-Spinner Tests and Pump Test in Well NC-EWDP-22S, Near Yucca Mountain, Nevada* (Questa Engineering Corporation 2003 [DIRS 178565]) and in *Analysis of Aquifer Pump Tests in Individual Well Zones at Site 22 Near Yucca Mountain, Nevada* (Questa Engineering Corporation 2004 [DIRS 178566]) below as appropriate.

F6.2 INPUT DATA AND INITIAL DATA PROCESSING

As discussed above, the input data were taken from the input DTNs: LA0705PR150304.008 [DIRS 181203], LA0705PR150304.009 [DIRS 181204], LA0705PR150304.010 [DIRS 181205], LA0705PR150304.011 [DIRS 181207], and LA0705PR150304.012 [DIRS 181208]. The data in the DTNs consist of a number of files generated by the MOSDAX data acquisition system. Each file has a header with the test identification information and a description of probes and actual readings consisting of the date and time of reading and the pressures and temperatures measured at the corresponding probes. The data are divided into a few time periods. Two sets of data are provided for each time period. The data in the first set (pressures and temperatures) are for well 22S and zone 1 in well 22PA. This set will be referred to as Set 1. The data in the second set (pressures and temperatures) are for well 22PA zone 2 and well 22PB zone 3 and zone 4. This

Table F-3. Results of the Correlation and Linear Regression Analysis Using Background Pressures in the Different Aquifer Zones

Estimated Parameters	Pressures (Zones 2 and 3)		Pressures (Zones 2 and 4)		Pressures (Zones 3 and 4)	
Correlation coefficient	0.89		0.93		0.95	
Linear Regression Equations	$p_2 = ap_3+c$	$p_3 = ap_2+c$	$p_2 = ap_4+c$	$p_4 = ap_2+c$	$p_3 = ap_4+c$	$p_4 = ap_3+c$
Slope (a)	1	1	1.052	0.83	0.99	0.80
Intercept (c)	0	0	−1.166	4.017	0.27	4.805

Output DTN: LA0701EK150304.001.

NOTE: p_2, p_3, and p_4 are the background pressures in zones 2, 3, and 4 correspondingly.

(b) Multiple-Layers Conceptual Model

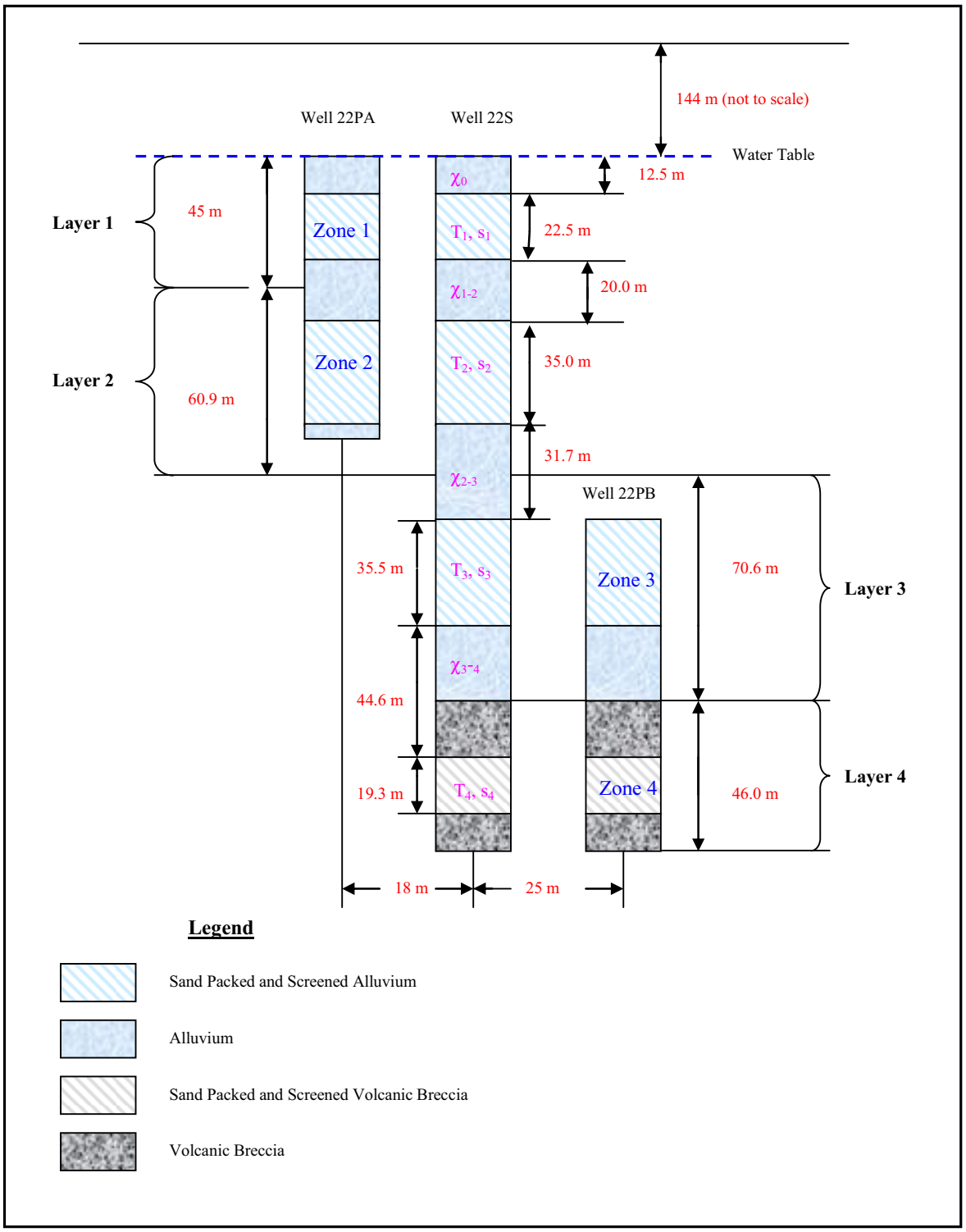

NOTE: For illustration purposes only.

Figure F-28. Site 22 Schematic in the Vertical Cross Section (Continued)

- Leakage parameter χ_{i-1} [T^{-1}]
- Leakage parameter χ_{i+1} [T^{-1}].

The parameter, χ_{i+1}, represents the connection of the adjacent aquifer to the 3rd aquifer that may contribute water to this aquifer, but which is not affected by pumping of the main aquifer. The parameter χ_{i-1} represents the connection of the main aquifer to the adjacent aquifer that may contribute water to this aquifer, but which is not affected by pumping of the main aquifer. In the case of an isolated system, χ_{i-1} and χ_{i+1} are equal to 0. In the case of semi-open system, either χ_{i-1} or χ_{i+1} is not zero, or both of them are not zero.

The equations for non-steady multiple-aquifer flow towards a well are formulated by Maas (1986 [DIRS 178614]). In the case of two aquifers, the Maas (1986 [DIRS178614]) equations can be written as:

$$s_i \frac{\partial S_i}{\partial t} = T_i \nabla S_i + \chi_i (S_{i+1} - S_i) - \chi_{i-1} S_i$$

and (Eq. F-28)

$$s_{i+1} \frac{\partial S_{i+1}}{\partial t} = T_{i+1} \nabla S_{i+1} + \chi_i (S_i - S_{i+1}) - \chi_{i+1} S_{i+1},$$

$$\nabla S_i = \frac{1}{R} \frac{\partial}{\partial R} \left(R \frac{\partial S_i}{\partial R} \right) \quad \nabla S_{i+1} = \frac{1}{R} \frac{\partial}{\partial R} \left(R \frac{\partial S_{i+1}}{\partial R} \right)$$

where S_i and S_{i+1} are drawdowns in the main and adjacent aquifers correspondingly.

The boundary conditions are:

$$R \frac{\partial Si}{\partial R}\bigg|_{R->r_{well}} = \frac{Qi}{2\pi T_i} \text{ and } R \frac{\partial S_{i+1}}{\partial R}\bigg|_{R->r_{well}} = \frac{Q_{i+1}}{2\pi T_{i+1}} \quad \text{(Eq. F-29a)}$$

$$S_1\big|_{r\to\infty} = 0, \text{ and } S_2\big|_{r\to\infty} = 0 \quad \text{(Eq. F-29b)}$$

where r_{well} is the radius of the pumping well and Qi is the pumping rate from the main aquifer. In a general case, an adjacent aquifer may be pumped as well with the pumping rate Q_{i+1}. If it is not pumped, Q_{i+1} is set equal to zero.

The system of equations F-28, F-29a, and F-29b has an analytical solution in only a few special cases. One of these is when the system is closed ($\chi_{i+1} = \chi_{i-1} = 0$) and $T_i/s_i = T_{i+1}/s_{i+1}$ (Hantush 1960 [DIRS 178665]).

Equations F-28, F-29a, and F-29b can be rewritten using Laplace transforms as shown below to eliminate the time derivative and obtain a system of ordinary differential equations that can be solved analytically.

accurate. The simplified approach of correcting the pressures does not allow for excluding all the possible noises that affect the drawdowns in the adjacent zones. To provide a measure of the goodness of fit, the root mean square errors are calculated for the drawdowns in all the aquifers using the formula:

$$Err_i = [\sum_{j=1,N} [S_c^i(t_j) - S_m^i(t_j)]^2 / N]^{\frac{1}{2}} \quad \text{(Eq. F-39)}$$

i = 1,2 (2 aquifer system) and i = 1,3 (3 aquifer system)

F6.7 IMPLEMENTATION OF THE ANALYSIS

All three mathematical models described above were implemented using MathCAD®. One MathCAD application was developed for each pumping test (output DTN: LA0701PR150304.001). The built-in MathCAD® functions, such as the *Ko* (modified Bessel) function, the calculation of integrals and factorials, data smoothing function, and minimization procedure were used.

Each application does the following:

- Reads the drawdown versus time data for pumping and recovery periods. These data are copied from the corresponding Excel file where the initial data processing was done, into a built-in Excel file within MathCAD®. The data are already corrected for the ambient pressure fluctuation (if needed). This is discussed in more detail when each test is considered below.
- Displays the input data.
- Defines the pumping rate(s) and the distance to the monitoring wells.
- Implements the calculations related to the leaky aquifer conceptual model, Equations F-26 and F-27.
- Defines the objective function using Equation F-38.
- Uses minimization procedure to estimate leaky-aquifer parameters T_i, s_i, and B_i.
- Displays the calculated versus measured drawdowns versus time and calculates root mean square error using Equation F-39 and i = 1.
- Defines the input parameters required for the two-aquifer system conceptual model.
- Implements two-aquifer system calculations, Equations F-30, F-31, and F-32.
- Displays the calculated versus measured drawdowns versus time in the first and in the second aquifers and calculates root mean square errors using Equation F-39.

- Defines the input parameters required for the three-aquifer system conceptual model.
- Implements three-aquifer system calculations, Equations F-34, F-35, and F-36.
- Displays the calculated versus measured drawdowns versus time in the first, second, and third aquifers and calculate root mean square errors using Equation F-39.

The MathCAD® application developed for the pumping test when all four zones were pumped only implements the three-aquifer system solution as discussed in detail later in this appendix. The MathCAD® applications developed for the pumping tests from zones 2 and 3 implement the leaky aquifer and three-aquifer system solutions. The MathCAD® application developed for the zone 4 pumping test implements the leaky aquifer and two-aquifer system solutions. All three solutions are implemented in the MathCAD® application developed for the zone 1 pumping test.

In the discussion provided below the aquifer parameters are denoted in accordance with the Figure 28 notations. This is somewhat different from the general cases described in Equations F-26 through F-39. For example, the actual zone numbers are used instead of indexes $i-1$, i, and $i+1$.

F6.7.1 Pumping Test in Zone 1

During the pumping test from zone 1, the ambient fluctuations of the hydraulic heads were relatively small. The ambient fluctuations were taken to be the fluctuations observed in zone 4, which is separated from zone 1 by the two intermediate zones. Zone 4 appeared to be unaffected by pumping while zones 2 and 3 showed some response to pumping. The drawdown versus time and recovery versus time data were in good agreement in all 4 zones, indicating that ambient pressure fluctuations, which were different during the pumping and recovery periods, had negligible impact on the drawdown curves. Consequently, it was decided not to correct the drawdowns in zones 1, 2, and 3. The same conclusion was reached in *Analysis of Aquifer Pump Tests in Individual Well Zones at Site 22 Near Yucca Mountain, Nevada* (Questa Engineering Corporation 2004 [DIRS 178566]).

Zone 1 in 22S was pumped for 11 hrs and 3.5 min at a pumping rate of 237.1 m^3/day (43.5 gpm). The recovery was observed for 45 hrs and 25 min. The observations in zone 1 are available for well 22PA located 18 m from the pumping well. The observations for zone 2 are in 22PA deep (18 m from the pumping well), and for zones 3 and 4 they are in 22PB shallow and deep (25 m from the pumping well). All three mathematical solutions were applied to the data, as described below. The resulting parameter estimates provided at the end of Section F6.7.5.

F6.7.1.1 Leaky Aquifer Solution

Based on the model assumptions (no drawdowns in adjacent aquifers), only the drawdown data for zone 1 (22PA shallow) are used in this analysis. The drawdowns observed during pumping and recovery periods in well 22PA shallow were combined. As a result, the vector S_m in equation F-38 includes both pumping and recovery data. The total number of observations is 10,700. The drawdowns S_c in equation F-38 are calculated in the same 10,700 time points as the observed drawdowns.

As described above, the leaky aquifer solution has three parameters. The parameter estimates obtained by minimizing the objective function defined in equation F-38 are:

$T_1 = 264.2$ m^2/day
$s_1 = 0.00132$
$B_1 = 32.5$ m.

The measured and calculated drawdowns are shown in Figure F-29. The root mean square error is 6.3 mm.

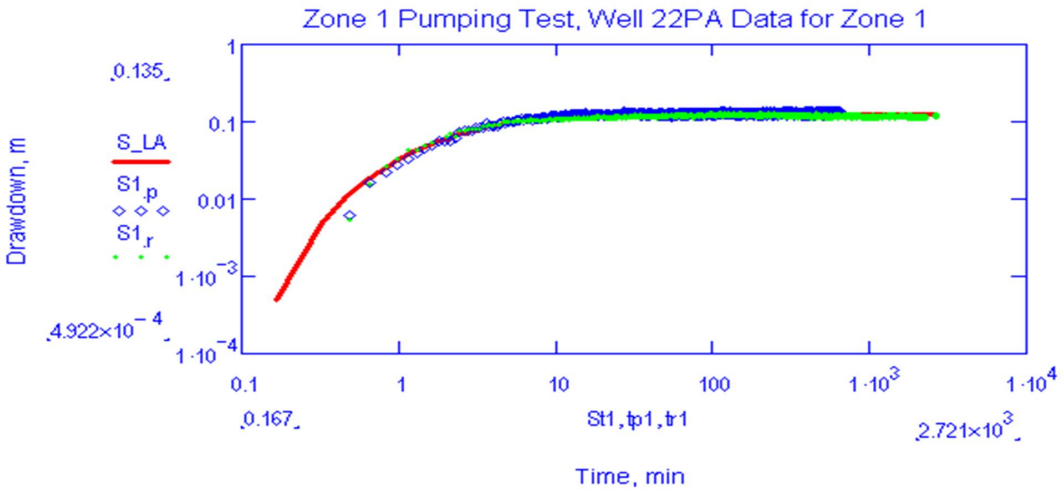

Output DTN: LA0701EK150304.001 (produced by MathCAD application *Zone 1.xmcd*).

NOTE: Red solid line shows the calculated drawdowns; blue diamonds show the drawdowns during pumping period; green dots show the drawdowns during the recovery period; and the green solid line shows the smoothed data (averaged drawdowns).

Figure F-29. Zone 1 Pumping Test, Leaky Aquifer Solution

Based on the zone 1 thickness of 22.2 m, the hydraulic conductivity of zone 1 is 11.9 m/day. Based on equation F-26, $(\chi_{1-2} + \chi_0) = 0.25$ day^{-1}. The high estimated storativity value indicates possible unconfined conditions in zone 1.

The parameter estimates reported in *Analysis of Aquifer Pump Tests in Individual Well Zones at Site 22 Near Yucca Mountain, Nevada* (Questa Engineering Corporation 2004 [DIRS 178566]) based on using the Hantush inflection point method (Hantush 1956 [DIRS 165169]) were:

$T_1 = 242$ m^2/day
$s_1 = 0.0016$
$B_1 = 29.9$ m.

These values are in good agreement with the estimates obtained from the method described above.

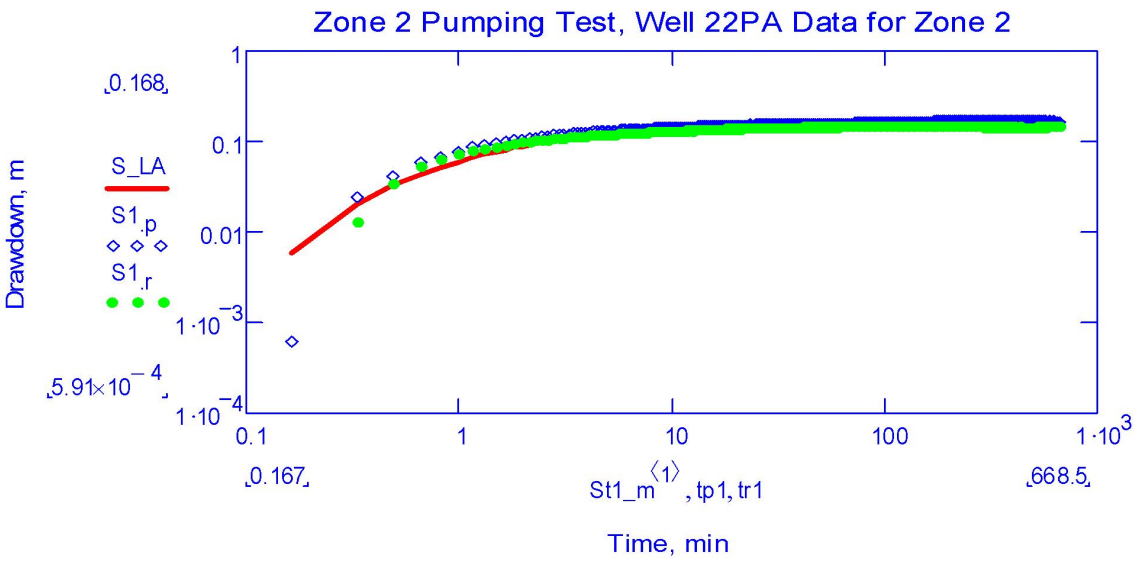

Output DTN: LA0701EK150304.001 (produced by MathCAD application *Zone 2.xmcd*).

NOTE: Red solid line shows the calculated drawdowns; blue diamonds show the drawdowns during pumping period; and green dots show the drawdowns during the recovery period.

Figure F-32. Zone 2 Pumping Test, Leaky Aquifer Solution

Assuming a zone 2 thickness of 35 m (sand pack thickness), the hydraulic conductivity of zone 2 is 9.3 m/day. Based on Equation F-26, $(\chi_{1-2} + \chi_{2-3}) = 0.11$ day^{-1}. This value is the same as the value estimated from the zone 1 pumping test.

The high estimated storativity value suggests it is likely that unconfined conditions exist in zone 2.

The estimated transmissivity and storativity of zone 2 are lower than the ones estimated from the zone 1 pumping test. The transmissivity and storativity are very sensitive to the absolute drawdown values. When zone 1 was pumped, the drawdowns in zone 2 were very small and affected by noise. This could have affected the estimation results. The parameters χ_{1-2} and χ_{2-3} are most sensitive to *differences* in the heads in zones 1 and 2 and these differences are less affected by noise in zone 2. Thus, the estimates of these parameters from pumping zones 1 and 2 are more consistent than the estimates of transmissivity and storativity.

The parameter estimates reported in *Analysis of Aquifer Pump Tests in Individual Well Zones at Site 22 Near Yucca Mountain, Nevada* (Questa Engineering Corporation 2004 [DIRS 178566]) based on using the Hantush inflection point method (Hantush 1956 [DIRS 165169]) were:

$T_2 = 427$ m^2/day
$s_2 = 0.00035$
$B_2 = 85.0$ m.

These estimates are somewhat different (transmissivity and leakage factor are higher and storativity is lower) from those provided above. The inflection point method uses the slope of the straight portion of the drawdown curve and maximum (steady-state) drawdown to estimate

these parameters. As shown in Figure F-33, the estimates are greatly affected by the way the actual data are approximated by the straight line and by the maximum drawdown selected.

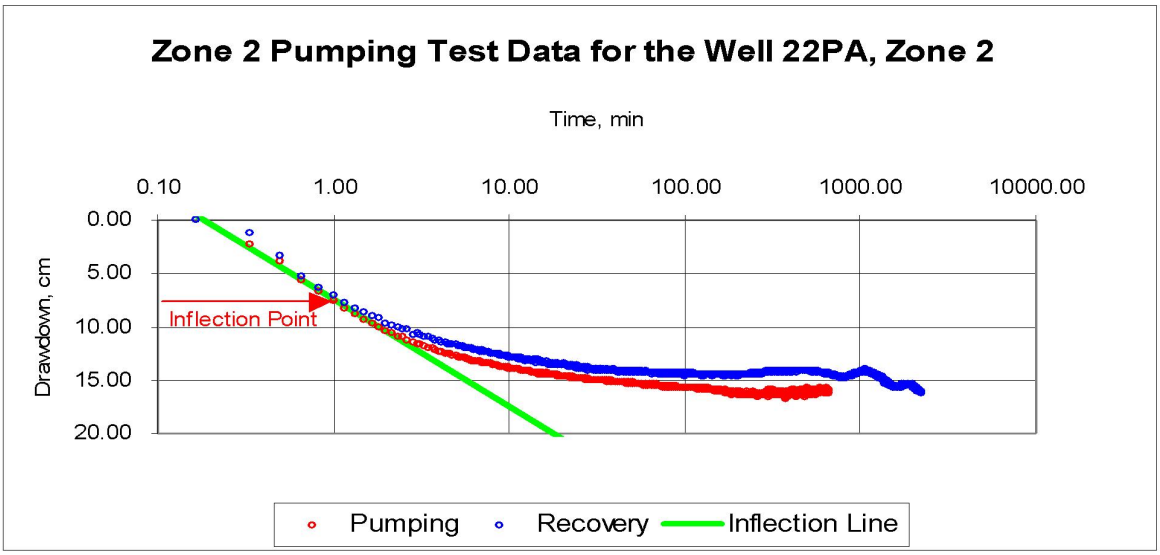

Output DTN: LA0701EK150304.001 (*Zone 2.xls*).

Figure F-33. Application of the Inflection Point Method to Zone 2 Pumping Test

The inflection line in this figure is drawn using linear regression and slope is calculated as the slope of the linear regression line. The maximum drawdown is assumed to be 0.15 m. The resulting parameters calculated using formulae (F-66) are:

$T = 299$ m^2/day
$s = 0.00054$
$B = 47.4$ m.

These estimates are very close to the ones obtained using minimization of the objective function defined in equation F-38.

F6.7.2.2 Three-Aquifer Solution

In this analysis, it was assumed that the pumping of zone 2 affects zone 1 and zone 3 and does not affect zone 4. The same data for zone 2 (22PA deep) are used in the analysis. In addition, the drawdowns in zone 1 (22PA shallow) and in zone 3 (22PB shallow) are used. The manually-adjusted parameter estimates providing the best visual fit to the drawdowns in zones 1, 2, and 3 are:

$T_1 = 280$ m^2/day
$s_1 = 0.0017$
$T_2 = 400$ m^2/day
$s_2 = 0.0007$
$T_3 = 170$ m^2/day
$s_3 = 0.0003$

(13 gpm) for zones 1, 2, 3, and 4, respectively. Pumping was interrupted after 19 hrs for about one hour and then it was resumed. Only the drawdown data obtained before this interruption were analyzed. The observations used in the analysis are from zone 1 in 22PA shallow (18 m from the pumping well), zone 3 in 22PB shallow (25 m from the pumping well), and zone 4 in 22PB deep (also 25 m from the pumping well). The three-aquifer solution was used to interpret the data. The resulting parameter estimates are summarized in Table F-4.

F6.7.5.1 Three-Aquifer Solution

To apply the three-aquifer solution, zones 1 and 2 were combined and assumed to be a single aquifer. The pumping tests from zones 1 and 2 indicated that these zones have very similar hydraulic properties and are well connected hydraulically. Consequently, combining these two zones is justified. The pumping rate from combined zones 1 and 2 was assumed to be equal to the sum of the individual zone pumping rates.

The manually-adjusted parameter estimates providing the best visual fit to the drawdowns in all three zones are:

$T_{1+2} = 1{,}000$ m^2/day
$s_{1-2} = 0.003$
$T_3 = 130$ m^2/day
$s_3 = 0.0003$
$T_4 = 250$ m^2/day
$s_4 = 0.0003$
$\chi_{2-3} = 0.01$
$\chi_{3-4} = 0.02$
$\chi_0 = 0.15$.

The measured and calculated drawdowns in zones 1+2, 3, and 4 are shown in Figure F-40. The root mean square error is 18.0 mm for zones 1 and 2, 14 mm for zone 3, and 14 mm for zone 4.

Table F-4. Summary of the Parameter Estimates for Nye County Site 22 (Continued)

Parameter Notation	Zone 1 Pumping Test			Zone 2 Pumping Test		Zone 3 Pumping Test		Zone 4 Pumping Test		All Four Zones Pumping Test	Range	Average	Questa Engineering Company 2003 [DIRS 178565], Table 2	Questa Engineering Company 2004 [DIRS 178566], Table 3
	Leaky Aquifer	Two-Aquifer System	Three-Aquifer System	Leaky Aquifer	Three-Aquifer System	Leaky Aquifer	Three-Aquifer System	Leaky Aquifer	Two-Aquifer System					
$\chi_{2-3} + \chi_{3-4}$, day^{-1}	—	—	—	—	—	0.0126	—	—	—	—	—	—	—	0.0119
T_1+T_2, m^2/day	—	—	—	—	—	—	—	—	—	1,000	—	—	—	—
s_{1-2}	—	—	—	—	—	—	—	—	—	0.003	—	—	—	—

Output DTN: LA0701EK150304.001.

NOTES: χ_0 = ratio of the hydraulic conductivity in m/day and thickness in m of the layer above zone 1; T_i = transmissivity of zone i in m^2/day; s_i = storativity of zone I; χ_{i-j} = the ratio of the hydraulic conductivity in m/day and thickness in m of the layer between zones *i* and *j;* T_1+T_2 = the transmissivity of the combined zone 1 and zone 2; s_{1-2} = storativity of combined zone 1 and zone 2.

Well efficiency can be estimated from equation F-42 as:

$$\varepsilon = \frac{Q}{2\pi TS_{\max}} \log\left(\frac{1.12B}{r_w}\right) \quad \text{(Eq. F-43)}$$

Equation F-43 was used to estimate well efficiencies in all 5 pumping tests. The maximum drawdown in 22S observed in each test was used in these estimations. The calculations were done for the transmissivity ranges obtained from the multiple-aquifer and multiple-layer solutions. The leakage factor B was set equal to the leakage factor obtained from the corresponding leaky aquifer solution. In the case when all four zones were pumped, the combined transmissivity (sum of transmissivities in all four zones) was used. The leakage factor B was calculated using equation F-26 assuming that $\chi_{1-2} = 0.15$ (influx from the water table) and $\chi_{2-3} = 0.0$ (no flow boundary condition at the bottom). The resulting well efficiencies are provided below. The numbers in the parentheses are the well efficiencies estimated in *Analysis of Aquifer Pump Tests in Individual Well Zones at Site 22 Near Yucca Mountain, Nevada* (Questa Engineering Corporation 2004 [DIRS 178566]):

- Zone 1 Pumping Test: $\varepsilon = 25.8\%$ to 27.5% (30%)
- Zone 2 Pumping Test: $\varepsilon = 10.5\%$ to 17.8% (16%)
- Zone 3 Pumping Test: $\varepsilon = 21.6\%$ to 29.9% (27%)
- Zone 4 Pumping Test: $\varepsilon = 11.6\%$ to 14.6% (15%).

The average well efficiency weighted according to the individual zone thickness is 17.0%. The average well efficiency estimated in *Analysis of Aquifer Pump Tests in Individual Well Zones at Site 22 Near Yucca Mountain, Nevada* (Questa Engineering Corporation 2004 [DIRS 178566]) is 22%. The well efficiencies estimates in *Analysis of Aquifer Pump Tests in Individual Well Zones at Site 22 Near Yucca Mountain, Nevada* (Questa Engineering Corporation 2004 [DIRS 178566]) agree with the well efficiency ranges estimated using this simplified approach.

The well efficiency calculated based on pumping all four zones in 22S is 16.8%. This is in good agreement with the average efficiency calculated from the individual zone pumping tests.

F6.10 SUMMARY OF THE SITE 22 HYDRAULIC TEST DATA INTERPRETATION

The interpretation of the pumping tests conducted at Site 22 was performed using different conceptual models and different methods. As a result, there are a number of estimates for each parameter. In some cases up to 6 estimates for a parameter are available (see Table F-4). The range of parameter estimates reflects the uncertainties in the system conceptualizations and in the mathematical solutions employed. A summary of the parameter estimates is provided below.

As discussed earlier, the transmissivity and storativity of each aquifer (layer) and the parameters χ_{1-2}, χ_{2-3}, and χ_{3-4} are the same regardless which system conceptualization (multiple-aquifers or multiple-layers) is assumed. However, the hydraulic conductivities are different because the aquifer thickness is different from the layer thickness (see Figure F-28). Similarly, the hydraulic conductivity of a low permeability layer between aquifers in the multiple-aquifer conceptualization may be different from the vertical hydraulic conductivity of a horizontal layer

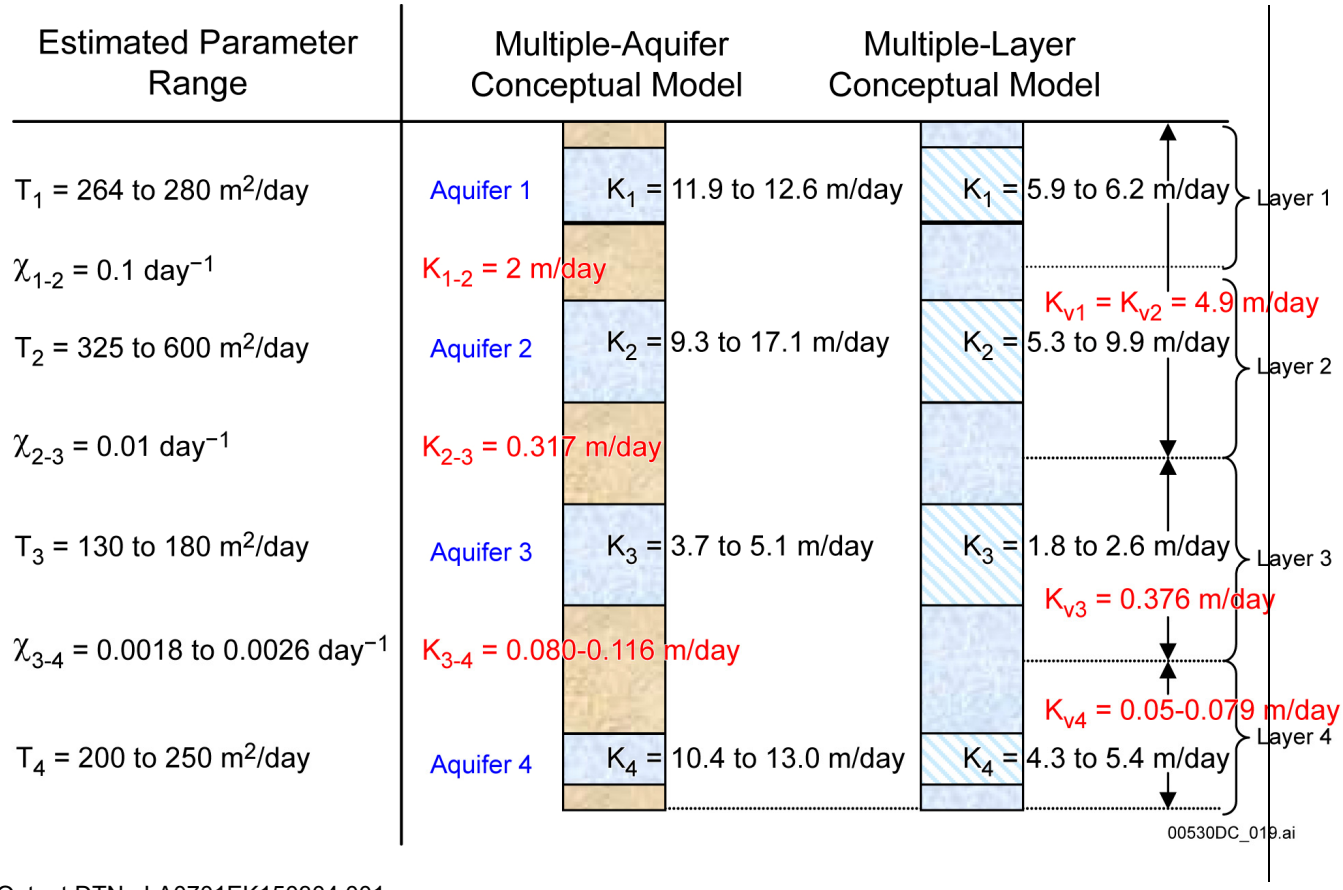

Output DTN: LA0701EK150304.001.

Figure F-45. Hydraulic Conductivities Obtained for Multiple-Aquifer and Multiple-Layer Conceptual Models Based on the Estimated Parameter Ranges

The confining layer between zone 1 and zone 2 has a hydraulic conductivity of 2 m/day assuming that the thickness of this layer is 20 m. The parameter χ_{1-2}, from which the hydraulic conductivity of this layer is estimated, is 0.10 day^{-1} to 0.11 day^{-1}. For the multiple-layer conceptualization, the vertical hydraulic conductivity estimate is 4.9 m/day for the two upper layers in the alluvium (Figure F-45).

Zones 1 and 2 are very well hydraulically connected, have similar hydraulic properties and exhibit unconfined aquifer behavior. It is concluded that zone 1 and zone 2 can be considered to be one unconfined aquifer with the average horizontal hydraulic conductivity of 7.1 m/day (multiple-layer conceptualization) and vertical anisotropy in hydraulic conductivity of 1.5. Because both zone 1 and zone 2 are unconfined, the storativity estimated from the conceptual models is considered a lumped parameter that has a value somewhere between the specific storage and specific yield. The specific yield can only be estimated in the case of an unconfined aquifer conceptual model since it is not a parameter of multiple-aquifer and multiple-layer conceptual models.

Six estimates of transmissivity were obtained for zone 3. The transmissivities range from 130 m^2/day to 180 m^2/day. Assuming equal weight of each conceptual model, the average transmissivity is 153 m^2/day. The transmissivity estimates of zone 3 obtained in *Preliminary*

Analysis of Pump-Spinner Tests and Pump Test in Well NC-EWDP-22S, Near Yucca Mountain, Nevada (Questa Engineering Corporation 2003 [DIRS 178565]) and *Analysis of Aquifer Pump Tests in Individual Well Zones at Site 22 Near Yucca Mountain, Nevada* (Questa Engineering Corporation 2004 [DIRS 178566]) are 237 m^2/day and 139 m^2/day, respectively. The thickness of zone 3 is 35.5 m. Consequently, the hydraulic conductivity of zone 3 ranges from 3.7 m/day to 5.1 m/day assuming the multiple-aquifer system conceptualization. The average hydraulic conductivity is 4.3 m/day. This is significantly lower than the hydraulic conductivity of the two upper zones. The thickness of layer 3 is 70.6 m. Consequently, the hydraulic conductivity of layer 3 ranges from 1.8 m/day to 2.6 m/day assuming the multiple-layer system conceptualization with the transmissivity of zone 3 assigned to all of layer 3. The average hydraulic conductivity is 2.2 m/day. This is significantly lower than the hydraulic conductivity of the two upper zones.

The layer between zones 2 and 3 has a significantly lower hydraulic conductivity than the layer between zones 1 and 2. The vertical conductivity is 0.317 m/day assuming that the thickness of this layer is 31.7 m. The parameter $\chi_{2-3,}$ from which the hydraulic conductivity of this layer is estimated is 0.01 day^{-1}. In the case of the multiple-layer system conceptualization, the vertical hydraulic conductivity of layer 3 calculated using formula (F-71) is 0.376 m/day.

Zone 3 is separated from the upper portion of the alluvial deposits by a layer with a noticeably lower permeability, and it exhibits confined aquifer behavior. Consequently, the storativity estimates obtained from the different conceptual models represent the actual specific storage. The storativity values range from 0.00022 to 0.0003. The average storativity is 0.00026 based on six estimates. The storativity values of zone 3 obtained in *Preliminary Analysis of Pump-Spinner Tests and Pump Test in Well NC-EWDP-22S, Near Yucca Mountain, Nevada* (Questa Engineering Corporation 2003 [DIRS 178565]) and *Analysis of Aquifer Pump Tests in Individual Well Zones at Site 22 Near Yucca Mountain, Nevada* (Questa Engineering Corporation 2004 [DIRS 178566]) are 0.00002 and 0.0001, respectively.

Four estimates of transmissivity were obtained for zone 4. The transmissivities range from 200 m^2/day to 250 m^2/day. The average transmissivity is 225 m^2/day, assuming equal weight of each conceptual model. The transmissivity values of zone 4 obtained in *Preliminary Analysis of Pump-Spinner Tests and Pump Test in Well NC-EWDP-22S, Near Yucca Mountain, Nevada* (Questa Engineering Corporation 2003 [DIRS 178565]) and *Analysis of Aquifer Pump Tests in Individual Well Zones at Site 22 Near Yucca Mountain, Nevada* (Questa Engineering Corporation 2004 [DIRS 178566]) are 269 m^2/day and 185 m^2/day, respectively. The thickness of zone 4 is 19.3 m. Consequently, the hydraulic conductivity of zone 4 ranges from 10.4 m/day to 13.0 m/day. The average hydraulic conductivity is 11.7 m/day. The thickness of layer 4 is 46 m. Consequently, the hydraulic conductivity of layer 4 ranges from 4.3 m/day to 5.4 m/day assuming the multiple-layer system conceptualization with the transmissivity of zone 4 assigned to all of layer 4. The average hydraulic conductivity is 4.9 m/day. This is very similar to the hydraulic conductivity of the two upper zones. Zone 4 is identified as volcanic breccia deposits. As such, it may have properties similar to the alluvial deposits.

The layer between zones 3 and 4 has even lower hydraulic conductivity than the layer between zones 2 and 3. The parameter $\chi_{3-4,}$ from which the hydraulic conductivity of this layer is estimated ranges from 0.0018 day^{-1} to 0.0026 day^{-1}. The conductivity is estimated as

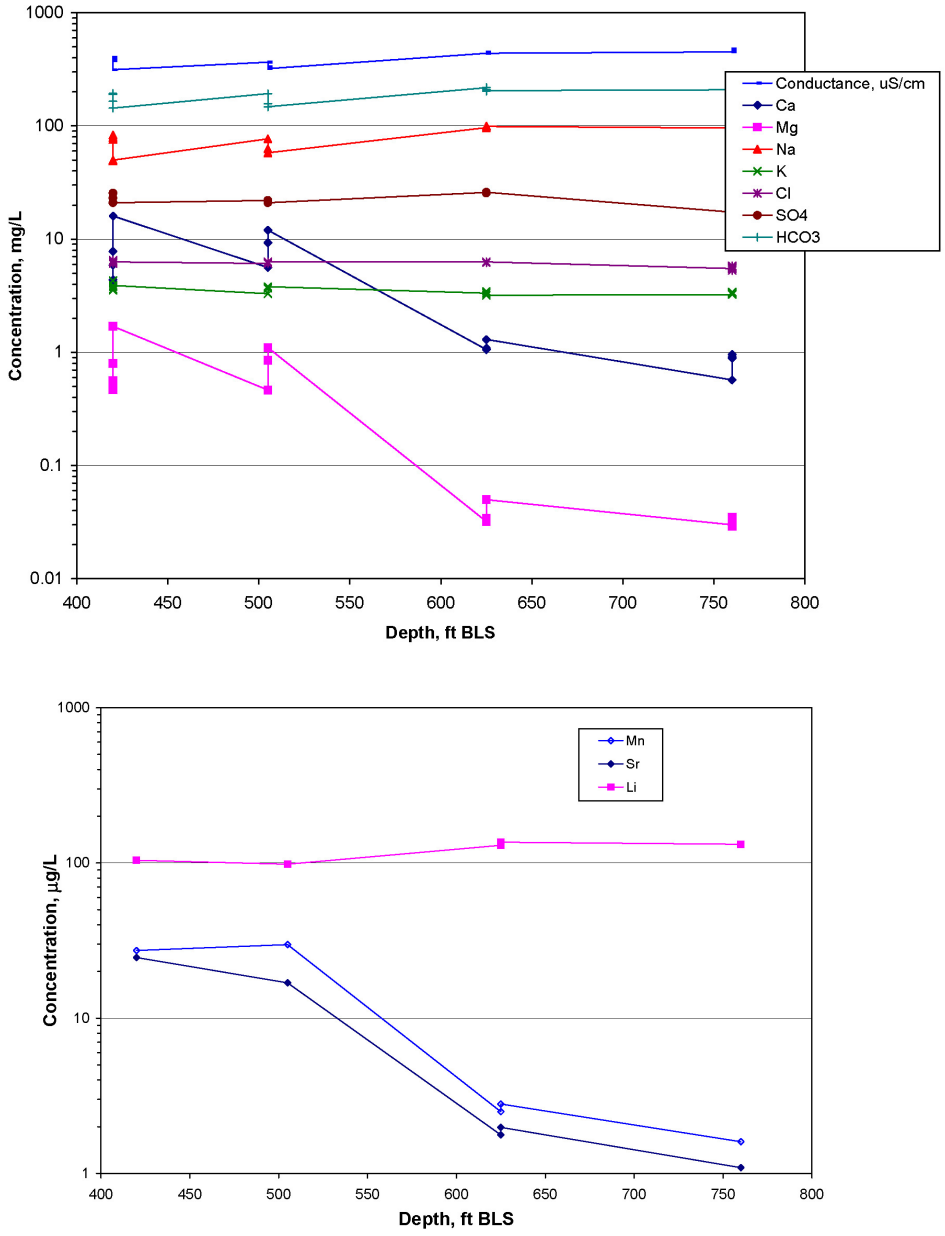

Sources: DTNs: GS011108312322.006 (19D data) [DIRS 162911], GS040108312322.001 (19IM1 data) [DIRS 179422].

Output DTN: LA0704PR150304.001.

NOTES: Depths correspond to the midpoints of screened intervals, and the data points do not distinguish between 19D and 19IM1. Plots show multiple samples from same interval when available. All divalent cations show a distinct decrease in concentration below zone 2 (505 ft), and sodium shows a corresponding increase below this depth, although this increase is not easy to see because of the generally high sodium concentrations and the log concentration axis. Note the log concentration scales.

Figure F-46. Geochemistry Depth Profiles of Major Cations and Anions (upper) and Minor Cations (lower) in Boreholes 19D and 19IM1

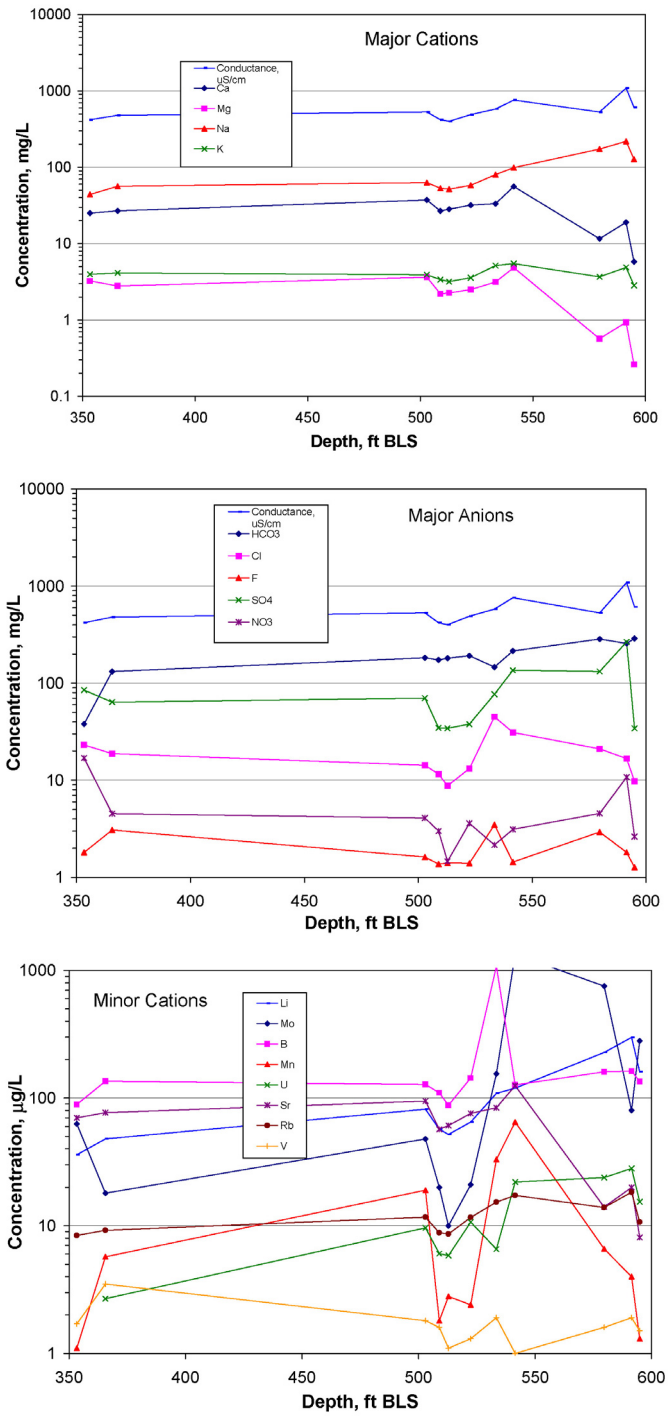

Source DTN: GS060808312272.003 [DIRS 179423].

Output DTN: LA0704PR150304.001.

NOTES: The data gap between 370 ft and 500 BLS provides a potentially false illusion of little variability in geochemistry over this depth range. There is some suggestion of changes in geochemistry that may be associated with flow stratification between 510 ft to 520 ft and 540 ft to 550 ft BLS and again between 540 ft to 550 ft and 580 ft to 590 ft BLS.

Figure F-47. Geochemistry Profiles of Major Cations, Major Anions, and Minor Cations in Samples from Sonic Borehole 19PB

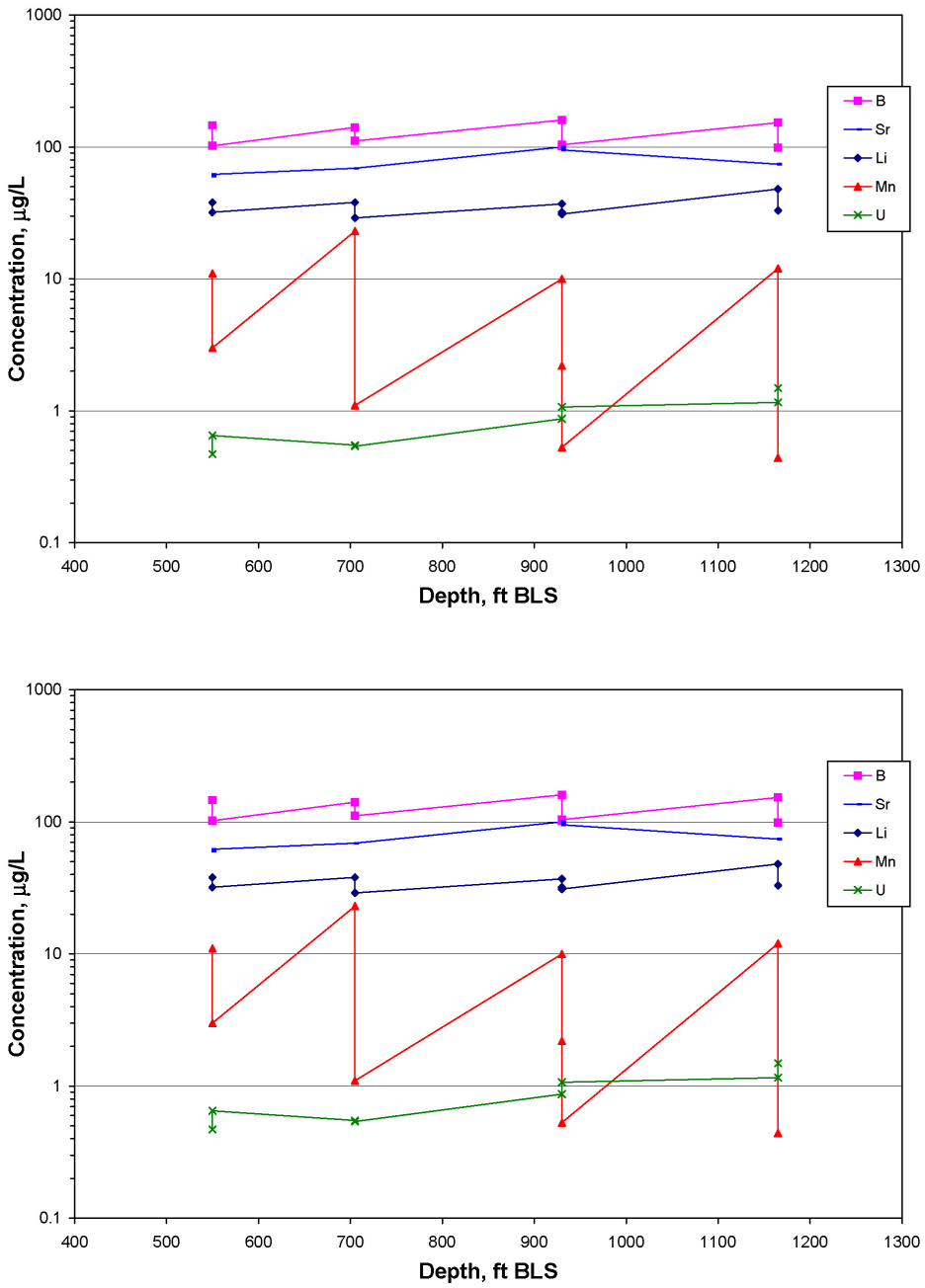

Source: DTNs: GS040108312322.001 (2002 data) [DIRS 179422], GS040808312322.006 (2003 data) [DIRS 179434].

Output DTN: LA0704PR150304.001.

NOTES: Depths correspond to the midpoints of screened intervals, and the data points do not distinguish between 22S, 22PA, and 22PB. The higher manganese concentrations at a given depth correspond to samples taken from 22S, and the lower manganese concentrations at the same depth correspond to samples taken from 22PA or 22PB. These results indicate that the presence (22S) or absence (22PA and 22PB) of steel in the borehole completions probably influences manganese concentrations. There are no obvious trends in concentrations with depth except a hint of increasing calcium concentrations with depth and a minor spike in strontium concentrations at ~940 ft BLS. Note the log concentration scales.

Figure F-48. Geochemistry Depth Profiles of Major Cations and Anions (upper) and Minor Cations (lower) in Boreholes 22S, 22PA, and 22PB

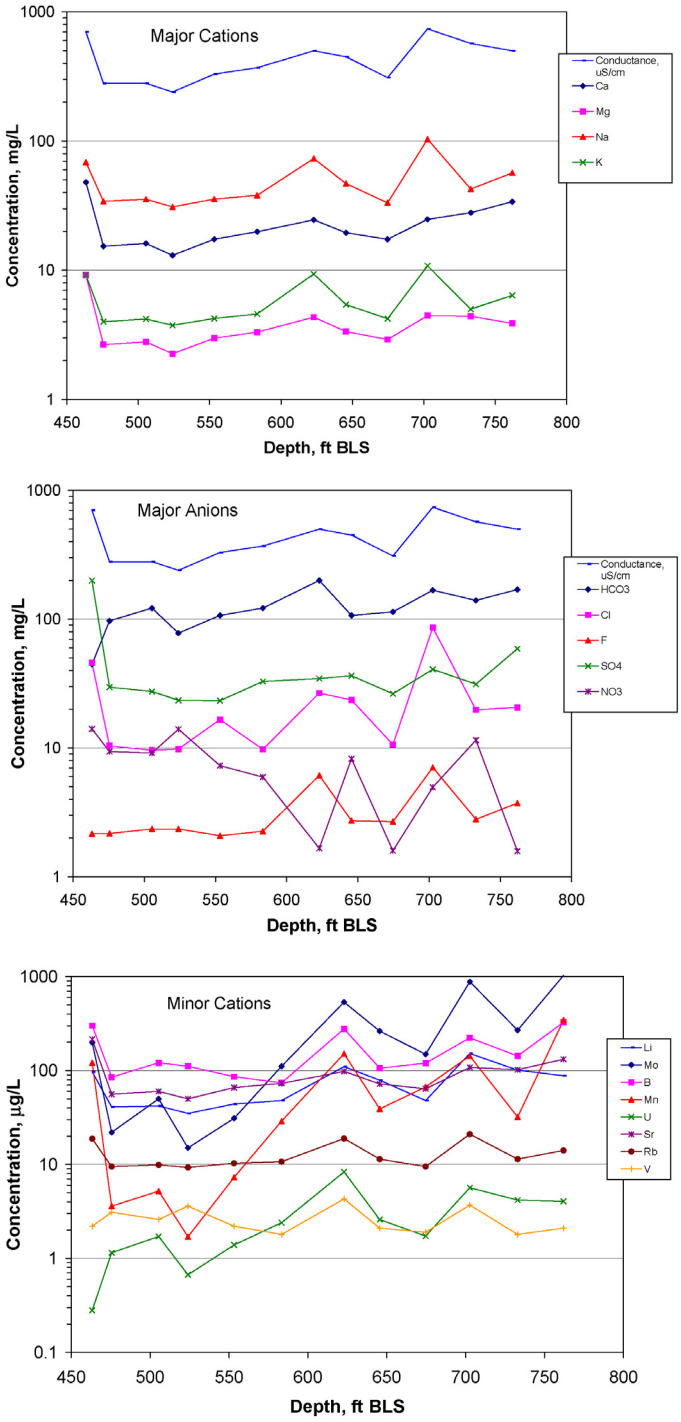

Source: DTN: GS060808312272.003 [DIRS 179423].

Output DTN: LA0704PR150304.001.

NOTE: Note the suggestion of flow stratification associated with the spikes in cation and anion concentrations at ~620 ft and ~700 ft BLS.

Figure F-49. Geochemistry Profiles of Major Cations, Major Anions, and Minor Cations in Samples from Sonic Borehole 22PC

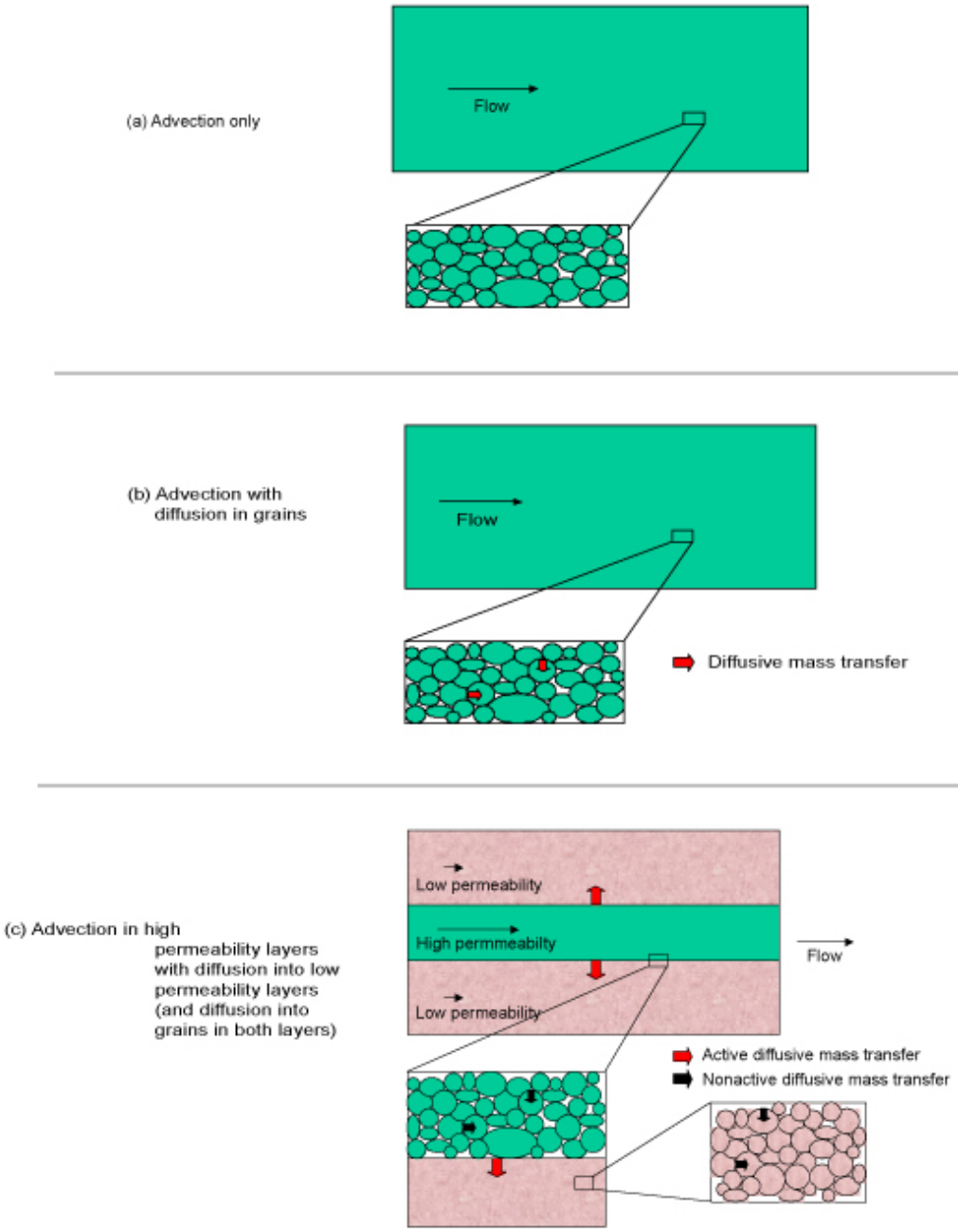

NOTE: For illustration purposes only. Red arrows in (c) indicate diffusive mass transfer options that were exercised in this scientific analysis, and black arrows indicate options that were not exercised.

Figure G-1. Schematic Illustration of Alternative Conceptual Transport Models for the Valley-Fill Deposits South of Yucca Mountain

Table G-1. Flow System Parameters Used in the Single-Well Simulations

Parameter	Figure G-1a Model	Figure G-1b Model	Figure G-1c Model
Porosity in advective layers	0.25	0.25	0.25
Porosity in nonadvective layers	N/A	N/A	0.25
Porosity of grains	N/A	0.15	N/A
Width of advective layers (cm)	N/A	N/A	10.0
Width of nonadvective layers (cm)	N/A	N/A	24.0
Grain diameter in advective layers (mm)	N/A	3.0 (2.2)[a]	N/A
Halide diffusion coefficient in advective layers (cm^2/s)[b]	N/A	3×10^{-6}	3×10^{-6}
Halide diffusion coefficient in nonadvective layers (cm^2/s)[b]	N/A	N/A	1×10^{-6}
Halide diffusion coefficient in grains (cm^2/s) [b]	N/A	1×10^{-6}	N/A
Drift velocity (cm/s)	0 [c]	0 [c]	0 [c]

Output DTN: LA0303PR831231.001.

[a] The number in parentheses is the standard deviation of ln (diameter) used for a lognormal distribution of grain sizes in one set of simulations (see text).

[b] The fluorinated benzoate diffusion coefficient is always assumed to be one-third of the halide diffusion coefficient (Section E.2).

[c] Drift velocity is assumed to be zero because of the small apparent hydraulic gradient in the vicinity of NC-EWDP-19D and NC-EWDP-22S.

Table G-2. Nonflow-System Input Parameters for the Single-Well Simulations

Parameter	Value
Volume of injection interval (including gravel pack) (L)	500
Radius of gravel pack (cm)	18
Duration of injection pulse (hr)	3
Duration of chase (hr)	28
Flow interruption duration (zero-rest-period test only) (hr)	24
Flow rate during injection and pumping (L/min [gpm])	approximately 57 [approximately 15]

Output DTN: LA0303PR831231.001.

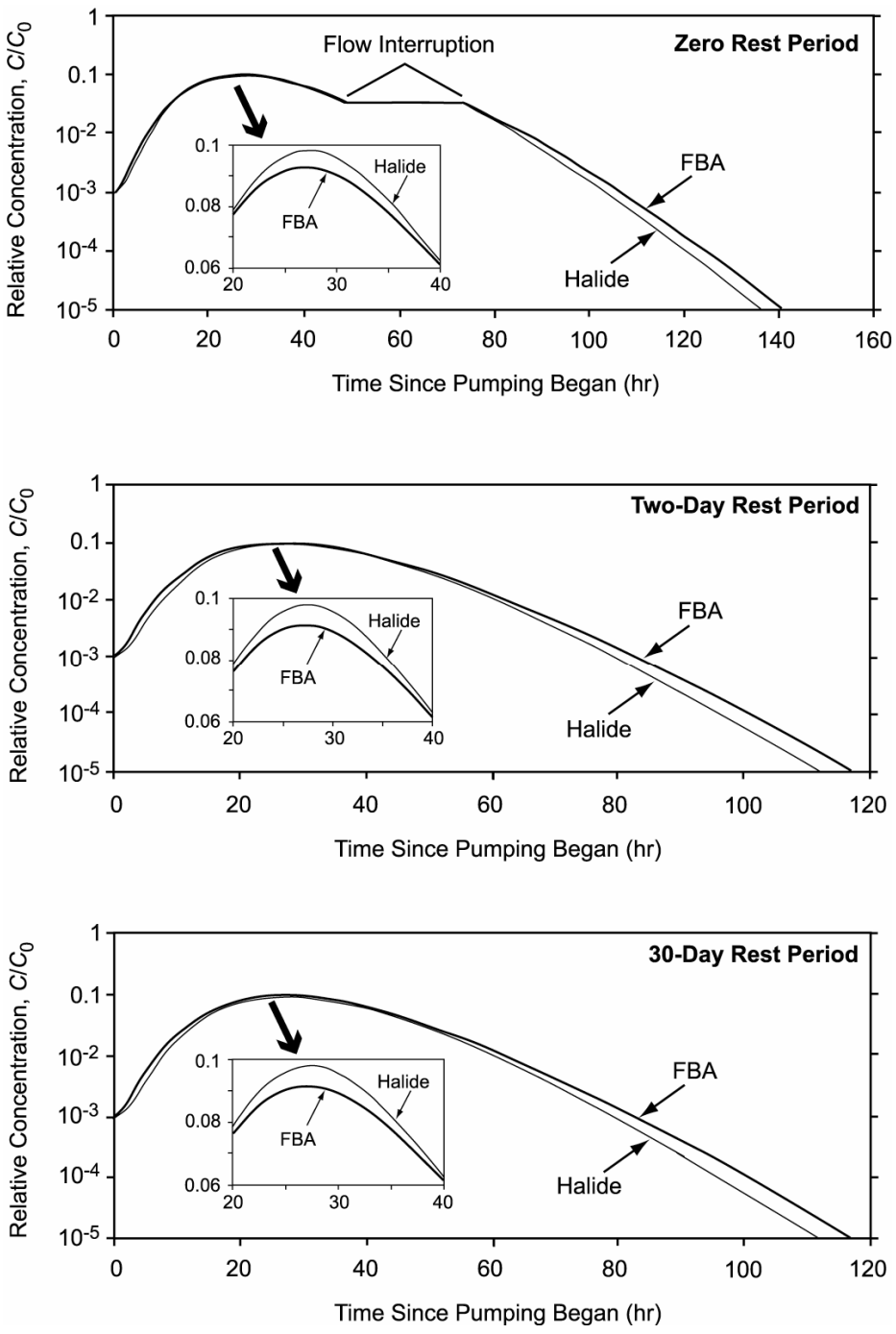

Output DTN: LA0303PR831231.001.

NOTE: The rest periods are zero (top), 2 days (middle), and 30 days (bottom); a 3-mm fixed grain diameter was used. X axis extends to 160 hr for zero-rest-period test because of 24 hours flow interruption. Insets show details of halide and FBA responses near their peak concentrations.

Figure G-3. Normalized Concentration Responses of a Halide and a FBA in Single-Well Tests for the Conceptual Transport Model of Figure G-1b Using a Fixed Grain Diameter

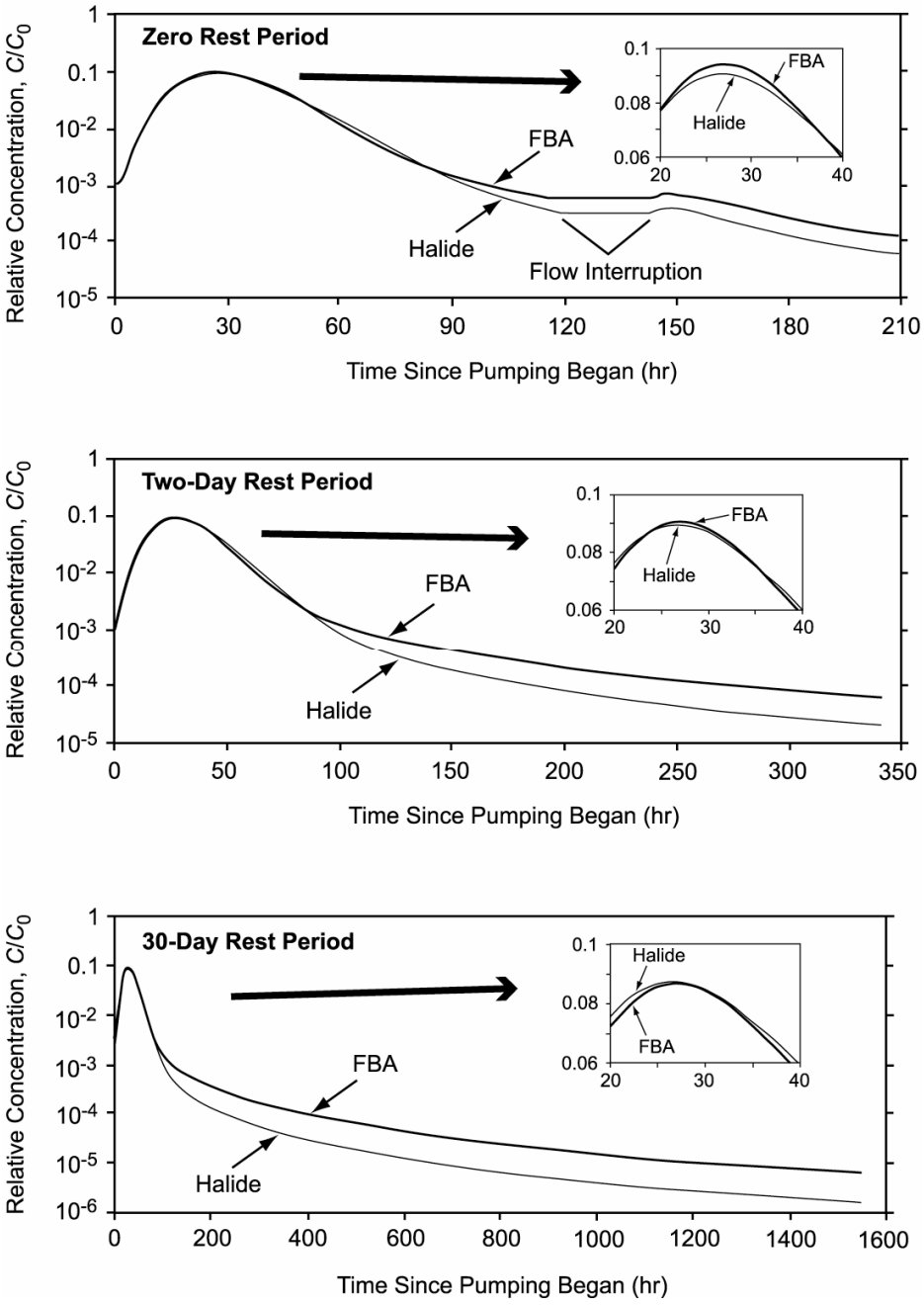

Output DTN: LA0303PR831231.001.

NOTE: The rest periods are zero (top) days, 2 days (middle), and 30 days (bottom); a mean grain diameter of 3 mm was used with a standard deviation for ln (diameter) of 2.2. X axes have different scales to reflect the different pumping durations planned for the three tests in 19D. Insets show details of halide and FBA responses near their peak concentrations.

Figure G-5. Normalized Concentration Responses of a Halide and an FBA in Single-Well Tests for the Conceptual Transport Model of Figure G-1b Using a Grain Size Distribution

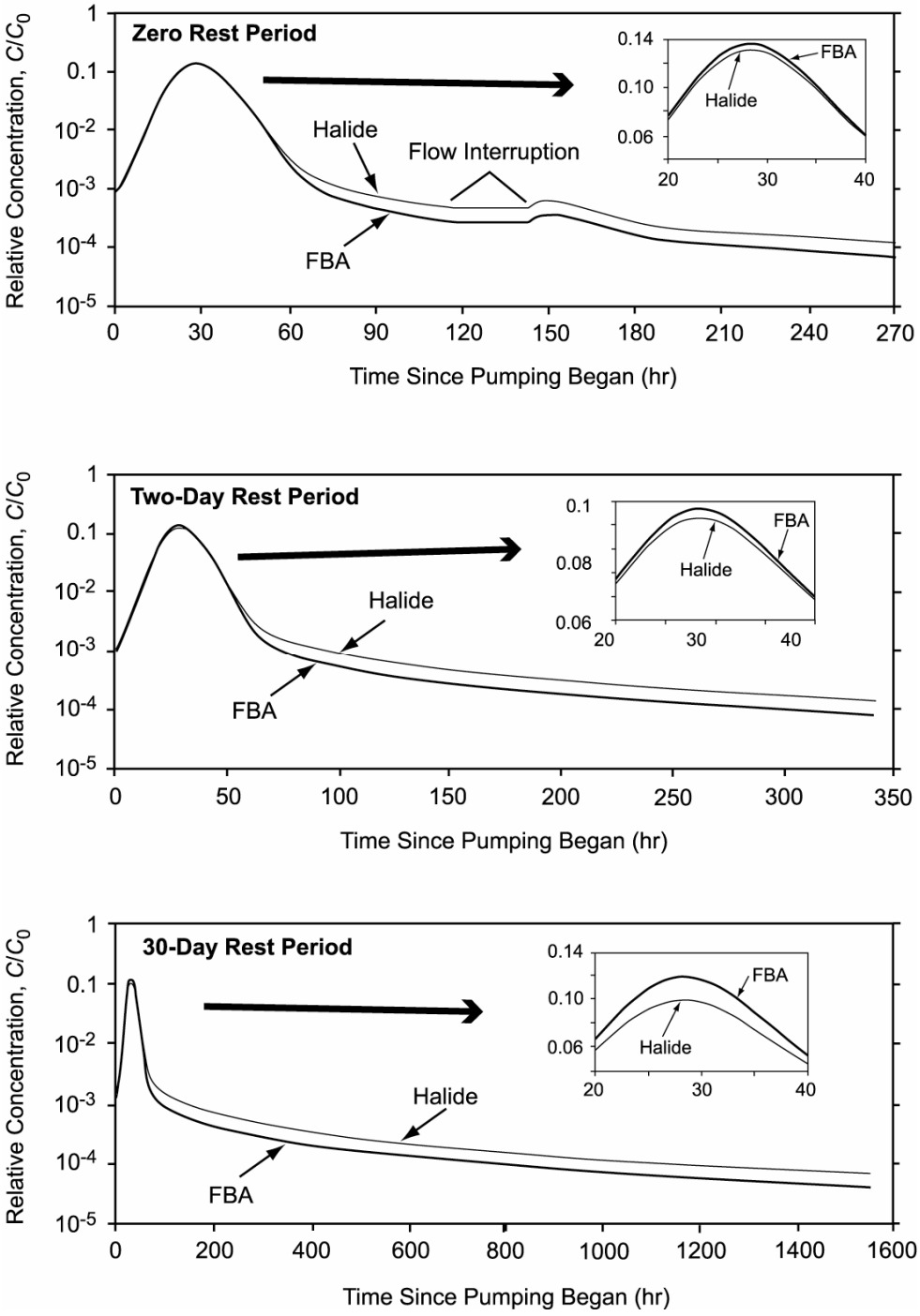

Output DTN: LA0303PR831231.001.

NOTE: The rest periods are zero (top) days, 2 days (middle), and 30 days (bottom). X axes have different scales to reflect the different pumping durations planned for the three tests in 19D. Insets show details of halide and FBA responses near their peak concentrations.

Figure G-6. Normalized Concentration Responses of a Halide and an FBA in Single-Well Tests for the Conceptual Transport Model of Figure G-1c

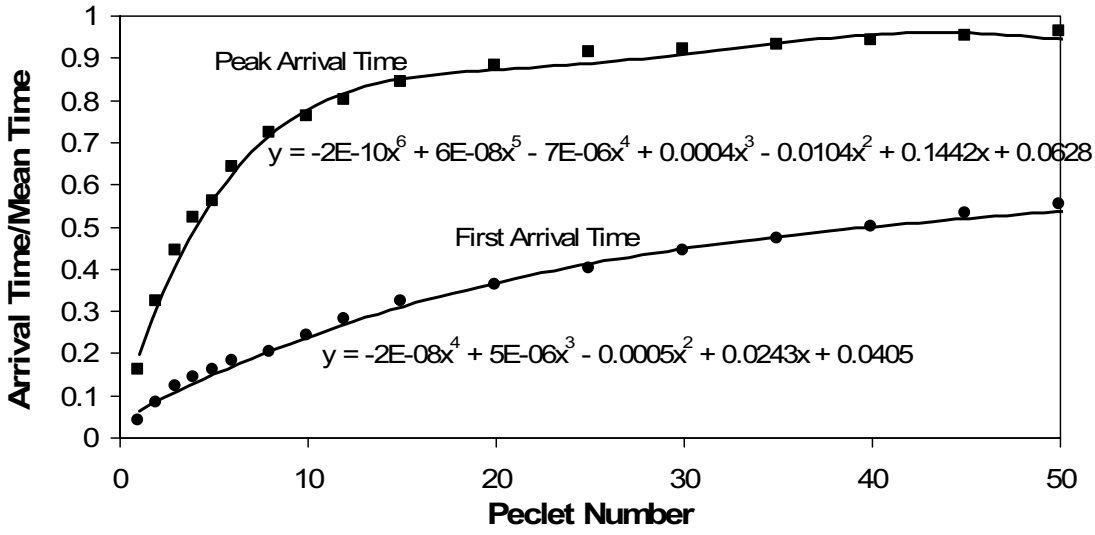

Output DTN: LA0403PR831231.001.

NOTE: Equations are polynomial fits to the "data." First arrival time is defined as the arrival time corresponding to 1% of the peak concentration.

Figure G-10. Ratios of First Arrival Time to Mean Arrival Time and Peak Arrival Time to Mean Arrival Time for Different Peclet Numbers

To obtain estimates of the mean, first, and peak arrival times for a sorbing tracer, the corresponding arrival times for a nonsorbing tracer can be multiplied by the retardation factor, R, given by (Freeze and Cherry 1979 [DIRS 101173], p. 404, Equation 9.14):

$$R = 1 + \frac{\rho_B}{\phi} K_d \qquad \text{(Eq. G-3)}$$

where

K_d = linear partition coefficient, mL/g
ρ_B = bulk density of medium, g/cm^3
ϕ = porosity of medium.

To obtain an estimate of transport times in an unbounded three-dimensional flow system, the 2WELLS_3D V 1.0 computer code was used (STN: 10667-1.0-00 [DIRS 159036]). 2WELLS_3D is a particle-tracking code that simulates tracer transport between two wells in a homogeneous, isotropic medium. It assumes that flow streamlines between the injection and production well follow trajectories given by the prolate spheroidal coordinate system, shown in Figure G-11. This coordinate system reduces to spherical coordinates in the limit of $c = 0$ (i.e., a point source instead of a line source). A number of 2WELLS_3D simulations with zero dispersion were conducted to determine mean nonsorbing tracer residence times as a function of the ratio of well separation to interval length (i.e., length of screen or gravel pack). Because 2WELLS_3D superimposes tracer movement (as particles) onto an analytical solution of the three-dimensional flow field, there is, effectively, no numerical dispersion in the simulated tracer

G4.2.1 Peak-Arrival-Time Analysis

For the analysis comparing the peak tracer arrival times, the mass contributing to the peak was assumed to move directly upgradient during injection. That is, the radial flow pushing the mass was assumed to be in the exact opposite direction as the ambient groundwater flow (Figure G-26). Any estimate of groundwater drift velocity using this assumption should be considered a lower bound because the peak mass will have the *greatest decrease* in arrival time as the rest period is increased when the mass is injected directly upgradient. Trigonometric calculations show that if the tracer mass corresponding to the peak concentration were injected at some angle relative to the ambient gradient direction, the groundwater velocity would have to be greater to result in the same decrease in arrival time (assuming a reasonably homogeneous system).

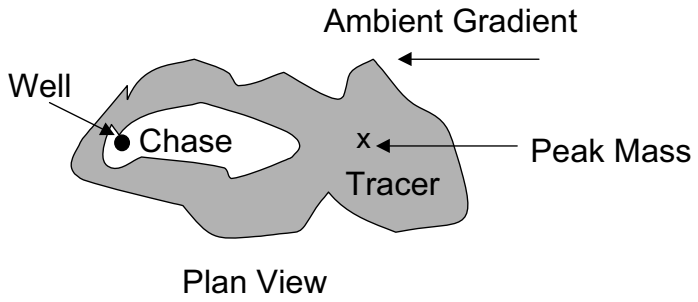

NOTE: For illustration purposes only. The shape of the distribution is not important; the key assumption is that the tracer mass associated with the peak concentration is located directly up-gradient.

Figure G-26. Depiction of Assumed Tracer Mass Distribution Immediately after Injection

Given the assumption of the peak tracer mass moving strictly upgradient, the distance that the tracer mass moved into the formation during the injection and chase phase is given by derivations of Equations G-7 to G-16, which are documented in a scientific notebook by Reimus (2003 [DIRS 165129]):

$$r_{inj} = \sqrt{\frac{(0.5\, V_{tracer} + V_{chase})}{\pi \eta\ h}} - v_{GW} \frac{(0.5\, V_{tracer} + V_{chase})}{Q_{inj}} \qquad \text{(Eq. G-7)}$$

where

r_{inj} = upgradient injection distance, m
V_{tracer} = volume of tracer solution injected, m^3
V_{chase} = volume of chase water injected, m^3
v_{GW} = groundwater velocity (seepage velocity), m/hr
Q_{inj} = injection flow rate, m^3/hr
h = interval thickness, m
η = flow porosity.

the calculated peak arrival volumes in the three tests had approximately the same ratios as in the actual field tests. It was considered more important to match the ratios of times than to match the actual times, although the calculated times were generally in reasonable agreement with the actual times, once the ratios were matched. In the case of the 19D tests, greater emphasis was placed on matching the volume ratio between the 30-day-rest-period test and the approximately 0.5-hr-rest-period test than on matching the volume ratios in any other pair of tests, particularly the two shorter tests. The uncertainty associated with a groundwater velocity estimate obtained from the two shorter duration tests at 19D was considered to be far greater than estimates obtained using the 30-day test results because of the much greater time allowed for drift to take place in the 30-day test. For this reason, only one short-rest-period test was conducted at 22S, and a rest period of 30 days was employed for the longer test.

The process of estimating v_{GW} was repeated for three different values of η - 0.05, 0.18, and 0.3. These values are approximately the lowest, expected (mean), and highest values, respectively, used for alluvium flow porosity in Yucca Mountain performance assessment simulations (SNL 2007 [DIRS 181650]). The value of v_{GW} was different in each case because of the dependence of equations G-7 and G-10 on η. For each case, a specific discharge, v_S, was calculated from v_{GW} using $V_S = \eta\ v_{GW}$.

G4.2.2 Analysis of Late Arrival Times (Associated with High Fractional Tracer Recoveries)

The analysis of late arrival times (arrival times associated with high fractional tracer recoveries) was similar to the analysis of peak arrival times except that the tracer mass associated with the late arrival time was assumed to have been injected downgradient rather than upgradient. This assumption seems reasonable, given that any mass injected upgradient should arrive earlier than the mean tracer arrival time, not later. Analogous to the peak arrival-time analysis, it was assumed that the mass was injected directly downgradient (in the same direction as the ambient groundwater flow). Any estimate of groundwater velocity using this assumption should be considered an upper bound because the late-arriving mass will have the *greatest increase* in arrival time as the rest period is increased if the mass is injected directly downgradient.

For the tests at 19D, the times/volumes associated with the final recovery in the approximately 0.5-hr-rest-period test (0.864), which had the lowest recovery of the three tests, were used as the basis of comparison of the late arrival times for the three tests. Although this is a somewhat arbitrary definition of the late arrival time because it depends on when pumping was stopped in the approximately 0.5-hr-rest-period test, it was considered to be the most objective measure because times associated with recoveries greater than 0.864 would require an extrapolation of the tracer responses in the 0.5-hr test. Clearly, if the 0.5-hr test had been pumped longer, the late arrival times in the tests would have all been greater, and the estimates of groundwater velocities would be slightly different. However, the pumped volumes associated with the arrival times would also have been greater, which would tend to have a moderating effect on the changes in velocity estimates. For the tests at 22S, the times/volumes associated with a fractional recovery of 0.967 were used in the late-arrival-time analysis.

The analysis requires that equations G-7, G-8, and G-9 be modified as shown in equations G-12, G-13, and G-14, respectively.

G4.3 GROUNDWATER VELOCITY ANALYSIS RESULTS

Table G-8 lists the results obtained for both v_{GW} and the specific discharge, v_S ($=\eta\, v_{GW}$) at the 19D location, as a function of assumed flow porosity (η) by all four methods of estimation. Similarly, Table G-9 lists the results obtained by the first three estimation methods at the 22S location. As expected, of the first three methods, the peak analysis method offers the smallest estimates, and the analysis of late-arriving mass (high recovery) offers the largest. The range of estimates from the three methods spans about a factor of three for a given assumed value of flow porosity. The 19D velocity estimate from the linked analytical solutions is in very good agreement with the peak analysis method. The peak-analysis method yields a velocity estimate of 17.5 m/yr (specific discharge of 1.75 m/yr), as compared to 15 m/yr (1.5 m/yr specific discharge) from the linked analytical solutions, when a flow porosity of 0.10 is assumed (the flow porosity obtained from the linked analytical solutions).

For the 22S location, groundwater specific discharge was independently estimated from hydraulic gradient and hydraulic conductivity data to compare with the estimates of Table G-9. These independent estimates of specific discharge were based on water levels in nearby wells (for gradient estimates) and on the local hydraulic conductivity in screen #2 at Site 22 from cross-hole hydraulic testing (Appendix F). Because water levels were essentially identical in all of the Site 22 wells (to within measurement error), the hydraulic gradient estimates were based on water level differences between wells 10S, 22S, and 19IM2, which are aligned along Fortymile wash in what is believed to be the principal direction of groundwater flow (Figure 6.1-6). The hydraulic gradients between each of the three possible well pairs were used as high, medium, and low estimates of the hydraulic gradient at Site 22. The hydraulic gradient multiplied by the hydraulic conductivity from cross-hole hydraulic testing yields an estimate of specific discharge. The high, medium, and low estimates are listed in Table G-10. It should be noted that the estimates in Table G-10 are non-Q and are presented for comparison purposes only because the water levels used to calculate the hydraulic gradients are unqualified Nye County data.

It is apparent that the specific discharge estimates from Table G-10 are slightly larger than those from Table G-9, although the ranges of values in the two tables overlap (0.5 m/yr to 5.4 m/yr for Table G-9, and 3.0 to 12.2 m/yr for Table G-10). The differences could be due to the fact that the local hydraulic gradient at Site 22 is somewhat different than any of the estimates based on the water levels in wells that are separated by several km. Also, the analytical methods involve several assumptions (see Section G.4.2) that undoubtedly do not hold true in a real system. Some of the limitations and uncertainties associated with the analytical methods are discussed in Section G4.4.

Table G-8. Groundwater Specific Discharges and Seepage Velocities at 19D Estimated from the Different Drift Analysis Methods as a Function of Assumed Flow Porosity

	Specific Discharge (m/yr) / Seepage Velocity (m/yr)		
Assumed Flow Porosity[a]	**0.05**	**0.18**	**0.3**
Peak Arrival Analysis	1.2 / 24.5	2.4 / 13.1	3.0 / 9.9
Late Arrival Analysis[b]	3.9 / 77.1	7.3 / 40.4	9.4 / 31.3
Mean Arrival Analysis[c]	2.0 / 40.3	3.8 / 20.9	4.9 / 16.4
Mean Arrival Analysis[d]	2.5 / 49.1	4.6 / 25.8	6.0 / 20.2
Linked Analytical Solutions	1.5 / 15 with a flow porosity of 0.10 and a longitudinal dispersivity of 5 m.		

Output DTN: LA0303PR831231.002.

[a] The three values are approximately the lowest, expected, and highest values of the alluvium flow porosity used in *SZ Flow and Transport Model Abstraction* (SNL 2007 [DIRS 181650]).
[b] Time/Volume associated with approximately 86.4% recovery in each test (the final recovery in the 0.5-hr rest period test, which had the lowest final recovery of any test).
[c] Mean arrival time calculated by truncating all tracer response curves at approximately 86.4% recovery in each test.
[d] Alternative mean arrival time calculated by extrapolating the tracer response curves in the 0.5-hr rest period test to 91.3% and truncating the response curves in the 2-day rest period test to 91.3% recovery (the final recovery in the 30-day rest period test).

Table G-9. Groundwater Specific Discharges and Seepage Velocities at 22S Estimated from Different Drift Analysis Methods as a Function of Assumed Flow Porosity

	Specific Discharge (m/yr) / Seepage Velocity (m/yr)		
Assumed Flow Porosity[a]	**0.05**	**0.18**	**0.3**
Peak Arrival Analysis	0.47 / 9.5	0.89 / 5.0	1.2 / 3.9
Late Arrival Analysis[b]	2.2 / 43.8	4.2 / 23.1	5.4 / 17.9
Mean Arrival Analysis[c]	0.82 / 16.4	1.6 / 8.6	2.0 / 6.7

Output DTN: LA0701PR150304.001.

[a] The three values are approximately the lowest, expected, and highest values of the alluvium flow porosity used in *SZ Flow and Transport Model Abstraction* (SNL 2007 [DIRS 181650]).
[b] Time/Volume associated with approximately 96.7% recovery in each test.
[c] Mean arrival time calculated by truncating the two tracer response curves at 96.7% recovery in each test.

Table G-10. Groundwater Specific Discharge and Seepage Velocity Estimates at 22S Using Different Natural Gradient Estimates and Assuming a Hydraulic Conductivity of 12 m/day from Cross-Hole Hydraulic Testing at Site 22

	Specific Discharge (m/yr) / Seepage Velocity (m/yr)		
Assumed Flow Porosity[a]	**0.05**	**0.18**	**0.3**
Gradient between 22S and 19IM2 (0.00279 m/m)	12.2 / 244	12.2 / 67.8	12.2 / 40.7
Gradient between 10S and 19IM2 (0.00196 m/m)	8.6 / 172	8.6 / 47.7	8.6 / 28.6
Gradient between 10S and 22S (0.00069 m/m)	3.0 / 60.5	3.0 / 16.8	3.0 / 10.1

Output DTN: LA0701PR150304.005 (non-Q; used for comparative purposes).

[a] The three values are approximately the lowest, expected, and highest values of the alluvium flow porosity used in *SZ Flow and Transport Model Abstraction* (SNL 2007 [DIRS 181650]).

G4.4 DISCUSSION OF GROUNDWATER VELOCITY ANALYSES

Some significant uncertainties are associated with each of the estimation methods for v_{GW} and v_S described in this report. Although it would be of interest to determine which of the methods provides the best estimate, a detailed analysis of uncertainties was not conducted. In the discussion that follows, qualitative comments are provided on several uncertainties, and some advantages and potential pitfalls of the different methods are discussed.

The linked-analytical-solution method offers the advantage of providing estimates of flow porosity and longitudinal dispersivity, which are very important parameters for repository performance assessment, in addition to providing flow velocity estimates. Although the parameter estimates in Table G-8 for this method were obtained after many trials using various values of flow porosity, dispersivity, and groundwater flow velocity to fit the three tracer responses simultaneously, an exhaustive sensitivity analysis to evaluate the uniqueness of the matches was not conducted. With such an analysis, it is possible that other combinations of flow porosity, dispersivity, and groundwater-flow velocity could yield essentially equally good matches to the tracer responses.

The value of longitudinal dispersivity obtained from the linked analytical solutions (5 m) intuitively seems large given that calculated injection distances from the well should have been only about 5 m to 6 m with a flow porosity of 0.1. This large dispersivity probably reflects that the aquifer was not truly homogeneous and isotropic as assumed, and a large dispersivity was the only way the analytical solutions could account for tracer plume spreading that occurred due to flow heterogeneity.

The impact of ignoring tracer drift during the injection and pumpback phases of testing for the linked-analytical-solution method is not clear. The error introduced by this assumption may be important for the two tests with the shortest rest periods, as the injection and pumpback phases were collectively longer than the rest period in both tests. The remaining discussion is focused on the other three estimation methods, although some aspects of it also apply to the linked-analytical-solution method.

The peak-analysis method would intuitively seem to have considerable uncertainty associated with it because of the inability to determine whether the tracer mass associated with the peak remained upgradient of the well during the rest period or if it drifted back downgradient of the well during the rest phase. The former case was assumed here, as it provides the lowest estimate of groundwater velocity and specific discharge. If the latter case were assumed, the estimated velocity would have been about twice the estimates obtained by the other methods instead of about half the other estimates. Another uncertainty associated with the peak-analysis method is that at least part of the shift in the peak-arrival time/volume may have been due to hydrodynamic dispersion in the system rather than pure advection (as was assumed). A considerable amount of dispersion during the rest phase could have shifted the peak-arrival time without significant translation of the tracer plume's "center of mass" due to advection. However, some advection is necessary for dispersion to occur.

Both the analyses of late-arrival times and mean-arrival times are potentially highly sensitive to diffusion into stagnant water and to density-driven flow resulting from density contrasts between

Additional insights into uncertainties associated with the estimation methods could probably be obtained by (1) generating random-stochastic-hydraulic-conductivity fields having statistics consistent with the current knowledge of the alluvium, and then (2) numerically simulating injection-withdrawal tests in these fields (for various assumed drift velocities). These methods could ultimately yield more refined estimates of groundwater velocities in the alluvium.

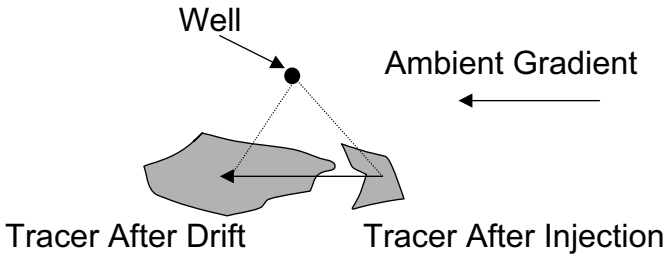

NOTE: For illustration purposes only. The dashed lines connect the well with the center of mass of the tracer "plume" before and after the rest period.

Figure G-30. Depiction of a Tracer Injection Scenario That Could Result in Underestimation of Groundwater Velocity

G4.5 SUMMARY OF GROUNDWATER VELOCITY ANALYSES

Four methods of estimating groundwater velocities from multiple single-well injection-withdrawal tracer tests conducted with varying rest periods in the saturated alluvium south of Yucca Mountain, Nye County, Nevada are presented in this report. All four were applied to the single-well tracer test data at 19D, and three were applied to the single-well tracer test data at 22S. The resulting estimates of groundwater velocity and specific discharge vary over a range of about a factor of 3 for a given assumed flow porosity, and by about a factor of 10 for a reasonable range of flow porosities. The estimates of specific discharge at 19D range from 1.2 m to 9.4 m per year, which is comparable to specific discharges being used in Yucca Mountain performance assessments (obtained from the calibrated site scale SZ Flow Model). Flow porosity and longitudinal dispersivity estimates of 0.10 m and 5 m, respectively (Output DTN: GS031008312316.003), were obtained for the 19D location using a linked-analytical-solution method. Estimates of specific discharge at 22S range from 0.5 m to 5.4 m per year, which compares reasonably well with estimates of 3.0 m to 12.2 m per year based on hydraulic gradient and hydraulic conductivity estimates at 22S.

The same aquifer parameter values obtained from analyzing the three injection-pumpback tracer tests in screen #1 of 19D were in the above linked-analytical-solutions to generate a theoretical breakthrough curve to compare with to the actual breakthrough curve from the 19D, screen #4 injection-pumpback tracer test (detailed documentation reported by Umari et al. 2003 [DIRS 164573]). The results are shown in Figure G-31. The close match indicates that the same aquifer parameters that were suitable for screen #1 in well 19D also appear to be suitable for screen #4 in the same well.

concluded that the observed separations reflect diffusion between flowing and stagnant water in the aquifer.

To conduct a semi-quantitative assessment of diffusion in the site 22 flow system, the MULTRAN V1.0 code (STN: 10666-1.0-00 [DIRS 159068]) was used to simulate the single-well tracer tests in flow systems with both the conceptual models of Figures G-1(b) and G-1(c). As discussed in Section G4.2, the MULTRAN model simulates radial outward and inward flow during the injection and pumping phases, respectively, of a single-well test, but it does not account for ambient groundwater flow, or drift, in the flow system during the rest period or any other phases of a test. Thus, the only way to account for the additional plume spreading that occurs during longer drift period tests is to increase the longitudinal dispersivity during the injection and pumpback phases in MULTRAN. Consequently, the longitudinal dispersivities from the MULTRAN interpretations of the single-well tracer tests should not be interpreted as meaningful longitudinal dispersivities.

Figure G-32 shows simultaneous fits to the tracer breakthrough curves in each single-well test at 22S using the conceptual model of Figure G-1(b), with diffusion into spherical grains (sometimes also referred to as "blocks") of varying size with a mean radius of 0.3 cm, and a standard deviation of the log of the grain radii of 0.5. Other model parameters are listed in Table G-11. The model curves shown in Figure G-32 were not obtained using an automated numerical optimization algorithm, but rather they are trial-and-error "fits" obtained by manually adjusting the dispersivity, grain size (radius of spherical grains), grain internal porosity, flowing porosity, and diffusion coefficients within the grains. As such, these fits should not be considered optimized, and they only serve to illustrate that the observed differences in the tracer breakthrough curves are qualitatively consistent with the conceptual model of Figure G-1(b) with variable grain sizes. The emphasis in the "fitting" process was on matching the tracer peak concentrations and the relative features of the tracer breakthrough curves (i.e., their relative peak heights, where they approach each other or cross-over), rather than on absolute matches. The slight mismatches between the data and model curves, particularly with respect to the timing of the peaks and the tailing behavior can likely be attributed to the lack of drift simulation in the MULTRAN code. The use of an adjustable longitudinal dispersivity in MULTRAN (see above) to account for tracer plume spreading during the drift period apparently does not approximate the effects of drift very well. It should be noted that assuming a constant grain size resulted in poorer matches to the breakthrough curves than assuming a variable grain size, so it appears that the multiple diffusion rates and diffusion distances offered by the variable grain sizes constitute a more representative conceptualization of the flow system.

It should be noted that four of the five parameters that were adjusted to obtain a good model fit (excluding longitudinal dispersivity) combine synergistically to define both a characteristic time scale and a mass transfer coefficient for diffusion between flowing and stagnant water in the flow system. These two lumped parameters govern the diffusive mass transfer behavior of the system, so the adjustment of the four model parameters effectively reduces to the adjustment of these two lumped parameters to fit the data. The grain radius (R) and the diffusion coefficient within grains (D_m) combine to define a characteristic time scale for diffusion ($t_{ch} = R^2/2D_m$), which is essentially a measure of the time it takes for the flowing and stagnant water domains to "equilibrate" with respect to solute diffusion gradients. When advective time scales are significantly greater than t_{ch}, solutes will experience single-porosity transport behavior with an

effective porosity equal to the sum of the flowing and stagnant water porosities. All four parameters combine to define a mass transfer coefficient, *MTC*, for diffusion between the flowing and stagnant water domains, given by $\frac{\phi_b \sqrt{D_m}}{R\phi_f / 3(1-\phi_f)} = \frac{3\phi_b(1-\phi_f)}{\phi_f \sqrt{t_{ch}}}$, where ϕ_b = grain internal porosity, ϕ_f = flowing porosity, and spherical grains are assumed. The ratio of stagnant to flowing water porosity in the system, r_{sf}, is given by $\frac{(1-\phi_f)\phi_b}{\phi_f}$, so the diffusive mass transfer coefficient can also be written as $\frac{3r_{sf}}{\sqrt{2t_{ch}}}$. Allowing the grain radius, *R*, to take on a range of values (defined by the standard deviation of the log of grain radius) effectively introduces an additional adjustable parameter (the standard deviation). The addition of this parameter can only improve the model fit, but the improvement must be significant to justify the addition.

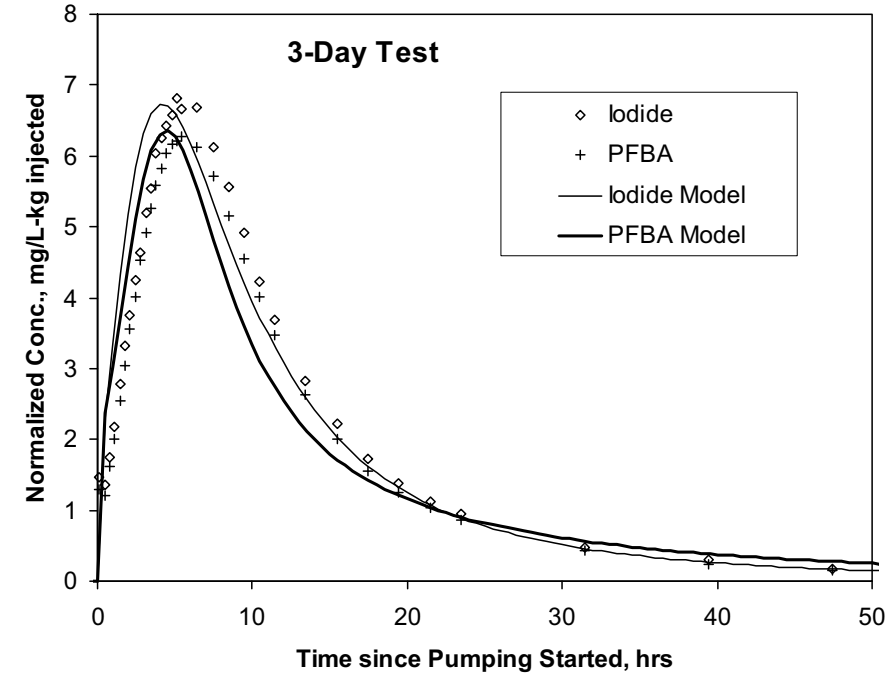

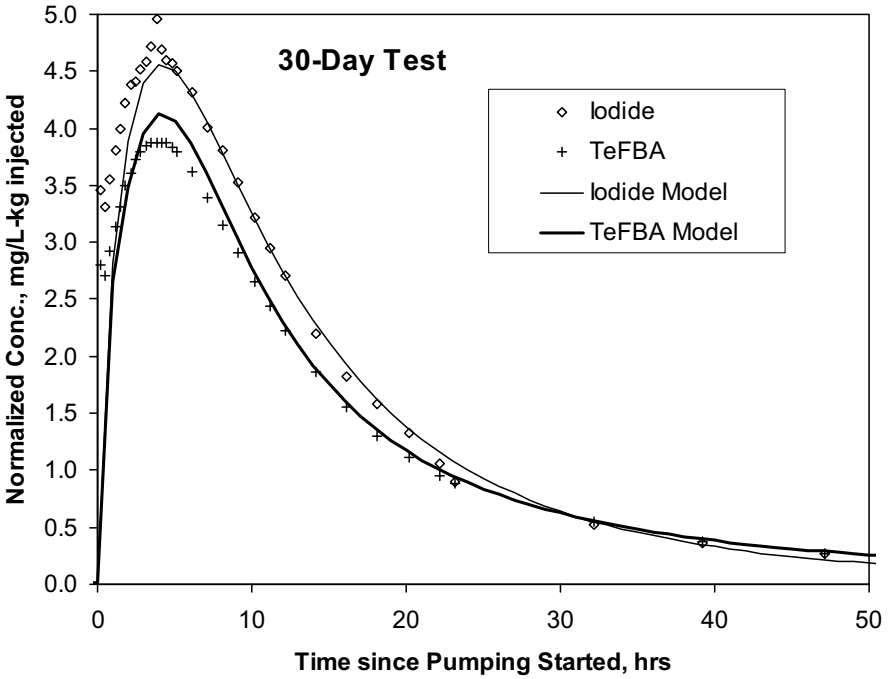

Sources: DTNs: LA0612PR831231.001 [DIRS 178733] (3-day test data), LA0612PR831231.002 [DIRS 178735] (30-day test data), and LA0701PR150304.007 (output).

NOTE: The data points are grab sample normalized concentrations. Model parameters are listed in Table G-11.

Figure G-32. MULTRAN Model Matches to the 22S Single-well Tracer Test Breakthrough Curves using the Diffusion-into-Grains Conceptual Model

Table G-11. MULTRAN Model Parameters Associated with the Matches to the 22S Single-well Tracer Test Breakthrough Curves Shown in Figure G-32 (diffusion-into-grains model)

Model Parameter	Parameter Value
Longitudinal Dispersivity, m	2 / 8[a]
Flowing Porosity	0.25
Porosity in Grains	0.1
Iodide Diffusion Coefficient in Grains (D_m), cm^2/s	3×10^{-7}
Mean Grain Radius (R), cm	0.31
Std. Dev. of Log Grain Radius	0.5
Characteristic Diffusion Time Scale ($R^2/2D_m$), hr	44.5
Diffusive Mass Transfer Coefficient, $\frac{\phi_b \sqrt{D_m}}{R\phi_f / 3(1-\phi_f)}$, $hr^{-1/2}$	0.095
Ratio of Stagnant to Flowing Water Porosity	0.3

Output DTN: LA0701PR150304.007.

[a]Values correspond to first test and second test, respectively.

Figure G-33 shows simultaneous fits to the tracer breakthrough curves in each single-well test at 22S using the conceptual model of Figure G-1(c), with diffusion between flowing and stagnant "layers" in a flow system. Model parameters are listed in Table G-12. As in the case of the conceptual model of Figure G-1(b) (Figure G-32), the model curves shown in Figure G-33 are not numerically optimized fits, but rather they are trial-and-error "fits" obtained by manually adjusting the dispersivity, layer thicknesses, layer porosities, and diffusion coefficients within the layers. The matches to the data in Figure G-33, though qualitatively reasonable, appear to be somewhat poorer than those in Figure G-32. However, a comparison of the conceptual models based on these differences is somewhat biased because the diffusion-into-grains model includes multiple diffusion rates and distance scales (because of the range of grain radii), whereas the layered model has only a single set of diffusion parameters. The additional adjustable parameter associated with the standard deviation in grain sizes in the diffusion-into-grains model provides much greater flexibility in matching the observed data than the layered model with a single effective diffusion rate and diffusion distance. For the diffusion-into-layers model, the characteristic time scale for diffusion, t_{ch} is given by $L^2/8D_m$, where L is the thickness of the non-flowing layers, and D_m is the diffusion coefficient in the non-flowing layers, and the mass transfer coefficient, MTC, is given by $\frac{\phi_l \sqrt{D_m}}{\phi_f (b + L/2)}$, where ϕ_l is the porosity within the non-flowing layer, ϕ_f is the flowing porosity, and b is half the thickness of the flowing layers.

As Tables G-11 and G-12 indicate, the best-fitting diffusion-into-grains and the diffusion-into-layers conceptual models both have relatively small ratios of stagnant to flowing water volumes (both less than 1.0). Also, the time scales for diffusion into the stagnant water are relatively short (less than 2 days) compared to the time scales of the rest periods in both tracer tests. These characteristics are necessary for the iodide to have higher peak concentrations than the FBAs, which occurs because diffusion into the accessible stagnant porosity essentially depletes the concentrations of both tracers in the flowing porosity by about the same relative amount during the rest periods of the tests, and the iodide diffuses back out of the stagnant porosity more quickly than the FBAs. While both the diffusion-into-grains and

diffusion-into-layers conceptual models match the tracer breakthrough curves reasonably well, the very short time and distance scales suggest that the former model is more plausible than the latter for solute transport in the saturated alluvium. The layer thicknesses necessary to have such short time scales with realistic solute diffusion coefficients are on the order of 2 mm for flowing layers and 6 mm for non-flowing layers. These are seemingly much too narrow to correspond to layer thicknesses in a material that has grain sizes much larger than this.

Thus, it is concluded from the 22S single-well tracer testing results that the diffusion-into-grains (or grains) conceptual dual-porosity model is most applicable for the saturated alluvium at this location. However, the very short diffusion time and distance scales suggest that the alluvium should behave as a single-porosity system over the much longer time and distance scales associated with performance assessment. That is, the flowing and stagnant porosities should effectively act as a combined flowing porosity for solute transport in the alluvium, with the solute transport velocity being less than the groundwater velocity in the flowing porosity by a factor of (flowing porosity)/(flowing+stagnant porosity), which is 0.53 for the diffusion-into-grains model and 0.77 for the diffusion-into-layers model. Of course, these conclusions must be tempered with the realization that the volume of the aquifer interrogated in the single-well tests was relatively small (on the order of 20,000 gal to 30,000 gal based on the tracer and chase water volumes and allowing for some plume spreading) and certainly can't be considered representative of km scales. Also, if the permeable layers were more than just a few cm thick, diffusion into adjacent low-permeability layers could have been masked by diffusion into grains within the permeable layers over the relatively short time scales of the tests. Thus, it is possible that over much longer time scales, additional diffusion between thicker alternating high and low permeability layers would have been observed.

G4.8 CONCLUSIONS FROM SINGLE-WELL TRACER TESTING IN ALLUVIUM

The single-well tracer tests at 19D showed no evidence of dual-porosity transport behavior based on the lack of any separation of the halide and FBA tracer breakthrough curves. However, the single-well tracer test results at 22S were consistent with a dual-porosity, diffusion-into-grains conceptual transport model with relatively short characteristic time and distance scales for diffusion. These were short enough that single-porosity transport behavior with an effective flowing porosity equal to the flowing plus stagnant porosity would be predicted for solutes over performance assessment time and distance scales. However, the caveats identified in the last three sentences of the previous paragraph should be kept in mind.

Differences in the tracer responses for the different rest periods in the three tests at 19D can be attributed to groundwater drift during the rest periods. At 22S, the differences in tracer responses between the two tests are also dominated by groundwater drift, although they can't be exclusively attributed to drift. Further evidence for a single-porosity flow/transport system at 19D was provided by the lack of an increase in tracer concentrations after flow interruptions during the tailing portions of the tracer responses in the two tests featuring flow interruptions.

Four methods were used to estimate groundwater drift velocities from the three single-well tracer tests in 19D, and three of these methods were also used to estimate groundwater velocities from the two single-well tests at the 22S location. The resulting estimates of specific discharge range from 1.2 m/yr to 9.4 m/yr at 19D and from 0.5 m/yr to 5.4 m/yr at 22S, with the estimates

Table G-12. MULTRAN Model Parameters Associated with the Matches to the 22S Single-well Tracer Test Breakthrough Curves Shown in Figure G-33 (diffusion-into-layers model)

Model Parameter	Parameter Value
Longitudinal Dispersivity, m	2 / 12 [a]
Flow Porosity	0.077
Porosity in Non-Flowing Layer	0.1
Iodide Diffusion Coefficient in Non-Flowing Layer (D_m), cm^2/s	5×10^{-7}
Flowing Layer Thickness, cm	0.2
Non-Flowing Layer Thickness (L) cm	0.45
Characteristic Diffusion Time Scale ($L^2/8D_m$), hr	14.1
Diffusive Mass Transfer Coefficient, $\frac{\phi_l \sqrt{D_m}}{\phi_f (b + L/2)}$, $hr^{-1/2}$	0.170
Ratio of Stagnant to Flowing Water Porosity	0.9

Output DTN: LA0701PR150304.007.

[a]Values correspond to first test and second test, respectively.

G5. RESULTS AND INTERPRETATION OF CROSS-HOLE TRACER TESTS IN SATURATED ALLUVIUM AT NC-EWDP SITE 22

Two cross-hole tracer tests were conducted in the saturated alluvium in the second screened interval from the surface at Nye County Site 22 in 2005 (the same interval in which the single-well tracer tests were conducted at this location – see Section G4). The first test involved the injection of several tracers into this interval in two different wells (22PA and 22PC) while the same interval was continuously pumped in 22S (see Figures 6.1-8 and 6.1-10). The two injection wells were located in approximately orthogonal directions to each other relative to 22S (22PA is north, and 22PC is east), so flow and transport anisotropy could be evaluated. Also, another nonsorbing tracer was injected into the first screened interval in 22PA, which was completed at a shallower depth than the pumped interval. The second cross-hole tracer test was conducted in the same configuration as the first test, but only two tracers, iodide ion and perrhenate ion, and one injection interval, the second interval from the surface in 22PA, were used.

The objectives of the first cross-hole test were to (1) further evaluate alternative conceptual transport models in the saturated alluvium, building on the information obtained from the single-well tracer tests, (2) evaluate flow anisotropy in the alluvium, both horizontal and vertical, and (3) obtain estimates of transport parameters for solutes and colloids in the saturated alluvium. The second test was conducted primarily to evaluate whether perrhenate transport is retarded relative to iodide in the saturated alluvium. Perrhenate was used in this test as a surrogate for pertechnetate, which is the predominant technetium species predicted to be present in oxidizing groundwaters at Yucca Mountain, and ^{99}Tc is one of the radionuclides that have been identified as potentially contributing significantly to future offsite doses because of its high solubility and weak sorption behavior. Both pertechnetate and perrhenate are predicted to be reduced to species of much lower solubility and significant sorption under reducing groundwater conditions, and perrhenate should be slightly harder to reduce based on standard tables of electrochemical potentials of half reactions (Lide 2006 [DIRS 178081], p. 8-24). Thus, if perrhenate were significantly retarded relative to a nonsorbing tracer (e.g., iodide), it would

suggest that local reducing conditions may exist in the alluvium that would also be capable of reducing, and thus retarding, pertechnetate.

The tracers injected into the second screened interval in 22PA in the first cross-hole test included two nonsorbing solutes (bromide ion and 2,4,5 TFBA) and a weakly sorbing cation tracer (lithium ion). These tracers were all injected simultaneously (co-dissolved in groundwater from 22S). Nonsorbing FBAs were also injected into the second screened interval from the surface in 22PC (2,6 DFBA) and into the first screened interval from the surface in 22PA (2,5 DFBA). This last tracer was injected to determine if there was any significant downward vertical flow through the alluvium induced by pumping from the deeper depth in 22S. Carboxylate modified polystyrene latex (CML) microspheres (200-nm diameter, and dyed with a fluorescent yellow dye to allow them to be distinguished from background colloids) were injected into the second screened interval of 22PA approximately ten days after the solute tracers to serve as colloid tracers. The delay in injecting the microspheres was to avoid the high ionic strength of the solute injection solution, which could have caused the microspheres to aggregate or to attach to the media surfaces more readily than in the much lower ionic strength ground water. The sorption parameters for lithium and the filtration parameters for the microspheres were to be determined by comparing the cross-hole responses of these tracers to that of the two nonsorbing solutes. Table G-13 provides a summary of the injection masses and volumes of the different tracers in both cross-hole tests at Site 22. The observed tracer recoveries are also summarized in Table G-13.

The 2,5 DFBA was never detected in 22S, so it is not discussed further and not included in Table G-13. This result suggests that vertical flow and transport through the alluvium at Site 22 is probably somewhat hindered relative to horizontal flow and transport, which is consistent with the hydraulic test interpretations that indicate the shallow alluvium at Site 22 (over the two shallowest intervals) has a horizontal-to-vertical hydraulic conductivity ratio of at least 1.5 to 2 (Section 6.4 and Appendix F). If the flow system were homogeneous and isotropic, the expected 2,5 DFBA travel time in the vertical direction from the bottom of zone 1 to the top of zone 2 (a distance of about 20 m) would be about 30 days. This estimate assumes a vertical hydraulic conductivity of ~12 m/day (based on the zone 2 hydraulic test interpretation), a drawdown difference of ~0.1 m between zones 1 and zone 2 (observed when zone 2 was pumped), and a flow porosity of 0.1 (based on the tracer test interpretations discussed below); (i.e., travel time = $L/(K\Delta H/L)/\eta$, where L = distance, K = hydraulic conductivity, ΔH = head or drawdown difference, and η = flow porosity, = 20 m / (12 m/day × (0.1/20) m/m / 0.1 = ~33 days). Given the observed horizontal tracer travel time of less than 10 days between wells 22PA and 22S, one would expect the 2,5 DFBA arrival time at 22S to be no more than about 30 + 10 = 40 days in a homogeneous, isotropic system. The fact that there was no 2,5 DFBA arrival at 22S in over 60 days of pumping (and also no arrival in another ~45 days of pumping during the second cross-hole tracer test) indicates that the flow system must have a lower effective vertical hydraulic conductivity relative to horizontal hydraulic conductivity. If the vertical travel distance were 20 m (the distance from the bottom of zone 1 to the top of zone 2), a lower bound estimate of the horizontal-to-vertical hydraulic conductivity ratio would be about 3:1 based on the fact that there was no arrival in over 100 days of pumping. However, if the vertical travel distance were greater than the minimum distance of 20 m, then the lower bound estimate of the conductivity ratio would be smaller. Also, the possibility that the 2,5 DFBA arrived at 22S in concentrations too low to detect cannot be discounted given that the 2,5 DFBA injection mass

was only about 18% of the injection mass of the 2,4,5 TFBA and 2,6 DFBA and that peak tracer concentrations tend to decrease approximately as 1/travel time.

For all tracer injections, a steady flow field was established between the injection wells and the production well (indicated by steady downhole pressures) prior to the tracers being injected, and the tracer solution was followed by a small volume of untraced "chase" water. This "chase" water was intended to "push" the tracers out of the injection wellbore and into the formation to minimize the possibility that they might linger in the wellbore, which would result in biased estimates of transport parameters. The chases were small enough in volume and duration that they should have had a negligible effect on the steady flow fields except very close to the injection interval. The production well was pumped at a steady rate of approximately 47.5 gal/min (180 L/min) during both tests, including throughout the tracer injections and chases.

Table G-13. Tracer Characteristics, Injection Masses, Injection Concentrations, and Fractional Recoveries in the Two Cross-Hole Tracer Tests at Site 22

Solute Tracers – Test 1 [a]				
Parameter	**2,4,5 TFBA**	**Bromide**	**Lithium**	**2,6 DFBA**
Free water diffusion coefficient at infinite dilution, D_f (cm^2/s)	7.2×10^{-6} [b]	2.1×10^{-5} [c]	1.0×10^{-5} [c]	7.5×10^{-6} [b]
Expected Sorption	None	None	Weak (ion exchange)	None
Target and directly measured injection mass (kg)	8.500	23.002	18.457 [d]	8.500
Injection mass based on measured injection concentration and volume (kg)	8.232	21.504	18.060	8.116
Approximate injection volume (L)	1,000	1,000	1,000	1,000
Tracer fractional recovery [e]	0.93 to 0.96 (0.06)	0.78 to 0.84 (0.03)	0.092	0.91 (0.14)

CML Microsphere Tracers – Test 1 [f]	
Parameter	**0.2-μm CML microspheres (yellow)**
Calculated free water diffusion coefficient, (cm^2/s)	2.15×10^{-8} [g]
Number of spheres injected	4.65×10^{14}
Injection concentration (number/L)	4.65×10^{11}
Approximate injection volume (L)	1000
Tracer fractional recovery	0.011

Solute Tracers – Test 2		
Parameter	**Iodide**	**Perrhenate**
Free water diffusion coefficient at infinite dilution, D_f (cm^2/s)	2.1×10^{-5} [c]	1.46×10^{-5} [h]
Expected Sorption	None	None or very weak
Target and directly measured injection mass (g)	4,233.13	68.123
Injection mass based on measured injection concentration and volume (g)	3,375.77	59.740

porosity within the stagnant domain (as opposed to the matrix porosity), D_m is the diffusion coefficient within the stagnant porosity, and b is the ratio of the volume of the flowing porosity to the interfacial area between the flowing and stagnant porosity (as opposed to the fracture half aperture). It can be readily confirmed that $\frac{\phi}{b}\sqrt{D_m} = \frac{\phi_b\sqrt{D_m}}{R\phi_f/3(1-\phi_f)}$ for the diffusion-into-grains conceptual model of the alluvium, and $\frac{\phi}{b}\sqrt{D_m} = \frac{\phi_l\sqrt{D_m}}{\phi_f(b+L/2)}$ for the diffusion-into-layers conceptual model.

Before attempting the RELAP fits, it was first noted that the rising limbs of the bromide and TFBA breakthrough curves (Figure G-34) had the unconventional appearance of being steepest at the point of initial breakthrough with gradually decreasing slopes until the peak concentration was reached and even a hint of one or two nearly linear segments between the initial breakthrough and the peak. Figure G-41 shows the derivative of the bromide concentrations with respect to time as a function of time in the early portion of the tracer test. The derivatives at any given time were calculated using the following 20-point moving-average formula, which served to smooth out the derivative data without compromising any of the information contained in the data:

$$\left(\frac{dC}{dt}\right)_i = \frac{Average(C_i, C_{i+19}) - Average(C_{i-20}, C_{i-1})}{Average(t_i, t_{i+19}) - Average(t_{i-20}, t_{i-1})}$$

where, C = concentration

t = time
i = data point corresponding to the time at which the derivative is calculated.
$Average(A_x,A_y)$ = average of A (concentration or time) for consecutive data points x through y (relative to the current data point i).

Three distinct maxima are shown on Figure G-41. Multiple maxima are not generally observed from breakthrough curves that result from a single dominant flow pathway. Furthermore, model fits of the data using only a single advective-dispersive pathway do not match the early portion of the breakthrough curve (Figure G-42). These two lines of evidence combined strongly suggest separate arrival of the tracers along separate flow pathways in the flow system. The derivative of concentration curve (Figure G-41) suggests that three pathways were dominant.

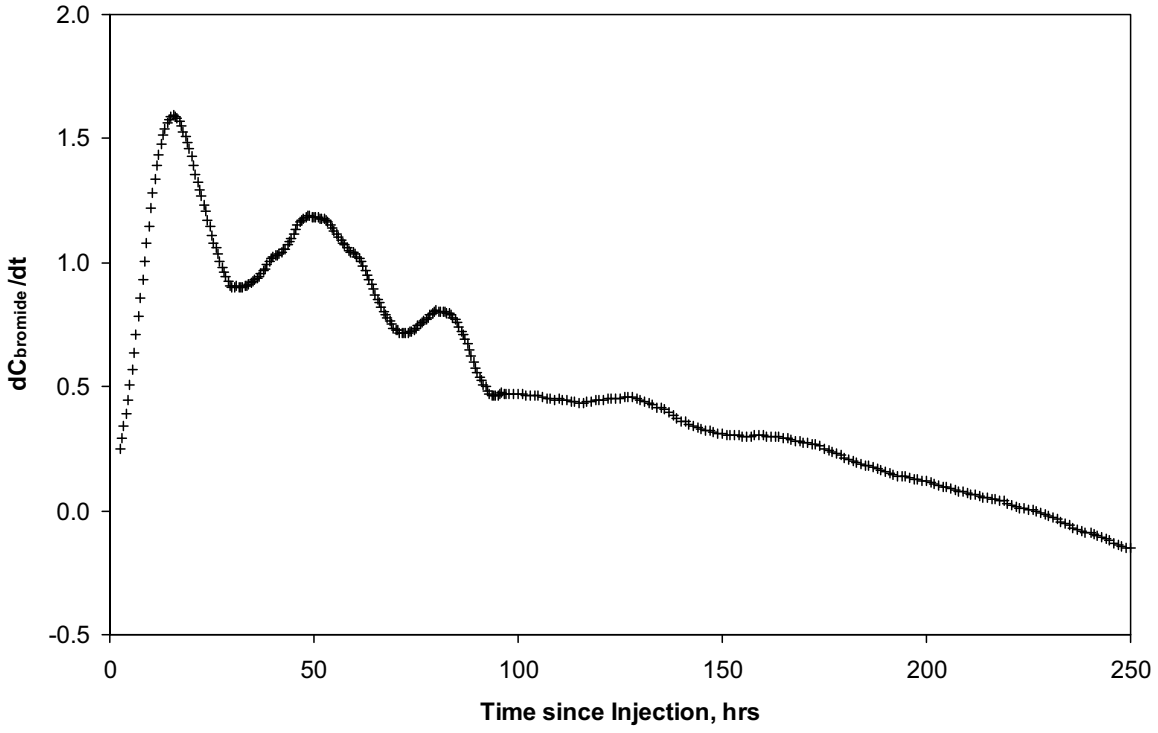

Source: DTN: LA0612PR831231.003 [DIRS 178736].

NOTE: The three prevalent peaks are interpreted as corresponding to separate tracer arrivals associated with different flow pathways.

Figure G-41. Derivative of Bromide Concentration with Respect to Time as a Function of Time since Injection in the First Cross-Hole Tracer Test at Site 22

For these reasons, the bromide and TFBA breakthrough curves were simultaneously fitted as three separate breakthrough curves in a sequential manner with RELAP. The earliest arrivals were fitted first, and then the model curves resulting from these fits were subtracted from the observed breakthrough curves and the differences were fitted. This process was repeated so that the overall fits to the bromide and TFBA breakthrough curves consisted of the sum of the three separate fits corresponding to the three separate flow pathways suggested by Figure G-41. The multiple pathway fits to the bromide and TFBA breakthrough curves with the minimum and maximum possible differences are shown in Figures G-43 and G-44. The model parameters corresponding to the these fits are provided in Tables G-14 and G-15, respectively. The dual-porosity pathways were simulated assuming a "diffusion-into-layers" conceptual model because RELAP does not have a diffusion-into-grains capability.

Figure G-43 and Table G-14 also show the results of a single-porosity RELAP fit to the 2,6 DFBA breakthrough curve, which represents transport between 22PC and 22S. A single-porosity model was used to fit these data because there were no other tracer responses that could be used to estimate diffusion parameters. A single-porosity assumption was considered justified because the third Br–TFBA pathway in the case of the minimum possible differences between these tracer concentrations was interpreted as having no diffusion (i.e., single-porosity

Table G-14. RELAP Model Parameters Yielding Fits to the Solute Responses for the Three Pathways in the First Cross-hole Tracer Test at Site 22 for the Case with the Minimum Possible Differences between the TFBA and Bromide Breakthrough Curves and for the Single Pathway Interpreted for DFBA (Figure G-43) (continued)

	22PA to 22S (2,4,5 TFBA)			22PC to 22S (2,6 DFBA)
Parameter	**Pathway 1**	**Pathway 2**	**Pathway 3**	**Single Pathway**
Ratio of stagnant to flowing water porosity	0.7	0.9	N/A	N/A
Characteristic diffusion time scale ($L^2/8D_m$), hr	68.1	1125	N/A	N/A
Lithium flowing porosity retardation factor, R_f	1.25	1.7	10.5	N/A
Lithium stagnant porosity retardation factor, R_s	33	800	N/A	N/A

Output DTN: LA0701PR150304.002.

NOTE: TFBA and bromide curves associated with fitted pathways 1 to 3 are shown on Figure G-43. The lithium fit is shown in Figure G-46.

[a] The mass transfer coefficient, $MTC = \frac{\phi}{b}\sqrt{D_m}$, for TFBA is ~0.58 times that for bromide.

MTC=mass transfer coefficient; TFBA = Trifluorobenzoic acid or trifluorobenzoate.

Table G-15. RELAP Model Parameters Yielding Fits to the TFBA, Bromide, and Lithium Responses in the First Cross-Hole Tracer Test at Site 22 for the Case with the Maximum Possible Differences between the TFBA and Bromide Breakthrough Curves (Figure G-44)

	22PA to 22S		
Parameter	**Pathway 1**	**Pathway 2**	**Pathway 3**
Mass fraction, *f*	0.05	0.68	0.27
Mean residence time, τ, for linear flow (hr)	100	400	400
Peclet number, *Pe*, for linear flow	2.1	2.2	8
Mean residence time, τ, for radial flow (hr)	67	270	346
Peclet number, *Pe*, for radial flow	3.5	3.6	11.3
$\frac{\phi}{b}\sqrt{D_m}$ for bromide ($s^{-1/2}$) [a]	0.001	0.00089	0.00022
Ratio of stagnant to flowing water porosity	0.7	1.9	0.63
Characteristic diffusion time scale ($L^2/8D_m$), hr	68.1	627	1125
Lithium flowing porosity retardation factor, R_f	1.3	1.9	5
Lithium stagnant porosity retardation factor, R_s	32	135	900

Output DTN: LA0701PR150304.006.

NOTE: TFBA and bromide curves associated with fitted pathways 1-3 are shown on Figure G-44. The lithium fit is shown in Figure G-47.

[a] The mass transfer coefficient, $MTC = \frac{\phi}{b}\sqrt{D_m}$, for TFBA is ~0.58 times that for bromide.

MTC=mass transfer coefficient; TFBA = Trifluorobenzoic acid or trifluorobenzoate.

An additional fit to the bromide and TFBA data was conducted after adjusting the normalized concentrations of the two tracer data sets so that the tracers had essentially the same recoveries. This adjustment raised the bromide breakthrough curve relative to the TFBA so that both tracers had approximately the same peak normalized concentration and the primary difference between the two tracers was the timing of the peaks. Furthermore, only the peaks of the tracer

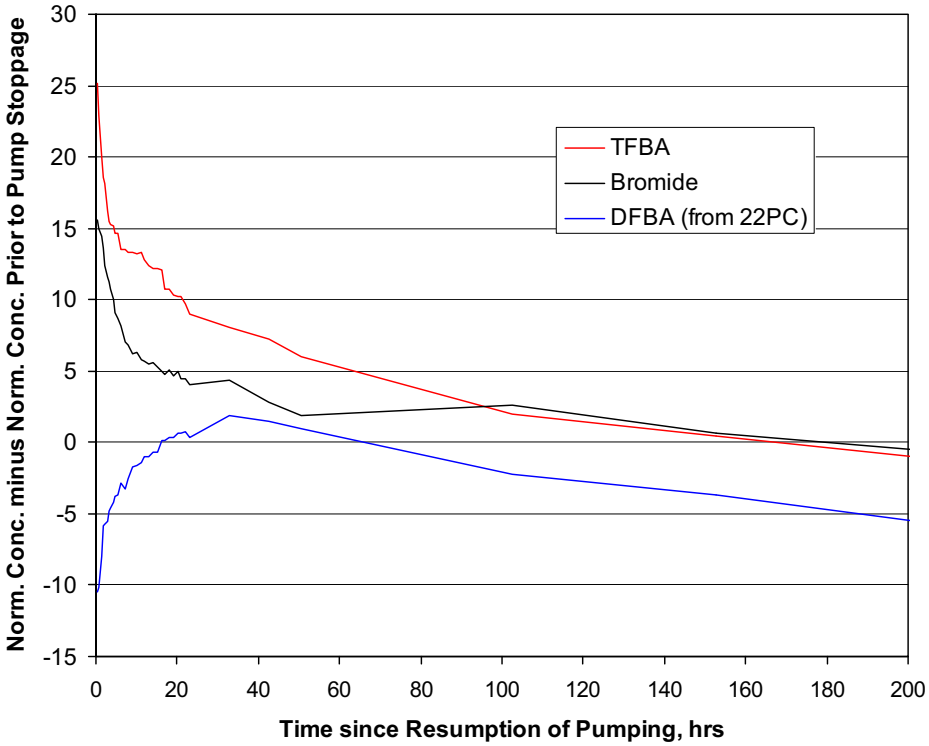

Output DTN: LA0701PR150304.004.

NOTE: There was no pumping for 159 days prior to time zero.

Figure G-52. Normalized Concentrations of Nonsorbing Tracers used in the First Cross-HoleTracer Test at Site 22 Minus Their Normalized Concentrations Prior to Pump Stoppage as a Function of Time Since Pumping Resumed

Qualitatively, the tracer responses are consistent with the groundwater drift illustrated schematically in Figure G-53. Unfortunately, it is not possible to obtain a well-constrained estimate of the groundwater drift velocity during the flow interruption because the distribution of the tracer plume around NC-EWDP-22S at the time of the flow stoppage was unknown. However, we can make a rough estimate of the drift velocity if the direction of drift was essentially in the direction from 22PA to 22S is assumed as follows (Output DTN: LA0701PR150304.004):

- It took about 150 hours for the TFBA and bromide concentrations to decline to their concentrations prior to the pump stoppage. It is reasonable to assume that during this 150 hours, the water being drawn into NC-EWDP-22S included at least some traced water that had drifted into the volume of water produced during this first 150 hours of pumping.

- The 150 hours that it took for the tracer concentrations to decline to preflow interruption levels represents about 75% of the time it took for *peak* tracer concentrations to arrive from -22PA (i.e., ~200 hrs). Assuming that the time to peak concentrations represents the approximate time it takes to "sweep out" a cylindrical volume of the aquifer with

assumed, the fact that the lithium breakthrough curve was better fit assuming dual-porosity behavior in all three flow pathways (Figure G-47 versus Figure G-46) argues for some dual-porosity character in all the flow pathways in the system.

In contrast, the results of single-well tracer testing in 19D do not support a dual-porosity conceptualization of the alluvium at that location. However, the volume of alluvium interrogated in these single-well tests is considerably smaller than the volume interrogated in cross-hole tests, so the former tests are considered less reliable than the latter in discriminating between conceptual transport models. Single-well tests are more likely to be influenced by local heterogeneities or local disturbances of the alluvium due to drilling and well completion.

While the data at 22S are consistent with a dual-porosity transport conceptualization, the tracer responses also suggest that the time scales for diffusion are quite short and the stagnant porosity is only 0.3 to 1.9 times the flowing porosity in the alluvium. It can be shown that if advective transport times are long relative to diffusion time scales, a nonsorbing solute will experience an effective physical retardation factor equal to 1.0 plus the ratio of stagnant to flowing porosity in a system (Robinson 1994 [DIRS 101154]). Advective time scales are clearly longer than deduced times scales for diffusion (Table G-20) in the alluvium under ambient flow conditions, so the range of porosity ratios of 0.3 to 1.9 translates to a range of effective physical retardation factors of 1.3 to 2.9 in the alluvium. In effect, over time and distance scales relevant for Yucca Mountain performance assessment, the saturated alluvium can be expected to behave as a single-porosity system with a flow porosity equal to the sum of the flowing porosity and stagnant porosity deduced from the relatively short-duration tracer tests. It is interesting to note that the mass-fraction-weighted sum of the flowing and stagnant porosities from the two pathways between 22PA and 22S in the second cross-hole tracer test (the test without density-driven flow issues) is slightly greater than 0.2, which is probably quite close to the total porosity of the alluvium (considered to have a maximum value of around 0.3). Thus, while we cannot rule out the possibility of longer diffusion time and distance scales in the alluvium than the tracer tests indicated, the test interpretations are consistent with tracers accessing the majority of the total porosity in the flow system.

It is also worth noting that the short diffusion time scales are more consistent with a diffusion-into-grains conceptual transport model (Figure G-1(b)) than a diffusion-into-layers conceptual model (Figure G-1(c)) because the latter will typically have significantly longer diffusion time scales than were observed. However, longer diffusion time scales cannot be ruled out in the alluvium because of the short time and distance scales of the tracer tests relative to performance assessment time scales. It is possible that the tests were strongly influenced by diffusion into grains within flow pathways, but the flow pathways were large enough in thickness or diameter (i.e., channels) that longer-time-scale diffusion into stagnant water surrounding the pathways was not observed.

Finally, it is noted that the quantitative estimates of the lumped diffusion mass transfer parameter, $\frac{\phi}{b}\sqrt{D_m}$, for halides in Table G-20 are based on the assumption that halides have a diffusion coefficient a factor of three greater than FBAs, which is based on matrix diffusion

coefficients measured in laboratory diffusion cell tests in consolidated tuff matrices (discussed in Section E2). It is worth repeating here that the individual parameters that comprise $\frac{\phi}{b}\sqrt{D_{\mathrm{m}}}$ have

slightly different interpretations in alluvium systems than in fractured rock systems. In alluvium, ϕ is the stagnant porosity (as opposed to the matrix porosity), D_m is the diffusion coefficient within the stagnant porosity, and b is the volume of the flowing porosity divided by the interfacial area between the flowing and stagnant porosity (as opposed to the fracture half aperture). It is also worth noting that, regardless of what the absolute values are for the diffusion coefficients, flowing and stagnant porosities, and length scales associated with flowing and stagnant porosities, the same transport behavior will be observed if the characteristic time scale for diffusion, $L^2/8D_m$ (diffusion-into-layers model) or $R^2/2D_m$ (diffusion-into-spherical grains model), the mass transfer coefficient, $\frac{\phi}{b}\sqrt{D_{\mathrm{m}}}$, and the ratio of stagnant to flowing water volumes (or porosities) are kept the same.

G5.4.2 Horizontal Flow Anisotropy and Flow Heterogeneity Considerations

Estimates of horizontal flow anisotropy in the saturated alluvium at Site 22 were obtained by comparing the nonsorbing tracer transport times between 22PA and 22S and between 22PC and 22S. 22PA and 22S are oriented almost due north–south (Figure 6.1-8), and 22PC and 22S are oriented almost due east–west. The flow anisotropy ratio (the ratio of largest to smallest hydraulic conductivity in the so-called conductivity ellipse that defines the two-dimensional anisotropy) was estimated simply as the inverse of the ratio of the mean nonsorbing tracer residence times between 22PA and 22S and between 22PC and 22S. As Table G-20 indicates, the estimates range from about 2.5 to 11, with the principal axis or preferred flow direction being north–south. The upper end of this range is based on using the travel times associated with the first flow pathway between 22PA and 22S, and the lower end is based on using the travel times associated with the second flow pathway between these wells. The third flow pathway observed in the first cross-hole tracer test was not considered because this pathway was not reproduced in the second cross-hole tracer test and was believed to be an artifact of density-driven flow of the very concentrated, high-density tracer solution used in the first test. Because the majority of the tracer mass in both the first and second cross-hole tests followed the second pathway between 22PA and 22S, this pathway is considered more representative for flow anisotropy estimates, and it forms the basis for the best estimate of 3.1:1 north–south for the anisotropy ratio in Table G-20.

Although not necessarily directly related to flow anisotropy, it is interesting that the first flow pathway between 22PA and 22S had very little tracer mass in it compared to the second pathway. This observation relates to the heterogeneity of flow in the alluvium. Normally, one would expect a faster pathway to also have the higher volumetric flow rate and therefore more mass associated with it. In this case, multiple pathways would probably not even be apparent in tracer breakthrough curves. The fact that the first pathway was observed in both tracer tests, under conditions with both a high density contrast and a low density contrast between the injection solution and the ambient groundwater, suggests that the small amount of mass in the fast pathway was probably not caused by density-driven flow effects in the vicinity of the injection wellbore (as suspected in the case of the multiple tracer test in the Bullfrog tuff at the C-wells – see Section D4.5). Rather, it appears likely that a low-volume, high-flow pathway exists. However, another possible explanation given the method of injection is that there is only a single fast-flow pathway that passes close to 22PA but does not directly intersect it, and the chase water that followed the tracer solution pushed a small amount of tracer mass into this

within the flowing porosity, but the R_s values are large, indicating strong sorption in stagnant porosity after diffusion into this porosity. The MULTRAN fit of Figure G-48 shows that even when multicomponent diffusion and cation exchange effects are explicitly accounted for, a single-porosity model cannot provide nearly as good of a match to the lithium breakthrough curve as a dual-porosity model without these features (RELAP). Qualitatively, these results provide additional support for a dual-porosity conceptualization of transport in the alluvium.

Estimates of lithium partition coefficients, or K_d values, were deduced from the fitted retardation factors by simple rearrangement of the expression defining the retardation factor (repeated here from Section D4.8.4):

$$K_d = \frac{\phi}{\rho_B}(R-1) \qquad \text{(Eq. D-5)}$$

Because the retardation factors in Tables G-14 and G-15 vary over such a wide range and the K_d values depend on the porosity within the stagnant or flowing regions of the flow system, K_d values are listed in Table G-21 for a wide range of potential porosities and for each retardation factor from Tables G-14 and G-15 (two values are lumped because they are very similar). In the K_d calculations, ρ_B was assumed to be equal to $2.65(1-\phi)$ g/cm^3, where 2.65 is the approximate density of many silicate phases present in the alluvium.

For comparison, Table G-22 lists lithium K_d values over a wide range of lithium concentrations measured in batch sorption experiments involving 22S water and alluvium material from two different zones within 22PC. The K_d values in Table G-22 do not reflect direct measurements, but rather they are calculated from the Freundlich isotherm parameters that provided the best fits to the experimental sorption isotherms, which are shown in Figure G-55 and provided in its caption (DTN: LA0703PR150304.001 [DTN 179625]). The wide range of concentrations in Table G-22 reflect the wide range that likely existed in the Site 22 field tracer test. The injection concentration of lithium was about 20,000 mg/L and the peak measured concentrations in the 22S production water were around 0.2 mg/L. The latter value should be considered an extreme lower bound estimate for concentrations in the aquifer, as there was probably considerable dilution with untraced water occurring in the production wellbore.

As Tables G-21 and G-22 indicate, the K_d values associated with retardation factors deduced from stagnant porosity in the field tests (32 or greater) are in relatively good agreement with or somewhat higher than the laboratory-derived K_d values. If the porosity within the stagnant porosity is 0.1 or greater, then the field values are all higher than would be expected from the lab measurements. In the case of the flowing porosity, the field retardation factors (10.5 or lower) are all consistent with K_d values that are in relatively good agreement with or lower than the laboratory-derived values. This result could indicate that there is relatively low effective surface area available for sorption within the flowing porosity and all the sorption in the alluvium effectively occurs after a diffusive mass transfer step into stagnant porosity. However, as pointed out in Section G5.4.1, for transport over long time and distance scales, it should be possible to treat the alluvium as a single-porosity system, and in this case, the distinction between retardation factors or K_d values in flowing and stagnant porosity becomes a moot point. However, the effective retardation factor in this case should be a volume weighted average of the two retardation factors. Although the laboratory data set is small and can't be considered

representative of all the mineralogical heterogeneity that likely exists in the alluvium, and there is also considerable uncertainty in the lithium concentrations that actually existed in the aquifer, it is concluded that the laboratory-derived K_d values are in reasonably good agreement with the field-derived values. If the average lithium concentrations in the field test were at the upper end or middle of the range in Table G-22, then it could be concluded that the lab K_d values would tend to underestimate field-scale sorption if they were used in field-scale predictive calculations.

An interesting trend in Tables G-14 and G-15 is that the lithium retardation factors in both the flowing and stagnant porosity appear to increase as flow pathway residence times in the alluvium increase. Given the time scales of the tracer responses and the fact that lithium sorption occurs by cation exchange (a rapid process), it seems unlikely that this trend could be explained by slow sorption kinetics. The reason for this apparent time-scale dependence of lithium sorption is unknown at this time. It could be just coincidence that the longer travel time pathways exhibit greater sorption, but a similar trend was also observed for the two flow pathways in the multiple-tracer test in the Bullfrog tuff at the C-wells (see Table D-6). These results suggest that the scaling behavior of reactive transport should perhaps be investigated further because of the important potential implications for transport of sorbing radionuclides over long time and distance scales in the alluvium near Yucca Mountain.

Table G-21. Calculated Lithium Partition Coefficients (K_d Values) for Various Assumed Porosities Using Retardation Factors Derived from Field Tracer Tests

	K_d Value				
Retardation Factor	**ϕ = 0.02**	**ϕ = 0.05**	**ϕ = 0.1**	**ϕ = 0.2**	**ϕ = 0.3**
1.25	0.002	0.005	0.011	0.024	0.040
1.7	0.005	0.014	0.029	0.066	0.113
1.9	0.007	0.018	0.038	0.085	0.146
5	0.031	0.079	0.17	0.38	0.65
10.5	0.073	0.19	0.40	0.90	1.54
32.5	0.24	0.63	1.32	2.97	5.09
135	1.03	2.66	5.62	12.6	21.7
800	6.15	15.9	33.5	75.4	129.2
900	6.92	17.9	37.7	84.8	145.4

Output DTN: Values calculated using equation D-5 with lithium partition coefficients (K_d values) from DTNs: LA0701PR150304.002 and LA0701PR150304.006.

dual-porosity transport regardless of the uncertainties in the normalizations of the tracer breakthrough curves.

Another uncertainty associated with the alluvium tracer test interpretations is the inherent and unquantifiable uncertainty associated with the conclusion that diffusion time and distance scales are quite small and that the alluvium should therefore behave as a single-porosity transport system over much larger time and distance scales than the tracer tests. The possibility exists that the time and distance scales of the tracer tests may have been too short to observe significant diffusion out of flowing pathways and into relatively extensive layers or grains of stagnant or near-stagnant alluvium in the flow system. Furthermore, the uncertainties associated with the tracer injection masses (above) make any assessment of larger diffusion time and length scales essentially impossible using the available data from Site 22.

It is well known that CECs of materials are dependent on the cation used to saturate the material surfaces (Anghel et al. 2002 [DIRS 164635], Section 3.1, pp. 821 to 822). The Cs^+ ion is often used to obtain a measure of the "total" CEC of a material because Cs^+ sorbs very strongly to mineral surfaces and will displace most exchangeable cations encountered in nature. To obtain an estimate of the Cs^+-exchangeable CEC, the above procedure was repeated on each of the half-gram alluvium samples that had been subjected to LiBr solution treatments using 1 M CsCl as the saturating solution. However, the CEC determined from the lithium saturation steps was the value used in subsequent modeling of the batch-sorption and column experiments (Section H2) because only cations displaced by lithium are of practical interest when lithium is the sorbing species.

H1.3 BATCH-SORPTION EXPERIMENTS

Lithium batch-sorption experiments were conducted on each of the sieved alluvium samples. Duplicate measurements were conducted at starting lithium concentrations of approximately 1, 3, 10, 30, 100, and 300 mg/L Li^+ for each material to obtain a sorption isotherm over a 2.5-order-of-magnitude range of concentrations. Starting solutions were prepared by dissolving a known mass of LiBr in a known volume of 19D well water and then diluting by weight with well water to the desired starting concentrations. In all of the batch tests, 20 mL of lithium solution was placed in contact with approximately 5 g of alluvium material in 50-mL polycarbonate Oak Ridge centrifuge tubes that were shaken for 48 hr on an orbital shaker. Separate control samples (lithium-spiked solutions in centrifuge tubes without any alluvium material) and blanks (nonspiked well water in contact with alluvium) were processed in parallel with the tubes containing both lithium and alluvium. The controls were used to verify that lithium sorption to tube walls was insignificant, and the blanks were used to measure any lithium background that might be leached out of the alluvium samples. After shaking, the tubes were centrifuged at 30,000x g (at an acceleration 30,000 times that of gravity) for 1 hr, and then an aliquot of supernatant was pipetted off for cation and bromide analyses. Cations (lithium, sodium, potassium, calcium, and magnesium) were analyzed by inductively coupled ICP-AES, and bromide (nonsorbing tracer) was analyzed by liquid chromatography with a conductivity detector.

The starting lithium concentration for each measurement was determined from both the corresponding bromide and lithium concentrations in the control samples. In general, lithium concentrations measured in the control samples were in good agreement with those determined from the bromide measurements, indicating that lithium sorption to centrifuge tube walls was negligible. The mass of lithium sorbed per unit mass of alluvium material was determined from:

$$S = \frac{V(C_0 - C)}{M} \qquad \text{(Eq. H-1)}$$

where

S = lithium mass sorbed per unit mass of alluvium, mg/g
V = volume of solution in contact with alluvium, L
M = mass of alluvium in contact with solution, g
C_0 = initial concentration of lithium in solution prior to sorption, mg/L
C = final concentration of lithium in solution after sorption, mg/L.

Table H-4. Major Ion Chemistry of NC-EWDP-19D Water Used in the Experiments

Species	Batch 1 [a] (mg/L)	Batch 2 [b] (mg/L)
Ca^{++}	2.2	7.5
Na^{+}	118	75.5
K^{+}	5.2	4.1
Mg^{++}	1.13	0.65
Li^{+}	0.15	0.09
Si	52.5	27.1
HCO_3^{-}	193	168
CO_3^{2-}	43.8	0
SO_4^{2-}	25.9	23.0
Cl^{-}	5.7	5.6
F^{-}	2.1	1.8
pH	9.2	8.1

Source: DTN: LA0303PR831232.001 [DIRS 162781].

[a]Batch 1 was collected in June 2000 from an open borehole.
[b]Batch 2 was collected from two isolated screened intervals in the upper 46 m (150 ft) of the saturated zone. This batch was used only for the 0.006 M LiBr column experiments.

Column experiments were conducted in duplicate using separate 30-cm-long by 2.5-cm-diameter glass columns equipped with polytetrafluoroethylene end fittings, including a 20-µm end frit and PTFE tubing. Each column was presoaked in deionized water to remove any residual ions. The columns were packed dry with a 50:50 mass ratio of the wet-sieved alluvium from the two intervals used in batch-sorption and CEC testing. The columns then were saturated by flushing with deaerated groundwater until air bubbles were no longer visible. They also were packed in ice for 8 hr to promote oxygen and nitrogen dissolution in the water. The saturated versus dry weights of the columns indicated a final porosity of about 40% with a pore volume of about 60 mL in each column.

Three transport experiments were conducted in each column at a flow rate of approximately 10 mL/hr with the two columns run in parallel. Each experiment involved the injection of approximately one pore volume of a tracer solution containing LiBr and 2 mg/L of an fluorobenzoate (FBA)(either pentafluorobenzoate or 2,4-difluorobenzoate) dissolved in 19D groundwater. The experiments differed in the concentrations of LiBr in the injection pulses. The first duplicate set of experiments was conducted using an injection concentration of 0.0275 M LiBr (190 mg/L Li^{+}), the second set had a concentration of 0.006 M LiBr (42 mg/L Li^{+}), and the third set had a concentration of 0.0013 M LiBr (9 mg/L Li^{+}). These concentrations were selected so that Li^{+} dominated the cation equivalents in solution in the first case (91% of total cation equivalents), accounted for about half of the cation equivalents in the second case (61%), and were a relatively minor fraction of the total cation equivalents in the third case (24%). These three situations represent a range of conditions that will likely occur during field testing, with relatively high concentrations present near the injection well immediately after injection, and concentrations decreasing as the tracer pulse advects and disperses through the flow system.

field transport behavior is consistent with the laboratory data if the existence of high concentrations is recognized.

The ability to distinguish between early and late dilution could help refine or constrain estimates of effective flow porosities derived from cross-hole tracer tests. When nonsorbing tracer responses are analyzed, flow porosity estimates are typically based on first, mean, or peak arrival times of nonsorbing tracers. Under ideal radial flow conditions in a two-dimensional aquifer, Equation D-6 (introduced in Section D4.8.5) can be used to estimate effective flow porosity. Equation D-6 (which is a rearrangement of equation 6 of Guimera and Carrera 2000 [DIRS 156830]) and the definitions of its variables are repeated here for convenience:

$$\eta = \frac{Q\tau}{\pi L^2 T} \qquad \text{(Eq. D-6)}$$

where

η = flow porosity
Q = production flow rate, m^3/hr
τ = mean residence time of a nonsorbing tracer, hr
L = distance between wells, m
T = formation thickness (assumed to be well screen length), m.

If flow heterogeneity exists, causing the flow field to not be radial, then estimates using equation D-6 will be erroneous. For instance, if most of the flow to the production well is channeled from a direction that does not intersect the tracer slug, then the interwell transport time for the slug can be very long, even if flow occurs in only a small fraction of the system volume. In this case, a considerable amount of dilution will occur late in the system (in the production well), and a misleadingly high flow porosity will be deduced from equation D-6. If an asymmetric lithium response curve with some apparent nonsorbing transport is detected at the production well, the degree of asymmetry in the response can, in principle, be used to estimate the volume that the tracer pulse flowed through within the system. Such an estimate can be obtained by first using MULTRAN V 1.0 (STN: 10666-1.0-00 [DIRS 159068]) in inverse mode to match the shape of the response curve, given a known injection pulse concentration, injection duration, alluvium CEC (estimated from laboratory tests), and a longitudinal dispersivity (estimated from the nonsorbing tracer responses). Once a curve shape is matched given these constraints, the flow system volume can be estimated by multiplying the volume of the injection pulse in the field test by the ratio of flow system volume to injection pulse volume assumed in the MULTRAN simulations. An estimate of flow porosity can then be obtained from:

$$\eta = \frac{V}{\pi L^2 T} \qquad \text{(Eq. H-2)}$$

where V = volume determined from MULTRAN matches to the lithium response.

Table J-1. Mineral Weight Percentages and Reported Errors (in Weight Percent Units) from Quantitative XRD Analyses of UE25c#2-2406 and UE25c#1-2346

Mineral	UE25c#2-2406 [a]	UE25c#1-2346 [b]
Smectite	5±2	2±1
Mica	1±1	3±1
Clinoptilolite	ND	ND
Mordenite	ND	ND
Analcime	ND	ND
Quartz	32± 2	34 ±2
Feldspar	62± 7	61± 9
Hematite	1± 1	Trace
Calcite	ND	1± 1
Kaolinite	ND	ND

NOTE: ND = Not Determined.

[a]Taken from DTN: LA9909PR831231.004 [DIRS 129623], SEP Table S99488_003 (unqualified).
[b]Taken from DTN: MO0012MINLCHOL.000 [DIRS 153370], SEP Table S00449_001 (qualified).

uncertainties associated with the testing). Thus, even inaccuracies of several feet in the test interval thickness would not have a significant impact on the uncertainties in the parameter estimates, as reported in Section 6.4.6. Furthermore, Section 6.4.6 also states that "hydrologic parameters derived from ATC and Site 22 testing are not used as direct inputs in *Saturated Zone Site-Scale Flow Model* (SNL 2007 [DIRS 177391]), but rather they are used primarily for qualitative/corroborative consistency checks with the hydrologic parameters that are derived from calibrations of *Saturated Zone Site-Scale Flow Model* (SNL 2007 [DIRS 177391])."

Given the reported accuracy of the data (Section 6.4.6), the ultimate end use of the hydrologic parameters derived from the data, and the fact that several Nye County well completion diagrams prepared by the same methods were previously qualified, the well completion diagrams in DTN: LA0705PR150304.007 [DIRS 181202] are considered qualified for their intended use in the analysis presented in Sections F2 and F6. The source DTN: LA0705PR150304.007 [DIRS 181202] will remain unqualified for other uses.

N3. NYE COUNTY TECHNICAL PROCEDURES

The two applicable technical procedures that Nye County personnel followed when conducting the hydraulic tests at NC-EWDP Site 22 were TP-9.2 (NWRPO 2005 [DIRS 178608]) and TP-10.0 (NWRPO 2002 [DIRS 178607]). These procedures were reviewed and found to be technically sound, and they are sufficiently descriptive that an independent investigator familiar with the testing equipment could quite easily reproduce the work. While the procedures and their supporting framework of procedures do not satisfy all the requirements of the Yucca Mountain/Lead Lab *Quality Assurance Requirements and Description* (DOE 2006 [DIRS 177092]), they are substantially equivalent in technical content to most YMP technical procedures, and following them should result in data of comparable technical quality to YMP-generated data (albeit with less stringent supporting procurement and vendor quality assurance requirements and less formal training, planning, documentation, and data management supporting requirements). The Nye County procedures reflect "standard industry practice" for conducting hydraulic tests that are used for water resource assessment and environmental remediation applications, and the data generated under the Nye County quality assurance program are certainly considered worthy of publication in peer-reviewed journals.

N4. VENDOR CALIBRATION RECORDS

Calibration records for key Westbay® Mosdax® pressure and temperature transducers used in the Site 22 hydraulic tests are included in Section N11. The serial numbers of the key transducers and the tests and borehole intervals in which they were used are listed in Table N-1.

Table N-1. Serial Numbers, Tests, and Borehole Intervals for Key Pressure Transducers Used in Site 22 Hydraulic and Tracer Tests

Serial Number	Mar 02, Combined	Aug 03, Zone 1	Aug 03, Zone 2	Sept 03, Zone 3	Sept 03, Zone 4	Jan 05, Zone 2	Aug 05, Zone 2
2291	—	atm	atm	atm	atm	—	—
2292	—	—	—	—	—	atm	—
2295	atm	—	—	—	—	—	atm
2323	22S-pump	22S-pump	22S-pump	22S-pump	22S-pump	22S-Pump	22S-Pump
2554	atm	—	—	—	atm	atm	atm
2565	—	atm	—	—	—	—	—
2693	—	—	atm	atm	—	—	—
2844	22PA S	22PB D	22PB D	22PB D	22PB D	22PB S	22PB S
2845	22PA D	22PA D	22PA D	22PA D	22PA D	22PA S	22PA S
2846	22PB S	22PB S	22PB S	22PB S	22PB S	—	—
3363	22PB D	22PA S	22PA S	22PA S	22PA S	—	22PA D

NOTE: January 2005 and August 2005 tests were not used directly in hydraulic test interpretations but were used for corroboration.

atm = atmospheric pressure measurement, S = shallow piezometer pump = pumped interval, D = deep piezometer.

Table N-1 includes transducers that were used in 2005 cross-hole tracer tests, because these tests were used for cross-comparisons between transducers and between tests to establish corroborative verification of transducer performance (Section N7). Several other transducers were used during the tests, but the ones in the observation well intervals (22PA shallow and deep

zone in hydrology boreholes USW H-3, H-4, and H-5 and water-table boreholes USW WT-10, UE-25 WT#12, UE-25 WT#14, and UE-25 WT#17 was performed with a stereomicroscope. Each cuttings sample represents 10 ft (3.05 m) of drilled rock. Readily available petrographic thin sections of drill core and cuttings were used; these were examined by reflected-light microscopy to provide additional data on sulfide mineral distribution and details of sulfide-mineral origin. The use of existing thin sections means that sample selection was not necessarily optimal for the study of sulfide occurrences. No quantitative determinations of sulfide abundance were made for this report. Visual estimates of sulfide abundance are included in some descriptions. Estimates are based on comparisons with standard charts such as those of Compton (1962 [DIRS 101588], pp. 332 to 333). Table O-1 lists all the boreholes from which samples were examined. Sample depths, unless otherwise indicated, are vertical depths below the land surface. Borehole identifiers in the text are abbreviated after first mention by dropping the prefix.

Table O-1. Summary of Borehole Samples Examined for Sulfide Occurrence

Borehole Identifier	Sample Types	Sulfide Observed
ESF-HD-CHE-3 (Alcove 5, Exploratory Studies Facility)	drill core chip (electron microscopy mount)	yes
UE-25b#1 (previously called UE-25b-1H)	thin sections	yes
UE-25 p#1	thin sections	yes
USW G-1	thin sections	yes
USW G-2	thin sections	yes
USW G-3 and GU-3	thin sections	yes
USW G-4	thin sections	yes
USW H-1	thin sections	yes
USW H-3	drill-bit cuttings	yes
USW H-4	drill-bit cuttings	yes
USW H-5	drill-bit cuttings	no
USW H-6	thin sections	no (observation in legacy notebook not verified)
UE-25 J-13	thin sections	no
USW WT-10	drill-bit cuttings	no
UE-25 WT#12	drill-bit cuttings	no
UE-25 WT#14	drill-bit cuttings	no
UE-25 WT#17	drill-bit cuttings	no

Source: DTN: LA0701SL150304.001 [DIRS 179620].

Published and unpublished works on Yucca Mountain mineralogy were checked for information on sulfide occurrences. Information was abstracted directly from the original sources unless the same samples were examined for this study.

In this report, the term *xenoliths* refers to rock fragments presumed to be foreign to the pyroclastic rock in which they occur. Literature sources for this report have used this term or a variety of generally synonymous terms, such as *accidental lithic fragment* (Castor et al. 1994 [DIRS 102495], p. 401).

but occurs only in the lower part of the Lithic Ridge Tuff penetrated by the borehole. The sulfide distribution reported by Castor et al. (1994 [DIRS 102495], p. 401) in borehole USW G-3 more closely resembles the distribution in H-4, rather than that in the more proximal hole, H-3. No sulfides were observed in the cuttings from USW H-5. The highest estimated sulfide abundance is about 1.8 vol % (H-3 3,560 to 3,570 ft; DTN: LA0701SL150304.001 [DIRS 179620], Table 1). Sulfides are most common in xenoliths, as noted by Castor et al. (1994 [DIRS 102495], p. 401).

Table O-3. Summary of Sulfide Occurrences and Lithostratigraphy in Cuttings from Boreholes USW H-3, H-4, and H-5

	USW H-3	USW H-4	USW H-5
Sulfide-bearing depth interval, ft (m)	3,500 to 3,660 (1,066.8 to 1,115.6)	3,450 to 3,820 (1,051.6 to 1,164.3) 3,900 to 4,004 (1,188.7 to 1,220.4) TD	none
Tctlv depth interval, ft (m)	3,120 to 3,595.1 (951.0 to 1,095.8)	3,228 to 3,788 (983.9 to 1,154.6)	3,150 to 3,412 (960.1 to 1,040.0)
Tctbt depth interval, ft (m)	3,595.1 to 3,637.1 (1,095.8 to 1,108.6)	3,788 to 3,819 (1,154.6 to 1,164.0)	3,412 to 3,421.9 (1,040.0 to 1,043.0)
Tlr depth interval, ft (m)	3,637.1 to 4,000 (1,108.6 to 1,219.2) TD	3,819 to 4,004 (1,164.0 to 1,220.4) TD	not present
Lava, unnamed, depth interval, ft (m)	not present	not present	3,421.9 to 4,000 (1,043.0 to 1,219.2) TD

Sources: DTNs: LA0701SL150304.001 [DIRS 179620]; MO0004QGFMPICK.000 [DIRS 152554] for lithostratigraphic intervals to base of Tctbt; Bentley et al. 1983 [DIRS 101193], pp. 11 to 12, Thordarson et al. 1984 [DIRS 103200], pp. 9 to 10, Whitfield et al. 1984 [DIRS 101366], p. 11 for intervals below Tctbt.

NOTES: Detailed information on abundances of sulfides at specific depths in the same lithostratigraphic units, but different boreholes is provided in Table O-4.

Tctlv = Tram Tuff, lower vitric (zeolitic) nonwelded to partially welded; Tctbt = pre-Tram Tuff bedded tuff; Tlr = Lithic Ridge Tuff; TD = total depth of borehole.

The groundwaters from water-table boreholes WT-10, WT#12, WT#14, and WT#17 were identified in *Impacts of Solubility and Other Geochemical Processes on Radionuclide Retardation in the Natural System* (BSC 2006 [DIRS 178672], pp. 2-4 to 2-5) as having reducing chemistry. These boreholes are all less than 2,000 ft deep, too shallow to reach the Tram or Lithic Ridge Tuffs. The lithostratigraphic units within the saturated zone in the lower parts of the boreholes are the Topopah Spring Tuff (WT-10), the Calico Hills Formation (WT#12, WT#14), or the Prow Pass Tuff (WT#17; DTN: MO0004QGFMPICK.000 [DIRS 152554]). Cuttings samples from the lowermost 10 to 20 ft of these holes were examined, but no sulfides were observed.

O3.2 PETROGRAPHIC EXAMINATION

Los Alamos National Laboratory legacy and active notebooks were searched for entries relevant to sulfide-mineral occurrences in Yucca Mountain drill cores and bit cuttings. The information documents numerous occurrences from petrographic thin sections and one occurrence from a scanning-electron microscopy mount. Most of the thin sections in the original studies were reexamined, and expanded descriptions of the sulfide occurrences are given in Table O-4. In a few cases, the original sulfide identifications were not confirmed during reexamination, and the legacy information is included in the table with a notation to that effect. There also were a few

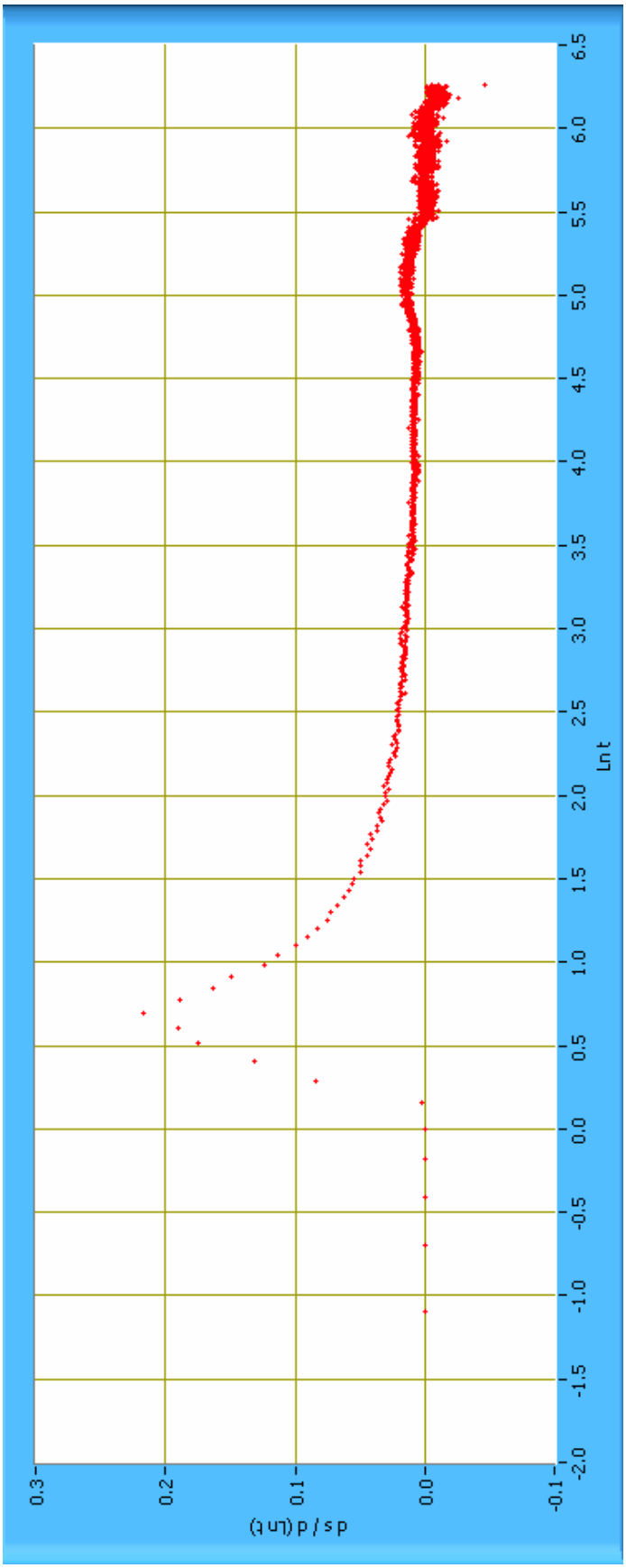

NOTE: In response to pumping Screen #2 in NC-EWDP-22S. The derivative of the drawdown decreases monotonically to almost zero at Ln (t) = 4.0 (which corresponds to $t = e^{4.0} = 54.6$ to approximately 55 minutes) and then oscillates and eventually becomes zero. Derivative calculated over a range of $\pm$ 0.25 Ln cycle.

Figure Q-2.7. Derivative of Drawdown Data in Screen #2 at NC-EWDP-22PA